Rheological and Mechanical behaviour of Block copolymers, Multigraft copolymers and Block copolymer Nanocomposites

Der Fakultät Maschinenwesen

der

Technischen Universität Dresden

zur

Erlangung des akademischen Grades

Doktoringenieur (Dr.-Ing.)

vorgelegte Dissertation

– – – – – – – – – – – – – – – –

Mahendra Thunga. M.Sc

geb. am 26.04.1980 in Eluru, INDIA

Tag der Einreichung: 17.11.2008

Tag der Verteidigung: 18.06.2009

Gutachter: **Prof. Dr. rer. nat. habil. Gert Heinrich**
Prof. Dr.-Ing. habil. Roland Weidisch
Prof. Dr. rer. nat. habil. Manfred Stamm

Vorsitzender der Prüfungskommission: **Prof. Dr.-Ing. habil. Rüdiger Lange**

Dedicated to my Family

Preface

Block copolymers are commercially significant and fundamentally interesting class of polymeric materials. The ability to undergo interfacial thermodynamics-controlled microphase separation from a completely disordered state in the melt to a specifically defined ordered structure through self-organization makes the block copolymers based materials unique. Block copolymers with a broad variety of architectural possibility can be designed by their synthesis and have been comprehensively studied regarding their phase behaviour and morphology during recent years. They provide the ability to design the targeted material behaviour by controlling the nanostructured morphology formed by self-assembling process. This nanostructure ordering in the phases is mainly governed by molecular weight (M_w), composition and chain architecture for constructing new materials with defined property profile. The most practical interests of block copolymers lie in the area of thermoplastic elastomers (TPEs). They provide the properties of irreversible cross-linked elastomers with better impact resistance and low temperature flexibility. In general TPEs prepared from block copolymers are phase separated systems consisting of a hard phase which provides physical cross-links and a soft phase which contributes in elastomeric property profile. Due to the presence of covalent bond between the hard and soft phases, the rigid domains can form physical cross-linking sites, resulting in a three-dimensional network, which make them comparable to vulcanised rubber. However, the main advantage in TPEs is due to their thermal reversible properties, which make them ideally suited for high throughput processing, such as melt extrusion and injection moulding. In recent days, the applicability of TPEs is widely extended in biomedical, automotive and IT industries due to the ability of high speed processing with better recycling capabilities when compared to vulcanised rubbers. Hence improving the physical and dynamic mechanical properties of block copolymers by controlling chemical architecture at synthesis level and by selective blending at production level gives an easy access for improvement of the material properties and this is one of my major tasks in the present research modules.

Further modification of block copolymer based TPEs by cross-linking in presence of radiation is relatively new technique for the development of TPEs with superior properties. The electromagnetic radiation has the ability to alter material parameters at molecular level for enhancing the macroscopic properties. The electron beam (EB) modification of polymers is relatively easy and direct method for cross-linking polymers when compared to chemical

processes. The desirable physical and chemical properties can be tailored by varying the radiation beam parameters.

Concerning the nanocomposites from TPEs, controlling the material at nanometer scale is one of the greatest challenges for current nanocomposite research. In elastomeric materials it is very prominent to fill the rubber matrix with nano particles from carbon or silica by melt mixing technique for enhancing the material properties. Other than conventional melt mixing technique, sol–gel processing is also a versatile technique, making it possible to produce a wide variety of materials and to provide existing materials with novel properties. A combination of in situ sol-gel reaction with electron beam (EB) cross-linking in TPE from triblock copolymer has been demonstrated for the first time as one of the novel nanocomposite system in this work. The main advantage of this system lies in controlling the size of silica nano particle generated inside TPE during in situ sol-gel reaction. The present investigation started with a thorough literature review of block copolymers, multigraft copolymers and block copolymer based nanocomposites in the first Chapter 1. The various experimental methods used for characterizing the investigated materials are described in Chapter 2. Chapter 3 to 6 is devoted to the discussion about the four critical topics that deals with Rheological and Mechanical behaviour of Block copolymers, Multigraft copolymers and Block copolymer Nanocomposites as listd below.

1. Symmetric linear styrene-b-(styrene-co-butadiene)-b-styrene S-(S/B)-S triblock copolymers with 80 wt.-% of PS content with varying molecular weights M_w have been studied. The influence of M_w on morphology, rheology and mechanical properties has been investigated. The scope of study lies in discussing the interrelation of M_w with the phase behaviour of S-(S/B)-S triblock copolymers with a S/B random middle block. The state of phase segregation, combined with high M_w has been observed to be the essential factors behind the tough response of the copolymer even at 80 wt.-% of PS.
2. The phase behaviour of symmetric and asymmetric triblock copolymers based on S-(S/B)-S chain architecture and their blends have been studied. A direct control over the final morphology and segregation strength for the block copolymer blends was achieved by blending of LN3 and LN4. The influence of SB random middle block on phase behaviour of triblock copolymers possessing different architectures was studied.

3. The *in situ* silica is synthesized in cross-linked triblock copolymer using sol-gel reaction technique. Control over size and distribution of silica particle is achieved through selective cross-linking of the butadiene phase (PB) in S-(S/B)-S triblock copolymer with the help of electron beam irradiation technique. The morphological observations reveals that the size of silica particle is decreasing from ~200 nm to ~35 nm with the increase of cross-linking dosage from 0 to 500 kGy. Further the interrelation between the three-dimensional cross-linked network structure and the growth of silica particles is studied.
4. Enhancement of tensile properties of superelastic multigraft copolymers having a polyisoprene (PI) backbone and polystyrene (PS) branches is studied by controlling chemical architecture at synthesis level and by cross-linking of PI phase with electron beam irradiation. The influence of number of branch points in the chain architecture on morphology and tensile properties of multigraft copolymers is studied. Selective cross-linking of the PI phase which is reinforced with PS microdomains by using electron beam irradiation technique has provided an easy and straightforward way for improvement in the tensile properties.

Coming to the experimental procedures employed for characterizing the materials: The phase behaviour and morphology, for the investigated materials was characterized by the dynamic mechanical analysis (DMA), transmission electron microscopy (TEM), atomic force microscopy (AFM) and the small-angle X-ray scattering (SAXS). The Dynamic mechanical properties of the melt within linear viscoelastic regime are studied by constructing master curves using time-temperature superposition (TTS) principle based on Williams-Landel-Ferry (WLF) equation. The morphological variations are critically correlated to the rheological response at reduced frequencies. The phase transitions in block copolymers were studied by using temperature dependent SAXS measurements and the observed transition temperatures are reconfirmed by Isochronal temperature scans in shearing mode. The mechanical properties are investigated by uniaxial tensile test. The thermal stability and the mode of decomposition of nanocomposites were comparatively studied by the Thermogravimetric analysis (TGA).

Contents

1. Introduction

1.1 Block copolymers

Block copolymers are macromolecules composed of sequence, or blocks of chemically distinct repeating units. Nanoscale self organization of polymers can be achieved simply by joining the polymer chains together in a block copolymer. As the polymer chains are tethered to each other, macroscopic phase separation cannot occur and structural organization occurs in domains with periodicities ≈1-100 nm. Development of block copolymers was originated with the discovery of anionic polymerization technique. The morphology and the nature of the microphase separated domains, including the nature and size of the phase boundaries depend up on chemical composition and chain structure, molecular weights of the constituent blocks, thermodynamic interaction parameters, casting solvent and solidification conditions and temperature. Depending on the synthesis procedure and conditions, the architecture of copolymers is controlled. As shown in Figure 1.1, diblocks, triblocks, multiblocks, starblock and graft copolymers are some of block copolymer architectures which are substantially commercialised materials with an extensive scientific interest.

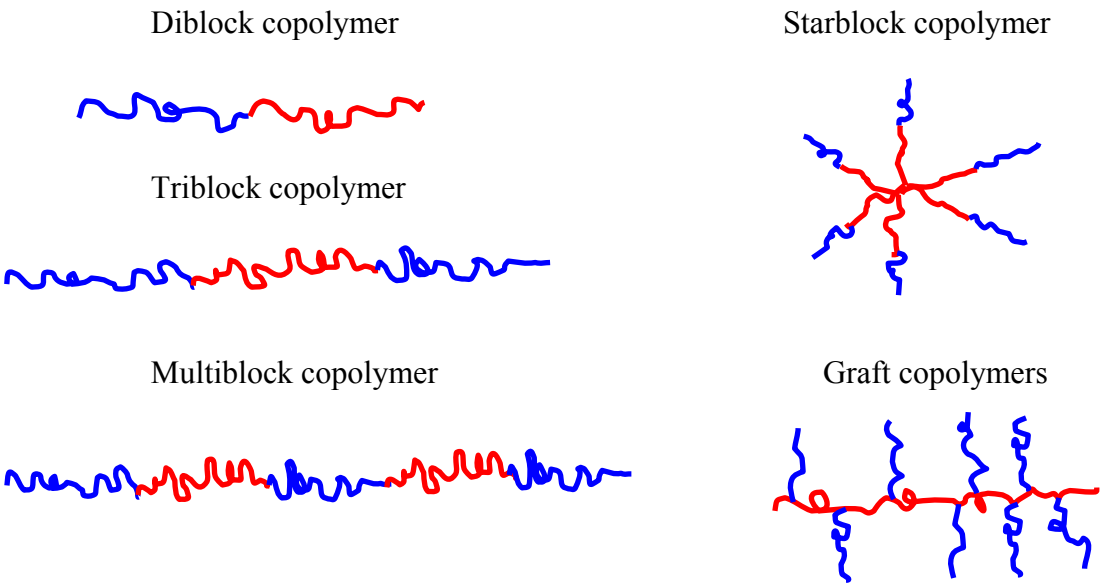

Figure 1.1 Possible block copolymer architectures

1.2 Phase behaviour and structure formation in block copolymers

The fundamental thermodynamics that describe the phase behaviour in homopolymer blends is also similar in case of block copolymers. When two polymers are mixed, the blended system mostly exhibits several different phases (regions with different compositions), which can be recognised as heterogeneous phase separated system. Whereas the state of equilibrium in this heterogeneous blend system is determined by the inter play between enthalpic and entropy during mixing. Entropy always favours mixing, but energetic

interactions resulting from enthalpic factor can either promote or inhibit mixing. A prerequisite for the miscibility of two polymers is decreased in the free enthalpy of mixing ($\Delta G_m < 0$), which is mathematically represented below [1]

$$\Delta G_m = \Delta H_m - T\Delta S_m \quad (1.1)$$

where, ΔH and $-T\Delta S$ represent the free energy of the chains due to local interactions and monomer moments and change in entropy due to motion of centre of mass of all polymers , respectively. According to Flory and Huggins, the enthalpy of mixing ΔH_m, can be expressed as

$$\Delta H_m = RT\chi_{AB}\phi_A\phi_B \quad (1.2)$$

R = universal gas constant
T = temperature
ϕ_i = volume fraction of component i

and the Flory - Huggins χ_{AB} is represented as below

$$\chi_{AB} = \left(\frac{Z}{k_B T}\right)\left[\varepsilon_{AB} - \frac{1}{2}\left(\varepsilon_{AA} + \varepsilon_{BB}\right)\right] \quad (1.3)$$

Z = number of nearest segments in other chains
k_b = Boltzman constant
ε_{AB} = interaction energy between segments A and B

The entropy of mixing is given by equation 1.4

$$\Delta S_m = -R\left(\frac{\phi_A}{N_A}\ln\phi_A + \frac{\phi_B}{N_B}\ln\phi_B\right) \quad (1.4)$$

Where N is the degree of polymerization

Hence, enthalpic and entropic contribution to free energy of mixing can be interrelated in terms of Flory-Huggins segmental interaction parameter (χ), where the temperature dependence of χ is represented as

$$\chi = \frac{A}{T} + B \quad (1.5)$$

A and *B* are the entropic and enthalpy terms respectively.

Modification of molecular chain architecture can dramatically influence the bulk physical, morphological and mechanical properties [1,2]. It has been reported that formation of microstructure mainly depends on the free volume of the phase. For example, in styrene-butadiene (S-B) block copolymers depending on the f_{PS} (free volume of styrene or volume composition of PS) different types of microstructures are observed [3], named as spherical,

cylindrical, gyroid, and lamellar morphologies (Figure 1.2). The dynamics of formation of several ordered nanostructures as shown in Figure 1.2 can be described in terms of volume fraction (ϕ) of individual blocks and a combined parameter; χN, where χ and N denote Flory-Huggins segmental interaction parameter and chain length respectively.

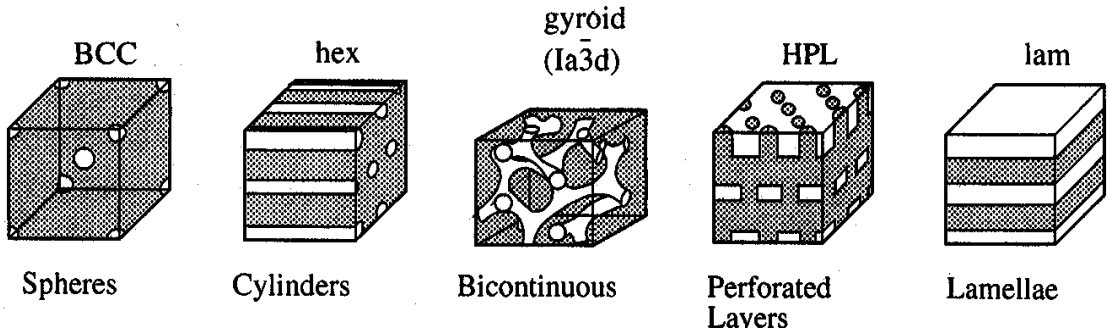

Figure 1.2 Microphase separated structures in block copolmers [3]

Accordingly, as shown in Figure 1.3 phase diagrams have been constructed in reference to relative block composition (ϕ) and the combined parameter (χN) [4]. The conceptual significance of the parameter, χN, remains in the fact that formation of ordered structures is facilitated when $\chi N > (\chi N)_{ODT}$ whereas the disordered structures formation will be favoured when $\chi N < (\chi N)_{ODT}$, where $(\chi N)_{ODT}$ is the critical value of χN for stability of the disordered state. On the other hand, formation of different morphologies from the ordered state (spheres, cubical, hexagonal packed rods, lamellar) typically depends on ϕ (Figure 1.3).

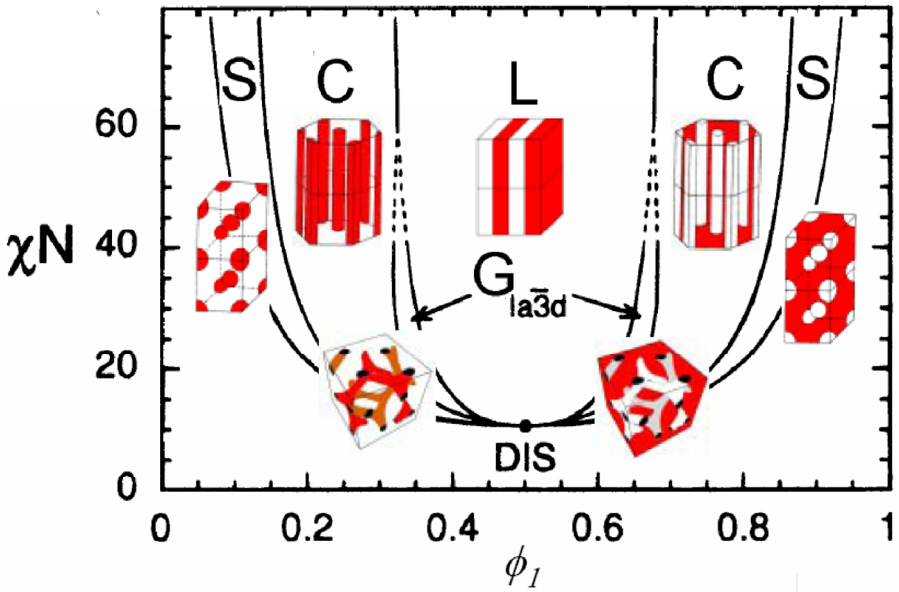

Figure 1.3 Mean-field phase diagrams for symmetric diblock copolymer [4].

1.3 Order to Disorder Transition (ODT)

In block copolymers at sufficiently high temperatures the incompatibility between the two phases in the system gradually diminishes resulting into a spatially homogeneous state and exhibiting the properties of a randomly mixed phase in the available free configurations of the polymer chains. As shown in Figure 1.4 at higher temperature the ordered microphase separated structure will go to disordered state which leads to the formation of an isotropic phase with the binary block chains interpenetrating each other. At high temperature, χ becomes sufficiently smaller leading to an increase in entropy, and hence contributes to minimizing ΔG_m. On decreasing the temperature, χ becomes larger and at critical value of χ the entropy term dominates causing an increase in free energy of mixing. Hence the number of contacts between the two blocks decreases which ultimately leads to phase separation at microscale. Since the two blocks are covalently bonded the phase separation is limited to a length scale of the radius of gyration (R_g) (about 10-100 nm).

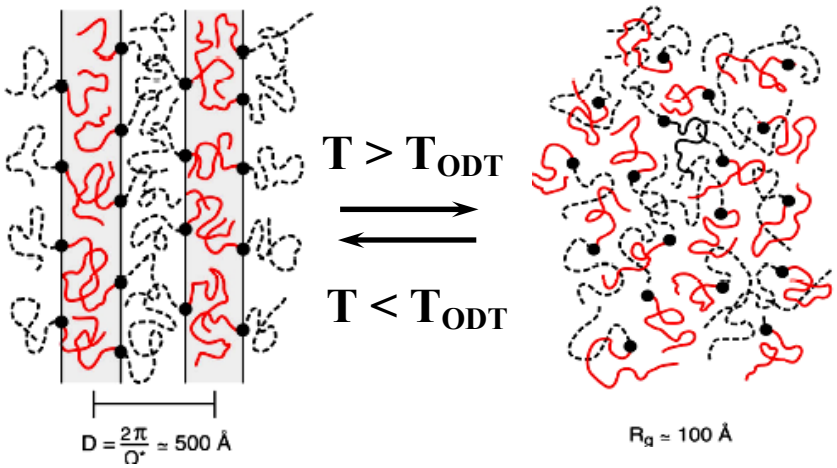

Figure 1.4 Order and disorder states in a symmetric PS-PI diblock copolymer

The product χN that expresses the enthalpy–entropic balance is then used to parameterize block copolymer phase behaviour. According to Leibler's mean field theory at the order-disorder transition in a symmetric PS-b-PI diblock copolymer the product χN can be expressed as [5]

$$(\chi N)_{ODT} = 10.495 \quad (1.6)$$

Fredrickson and Helfand [6] have subsequently extended the mean-field theory while taking into account of the fluctuation effects and this critical value was corrected later as

$$(\chi N)_{ODT} = 10.495 + 41.022N^{-1/3} \quad (1.7)$$

ODT in block copolymers can be experimentally identified via numerous methods out of which rheological measurements and temperature dependent Small-Angle-X-ray scattering

(SAXS) measurements are extensively used. From rheology, during shearing the block copolymer sample, the ODT can be identified from a sharp decrease in the isochronal dynamic elastic moduli obtained during heating ramp. Bates et al. [7] have investigated the ODT transitions in Polyethylenepropy1ene-Polyethylethy1ene (PEP-PEE) Diblock copolymers with the aid of rheology. They pointed out that the elastic moduli G' is decreasing discontinuously near ODT as shown in Figure 1.5. Further, they investigated the ODT from the master curves which are constructed by time-temperature superposition principle in order to attain low frequency rheological response. Although, application of time-temperature superposition principle on rheologically complex materials like diblock copolymers is not rigorously correct, this method is used to illustrate the qualitative changes that occur as a consequence of phase transitions near ODT.

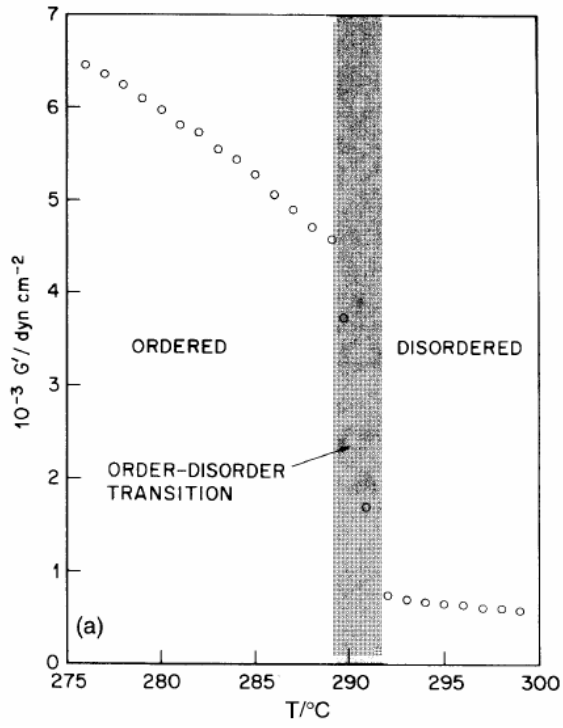

Figure 1.5 Temperature ramp for a nearly symmetric PEP-PEE diblock copolymer showing a transition from lamellar phase into a disordered phase at ~290 K[7]

The fairly accurate ODT temperature from the rheological measurements can be determined accurately by SAXS technique. This technique involves in measuring the intensity of X-ray or neutrons reflection as a function of angle of incidence. The main objective of this method is to calculate a scattering density profile representing the bulk nano structure in the block copolymers. The order-disorder transitions in polystyrene-polyisoprene (SI) diblock copolymer was critically investigated by Hashimoto et al.[8], they studied the temperature dependent SAXS profile for SI diblock copolymers as shown in Figure 1.6a . From Figure

1.6a a sharp and remarkable change in the SAXS profile can be clearly seen at temperature between 149.7 and 160.2 °C. This discontinuities change of the SAXS profile enables a clear –cut determination of ODT temperature of this block copolymer. A continues change in the scattering profile in terms of peak width and peak position at $T>T_{ODT}$ can be observed.

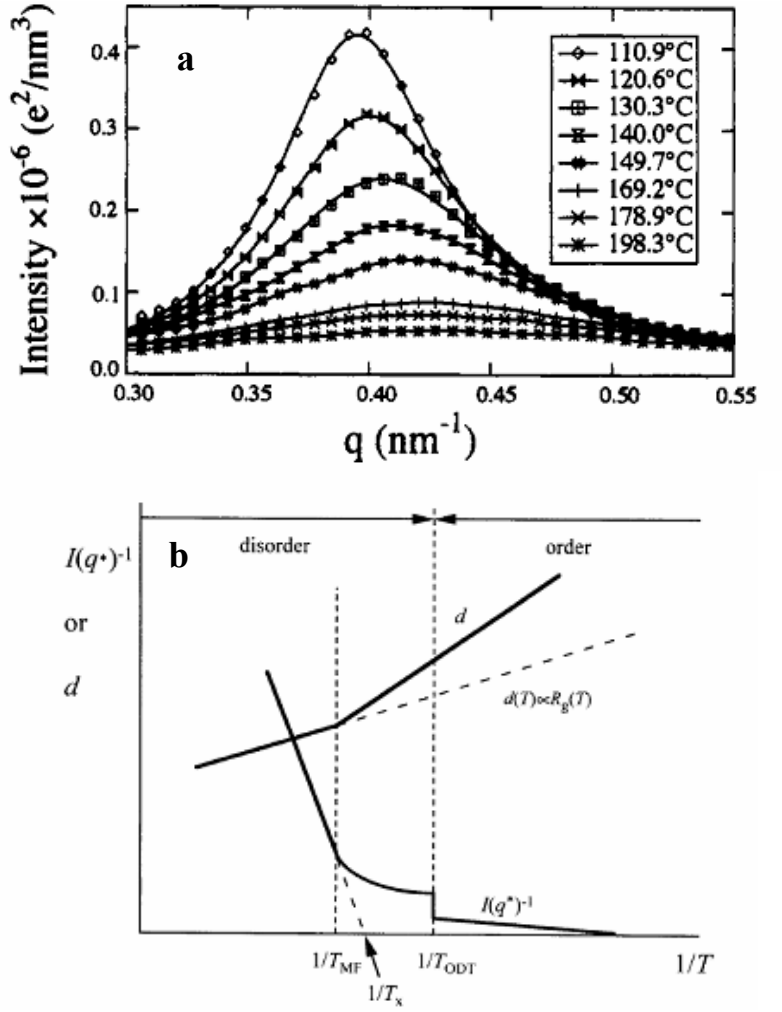

Figure 1.6 Temperature dependency of SAXS profile for SI diblock copolymers Represents (a) change in SAXS profile across ODT (b) The variation of inverse scattering intensity and domain spacing across the ODT [8]

Further, the scattering intensity (I_m), scattering vector (q_m) at the maximum scattering intensity or the characteristic length $D=2\pi/q_m$ are studied for screening the variation of the microstructure with respect to temperature. The ODT was determined from the scattering experiment on the basis of Leibler's mean-field theory [5]. According to the theory the correlation function for a homogeneous block copolymer melt is given by

$$S(Q) = \frac{N}{\left(F(Q) - 2\chi N\right)} \tag{1.8}$$

Where

$$F(Q) = \frac{g_1(R)}{g_1(R_1)g_1(R_2) - \frac{1}{4}\left[g_1(R) - g_1(R_1) - g_1(R_2)\right]^2} \text{ and}$$

$$g_1(x) = \frac{2\left[Q^2x^2 + \exp(-Q^2x^2) - 1\right]}{R^4Q^4}$$

$$R^2 = R_1^{\ 2} + R_2^{\ 2}$$

F(q) is the function which depends on the *R* and the composition *f* of the block copolymer. According to Equation 1.8 and 1.5, as χ is strongly depending on T. At high temperature i.e. in the disorder state I_m^{-1} should change linearly with 1/T as shown in Figure 1.6b. Further as $D=2\pi/q_m$, it should change linearly with 1/T with in the narrow temperature range of $T>T_{ODT}$. Thus a deviation of D or I^{-1} from linearity at $T<T_{ODT}$ was considered to be an onset temperature (T_{MF}) of ordering which can be predicted on the basis of mean-field theory. On the other hand Bates et al. [7] reported that the discontinuity in the plot of I_m^{-1} vs T^{-1} was identified as T_{ODT} for PEP-PEE diblock copolymer system as shown in Figure 1.6b.

1.4 State of ordering in block copolymers

The scaling relation between the characteristic length and the chain length in block copolymer systems has gained considerable interest. As illustrated in the phase diagram of block copolymers the two important regimes that are postulated to describe the phase segregation in block copolymers are weak segregation limit (WSL) and strong segregation limit (SSL). When the combined parameter $\chi N<10$, the copolymer melt exists in a disordered state and the interaction between A-B blocks is sufficiently low and the composition profile of the heterogeneous phases exists in a sinusoidal wave profile as shown in Figure 1.7a. The interface between the heterogeneous phases is broader and the domain periodicity D scales similar to that of radius of gyration in random (R_g) coil confirmation of homopolymers [9].

$D \alpha aN^{1/2}$ (1.8)

Where 'a' and N are characteristic segment length and degree of polymerization respectively. This regime is termed as weak segregation limit (WSL).

On the other hand when the value of $\chi N >>10$, then the purity of the phases will be enhanced with sharp interface between neat A and B blocks as shown in Figure 1.7b. This regime is termed as strong segregation limit (SSL). In this regime the interaction associated between A and B blocks is localised with in the interface. The system tries to attain equilibrium state by minimising the total area of such interfaces and the periodicity D scales as

$D\alpha aN^{2/3}\chi^{1/6}$ (1.9)

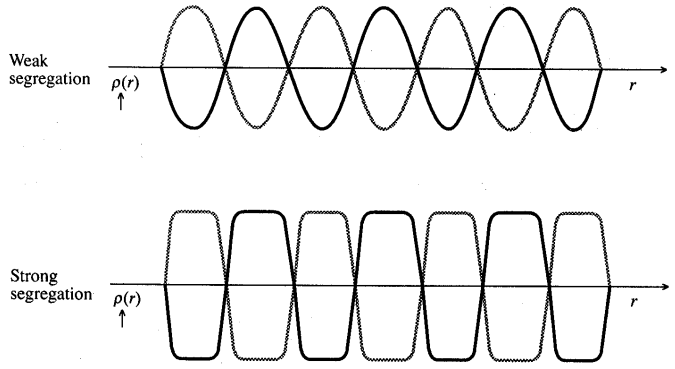

Figure 1.7 Composition profiles of A and B components (a) weak segregation limits (b) strong segregation limits, compared to the mean (straight line)

Depending on the volume fraction of the individual phases, in the SSL various ordered microphase separated structures can be observed as listed in Table 1.1 [9]. On further increasing of the block A content above 62 vol.-% leads to the corresponding ordered phase invertion.

Table 1.1 Expected microphase separated structures based on free volume of styrene

Vol.-% of A block	Type of structure
Up to 17	BCC (Spheres)
17 to 28	HDP (Hexagonal packed cylindrical structure)
28 to 34	Gyroid
34 to 62	Lamellar

Recently, an Intermediate Segregation Regime (ISR) was also proposed when $10.5<\chi N<29$ and the domain periodicity was represented as [10]

$$D\alpha N^{0.83} \quad (1.10)$$

As shown in Table 1.1, the systematic variation in the microphase separation structure with the increase in the vol.-% of individual block is due to a relevant change in the chain architecture [9].

As a matter of fact, a symmetric diblock copolymer with compositionally symmetric can form a flat interface as shown in Figure 1.8a and such chain organisation in the heterogeneous phases constrained by the interface results in showing a lamellar morphology. However, a diblock copolymer with compositionally asymmetric nature will show a high tendency to form curved interfaces as shown in Figure 1.8b and the interfacial curvature can be controlled by varying the asymmetric parameter. The reason behind the systematic

variation of the interfacial curvature with respect to asymmetric parameter is to maintain an uniform segmental density within the heterogeneous phases which should be equal to the bulk density of the homopolymer.

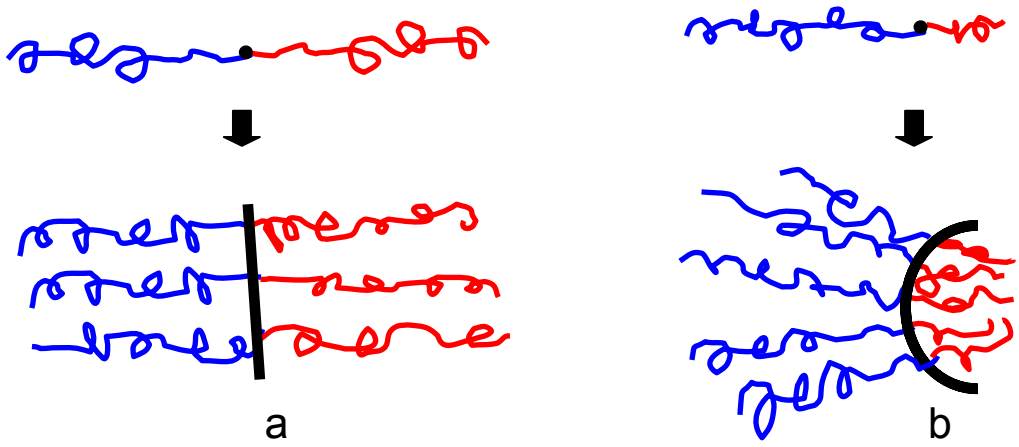

Figure 1.8 Schematics of chain conformation at the microphase separation state. (a) Stable flat interface from compositionally symmetric architecture (b) Stable curved interface from compositionally asymmetric architecture

1.5 Phase behaviour in triblock copolymers

The change in molecular architecture from diblock to a triblock copolymer at constant chain length and composition could show similar morphologies but show a dramatic influence on the structure-property interrelation. During the phase separation, the two block junction points in triblock copolymer will try to locate at the interface with a significant reduction in the conformational entropy in its ordered state when compared to the diblock copolymer with same composition and chain length. As a consequence, in the disordered state the triblock copolymer is more stable than a diblock copolymer processing same molecular chain architecture and composition. This phenomenon is described more clearly in relevance with the theoretical predictions by comparing the phase behaviour in triblock copolymer melt with that of a hypothetical melt formed by snipping the same triblock copolymer at half [11] . Such comparisons result in concluding that the oder-to-disordered transition in triblock copolmers stay at higher values than diblock copolymers with chain length equal to half of the triblock copolymer. The Mean-Field-Theory (MFT) proposed by Leibler was also used in the calculation of the triblock copolymer phase diagram. As shown in Figure 1.9, the phase behavior in triblock copolymers near ODT was investigated theoretically by Mayes and Olvera de la Cruz [12]. They showed that the critical $(\chi N)_{ODT}$ for microphase separation in triblock copolymers is 18, which is equal to 10.5 in

case of diblock copolymers having similar molecular parameters. Further, the phase diagram of ABA triblock copolymer which is having either symmetric architecture or asymmetric architecture is highly asymmetric. The composition, ϕ at which a continuous transition from disordered to lamellar phases occurs, was found to shift as a function of symmetric parameter τ. For an asymmetric parameter τ =0.25 at ϕ=0.5 a transition from disordered phase to a BCC phase and to hexagonal and then to lamellar phase can be expected on lowering the temperature.

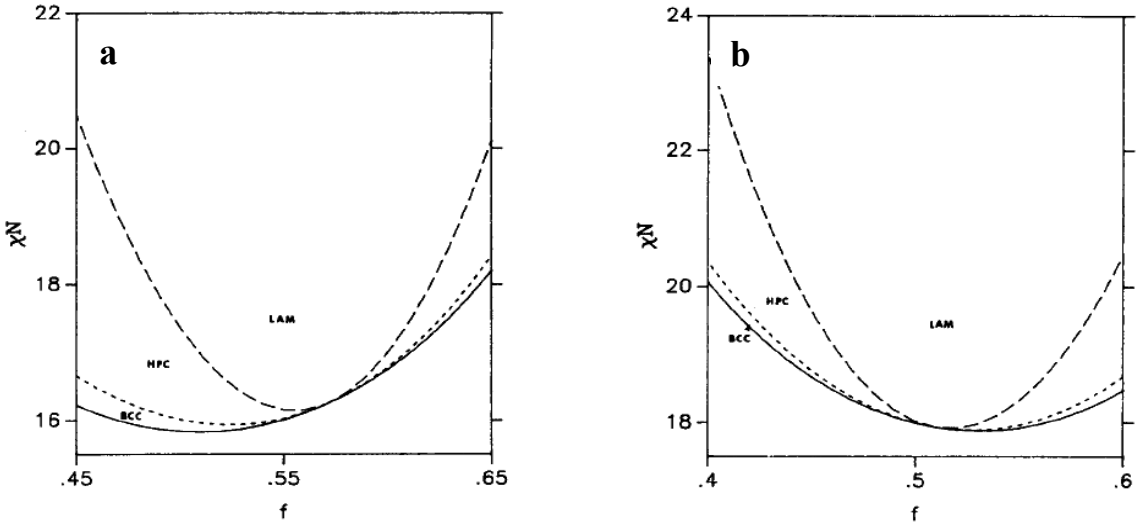

Figure 1.9 Phase diagram of ABA triblock copolymer with different chain architectures (a) asymmetric architecture with asymmetric parameter τ = 0.25 and (b) symmetric architecture with asymmetric parameter τ = 0.5 [12]

This phase behaviour is contrasting to the diblock copolymers, where a direct transition from disordered structure to lamellar phase can be observed at ϕ=0.5. On the other hand when the τ =0.5 (Figure 1.9b), when χN≈18 and ϕ=0.4 the melt is predicted to be disordered, where as at same χN a hexagonal phase is found to be more stable when ϕ is increased from 0.4 to 0.6.

Very recently by using self–consistent field theory (SCFT) , Matsen has examined the phase behaviour of ABA triblock copolymers and found that there is a drastic phase shift in phase transition lines relative to the symmetric ABA copolymer in asymmetric copolymers [13]. He showed that the molecular asymmetry can alter microdomain dimensions and order-order transitions due to the presence of shorter block that remain mixed upon microphase ordering of longer A and B blocks in the asymmetric architecture. Further, phase diagrams describing a systematic variation in the region of ordering with respect to the molecular composition (*f*) and asymmetric parameter (τ) at different degree of segregations were constructed. The phase diagrams with respect to segregation strengths χN = 20 and 40 are shown in Figure 1.10a and 1.10b respectively. As the asymmetry changes,

the various ordered regions of diblock system at τ=0 in Figure 1.10a is eventually going into those of symmetric triblock system at τ=1/2 as shown in Figure 1.10b. As diblocks are more strongly ordered than symmetric triblock copolymers of same M_w, the ordered region tends to narrow as τ increases at specific segregation strength.

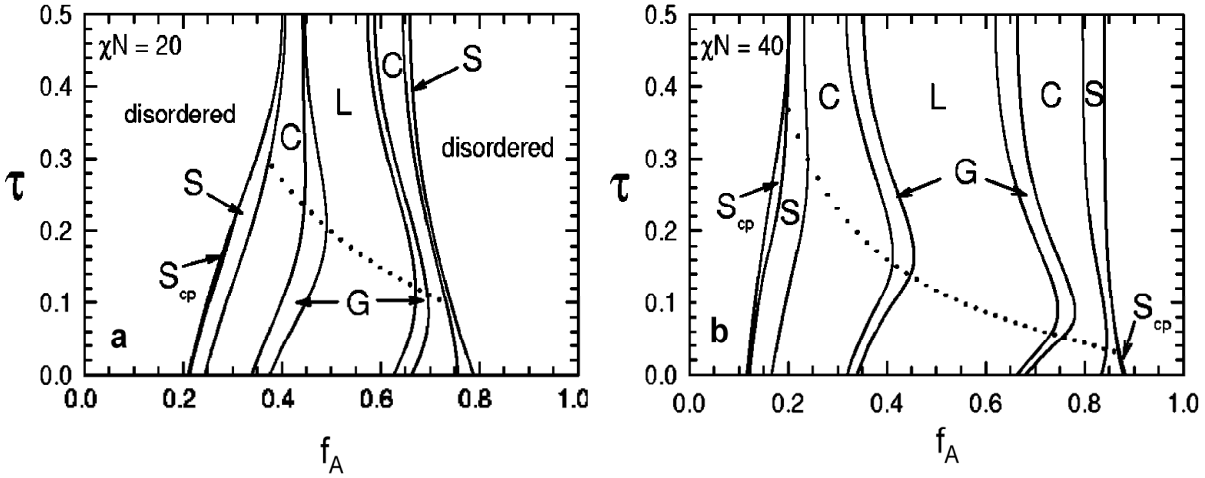

Figure 1.10 Mean-field phase diagram for asymmetric ABA triblock spanning between diblock (τ=0) and symmetric triblock (τ=0.5) limits at segregation of (a) χN = 20,(b)χN = 40 [13]

On the other hand a significant deflection in the order-order transition (OOTs) towards large f_A value can be seen. As the value of τ deviates from 0.5, the A segments distribution moves away from the interface without stretching the A chains and this causes an increase in the domain spacing as shown in Figure 1.11

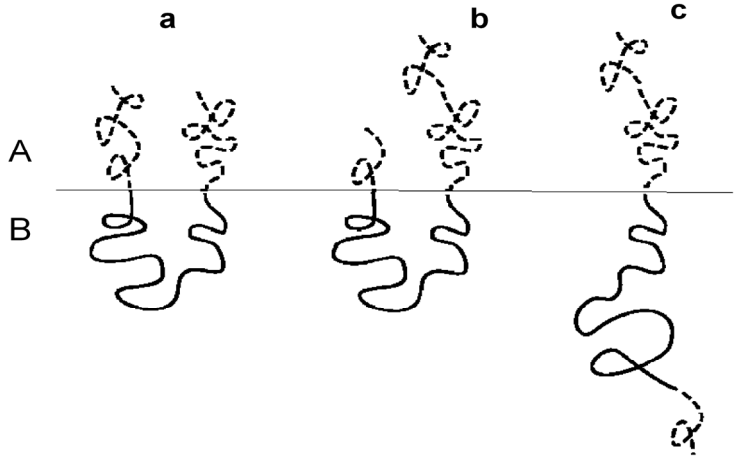

Figure 1.11 Schematic diagrams of three triblock configurations all with equal degrees of chain stretching. Dashed and solid curves denote the A and B blocks, respectively. (a) The symmetric triblock having its segments closest to the interface, (b) asymmetric triblock having its A segments further away from the interface and (c) asymmetric triblock having its short A block extended from A domains [13]

Hence the stretching energy in A domains is decreased. Further, the spontaneous curvature changes, since transferring some of the B domain stretching on the softer A domain by curving the interface away from B domain lowers the overall energy. This change in spontaneous curvature shift OOTs towards large f_A as τ decreases from 0.5, i.e., when the outer block become more asymmetric. At sufficient large asymmetry, the A chains begin to pull out of their domains. Although unfavourable interactions occur when A blocks leave A domains, it is more than compensated for the fact that its B domains can relax.

1.6 Blends of block copolymers

The most important application of block copolymers lies in compatiblization of two immiscible homo-polymers. The phenomenon of compatiblization results in the reduction of interfacial tension due to segregation of copolymer to the interface between homopolymers. However, concerning the binary blends of block copolymers, M_w of the two blend components plays a vital role in the blending process. A mismatch in the M_w causes macrophase separation and on the other hand blending of similar molecular weight polymers allows microphase separation.

The morphology of a blend does not necessarily correspond to that of the pure copolymer with the same composition. A change in morphology can be driven by change in interfacial curvature and packing density. Blends of diblock copolymers with similar compositions and satisfying $\chi_{eff} << \chi_{s,macro}$ exhibit the same morphology as pure diblocks with same overall composition. The phase miscibility aspects need to be critically understood for attaining desired morphologies via molecular level mixing, since nature of the components in a blend affect the ultimate morphologies decisively. For example, a morphological transition from lamellar to cylindrical structure was observed by adding a homo-PS in PS-PI diblock copolymers by Hashimoto et al. and Tanake et al. [14, 15]. Such changes are illustrated in the vicinity of variation of the interfacial curvature which appear from the difference in the segmental volume between PS and PI due to the localization of PS homopolymer in the PS-phase of block copolymer. These blend systems have remarkable adaptability in order to tailor polymer nanostructures. However, the two limiting factors influencing the morphology in blending a homopolymer with a block copolymer are, (a) the ratio of M_w of homopolymer to that of the block copolymer and (b) the fraction of the homopolymer that can be added in the blend [14,16]. In order to overcome such limitations, the strategy of blending of two block copolymers for precisely accessing control over the ultimate morphology has been widely adopted. Apart from the M_w and compositional ratio, like in homo-polymer / block-copolymer blends, the chain architecture of the blend-

components and the blend-composition can be manipulated for attaining novel morphologies which could potentially lead to excellent physical and mechanical properties [17]. In this direction, Matsen and Bates have calculated the phase diagram for the A-B type diblock copolymer based blends where both components have similar degree of polymerization (N) but differ in A-block fraction by making use of self consistent field theory and thus describing the phase behaviour in such blend systems to be comparable to that of the phase behaviour of neat diblock copolymers [18].

However, Spontak et al. [17] noticed coexisting morphologies in some block copolymer blends. Addition of an asymmetric copolymer to a symmetric block copolymer causes a change in morphology. Initially this was observed in swelling of the lamellar domains of the symmetric diblock, which was subsequently modelled using a simple strong segregation limit theory. On further increasing the asymmetric copolymer, coexistence of a cylindrical phase with a lamellar structure or bicontinuous morphology was observed. Comprehensively, Hashimoto et al. [19-21] have studied the systems involving lamella forming diblock copolymers and their blends and later extended their investigations to several other morphologies. They explored the phase behaviour of diblock copolymers with equilibrium morphologies attained via self-organization of the block copolymer chains from blend components, where the blend components differ substantially not only in composition but also in architecture [19-21]. Subsequently Sakurai et al. [22] have applied these developments from Hashimoto's work based on diblock copolymers to more complex architectures like triblock copolymers from SBS and illustrated that the variation in the microstructure remained sensitive to composition.

1.7 Rheological Properties

The persistent microphase separated morphologies in block copolymers show a strong significance on their corresponding rheological response. Shearing the material at small amplitudes does not affect the morphology and hence can be used to study the effect of morphology on rheology in a non-destructive manner. Dynamic mechanical measurement techniques are generally used in studying the rheological behaviour of block copolymers. Since the dynamic data gives information about both the molecular and the physical characteristics of polymers. Application of dynamic mechanical testing techniques while shearing are particularly advantageous in the study of block copolymers because they probe time scales that are closely correlated with the microstructural length scales which is being intended to study.

In block copolymers or in blends with multicomponent systems there is emergence of pronounced elasticity at low frequency. Due to the interfacial tension under flow conditions the drop break-up and coalescence processes between these multiphases are rendering the rheology-morphology interrelation. The main aim of applying rheology on polymer systems is to analyse the elementary building blocks of the polymer system, such as polymer chains, crystalline structure, liquid crystal mesogens and phase-separation structures. There can be a variation in chain conformation in different types of block copolymers but all of them can show the same morphology dependent on the composition. The chain conformation in the microphase separated morphology will effect the parameters such as interaction between phases and phase segregation strength, which ultimately controls the material properties. For example, in triblock copolymers like SBS the middle butadiene block can either form a loop so that the two styrene blocks are anchored in the same microdomain or can form a bridge between the two outer blocks. In the above two cases the material mechanical properties will vary even though they show nearly same microstructures. Such variations are characterized by rheology. Using linear viscoelastic rheology as a tool, one can distinguish the mechanism of polymer chain relaxation under shearing for different types of block copolymers. The behaviour of the block copolymer in a flow field is a complex phenomena which can be investigated by three externally correlated parameters like temperature (T), shear strain (%) and deformation rate (ω or $\dot{\gamma}$) The first key step is recognition and understanding of the time–dependent relationship in polymers. Relaxation times of polymers and the relative characteristic time of the deformation play an important role in determining their constitutive relation of time dependency. Thus Deborah number is introduced which is the ratio between the relaxation time (λ) and the characteristic deformation time (t), and is given by,

$$De=\lambda/t . \qquad (1.11)$$

In the above equation t will be in different forms in different experiments, e.g $t = \dot{\gamma}^{-1}$ in steady shear where as it is represented as $t =(\gamma_o\omega)^{-1}$ in dynamic shear tests. Polymers have some special properties like a rich inner structure and wide relaxation spectra. As the polymers are sheared far away from their equilibrium state, nonlinear behaviour can be expected. Thus the amplitude of deformation, expressed as strain amplitude (γ_o),is another important parameter while considering the constitutive relations of block copolymers. Thus, based on the shear amplitude and the shear rate the viscoelastic behaviour of polymers in the limits of low strain rate, low amplitude deformation, and high strain rate is schematically summarized in Deborah number versus strain amplitude in Figure 1.12 [23].

As the Deborah number is very small, i.e. the characteristic time of deformation is much larger than the relaxation time of a polymer (t>>λ), the polymer behaves like an ideal Newtonian fluid and its constitutive relation can be expressed using Newton's law

$$\tau = \eta_0 . \dot{\gamma} \qquad (1.12)$$

where τ and $\dot{\gamma}$ are stress and strain rate, respectively, η_0 is an intrinsic constant of the polymer, called steady-flow viscosity.

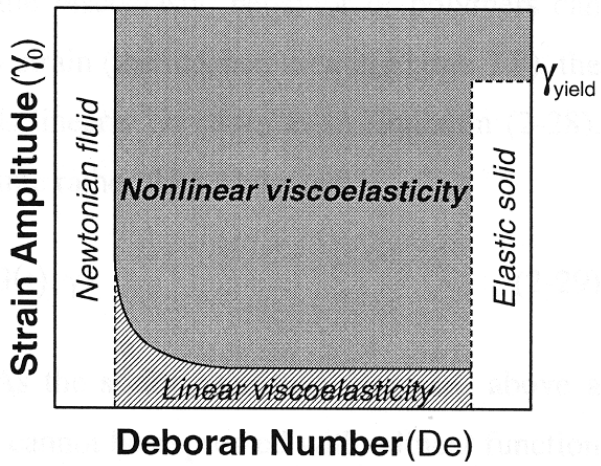

Figure 1.12 Schematic diagram showing the viscoelastic behaviour of polymers in the limits of low strain rates, low amplitude deformations, and high strain rates [23]

Another extreme is observed at high Deborah numbers in the diagram. In this case the characteristic time of deformation is much shorter than the relaxation time of the polymer and the rheological behaviour is governed by Hooke's law

$$\tau = G_g . \gamma \ , \qquad (1.13)$$

where γ is the strain and G_g is the glass-like modulus.

Depending on the strain amplitude the viscoelastic behaviour of polymer can further be categorized into two types

- Linear viscoelasticity: In this case at low strain the stress in a polymer under deformation depends linearly on strain and is given by the relation,

  $$\tau = G(t) . \gamma \ . \qquad (1.14)$$

- Nonlinear viscoelasticity: In this case the strain amplitude increases above a critical value and the stress can not be expressed with a linear function of strain.

In the present work rheological techniques are extensively employed for describing the interrelation between structure and property in the nano structured materials. The materials

are characterised within the linear viscoelasticity regime in order to restore the microstructure even at elevated measured temperature range.

1.8 Linear viscoelasticity of polymers

As a consequence of viscoelasticity in polymeric liquid or melt, they show a stress relaxation behavior in an exponential fashion when subjected to step increase in strain. This strain dependence of measurable stress in polymer under external deformation fields in the linear regime makes time dependent studies quite easy. Thus one can use viscoelasticity of polymers as a spectroscopic tool to investigate polymer dynamics.

1.9 Dynamic shear experiment

In the present work the characterization of the polymer melts is done with the help of dynamic test data. This method is one of the important experimental techniques that can be applied for characterizing nanostructure materials at small strains. In this method the material response will be acquired by deforming the sample in a sinusoidal manner for few cycles in dynamic mode.

The stress will also oscillate in sinusoidal manner with the same frequency with some phase angle shift δ , with respect to the strain wave. This phenomenon can be expressed mathematically as

$$\gamma(t) = \gamma_0 . \sin \omega t \tag{1.15}$$

where $\gamma_0 = \frac{\Delta_0}{h}$

Δ_0 is the maximum lateral deflection of the sample from the initial position, h is the sample thickness, ω is the angular frequency. The strain rate can be represented as

$$\dot{\gamma}_0 = \gamma_0 . \omega . \cos \omega t \, . \tag{1.16}$$

Due to the viscoelaticity, the relation between induced shear stress τ(t) in the polymer oscillates with a shear amplitude producing a phase angle δ can be represented as

$$\tau = \tau_0 \sin(\omega t + \delta) \, . \tag{1.17}$$

The acquired experimental data can be expressed by decomposing the stress wave into two waves of same frequency , one in phase with the strain ($\sin \omega t$) and another 90^0 out of phase with this wave ($\cos \omega t$)

$$\tau = \tau' + \tau'' = \tau_0' \sin \omega t + \tau_0'' \cos \omega \tag{1.18}$$

Thus from equation 1.18

$$\tau'(t) = \tau_0 . \cos \delta . \sin \omega t$$

$$\tau''(t) = \tau_0 . \sin\delta . \sin\omega t \tag{1.19}$$

To consider phase relation between the strain and the induced stress, it is convenient to express the sinusoidal varying strain and stress as complex quantities.

$$\gamma^* = \gamma_0 . e^{i\omega t} \tag{1.20}$$

$$\tau^* = \tau_0 . e^{i\omega t} \tag{1.21}$$

Thus the three viscoelastic moduli in shear can be defined as

$$G^*(\omega) = \frac{\tau^*}{\gamma^*} = G' + iG'', \tag{1.22}$$

Where

$$G'(\omega) = \frac{\tau_0}{\gamma_0}\cos\delta \tag{1.23}$$

$$G''(\omega) = \frac{\tau_0}{\gamma_0}\sin\delta \tag{1.24}$$

Where G*, G', G'' are called complex, storage and loss modulus, respectively. The storage modulus reflects the elasticity of a polymer while the loss modulus corresponds to the viscous contribution to the complex modulus. Similarly, the three viscosities are defined as

$$\eta^*(\omega) = \frac{\tau^*}{\gamma^*} = \eta' + i\eta'' \tag{1.25}$$

where

$$\eta'(\omega) = \frac{\tau_0}{\omega\gamma_0}\sin\delta = \frac{G''}{\omega} \tag{1.26}$$

$$\eta''(\omega) = \frac{\tau_0}{\omega\gamma_0}\cos\delta = \frac{G'}{\omega} \tag{1.27}$$

η* (ω) is called the complex viscosity. η'(ω) and η''(ω) are its components which are in phase and out of phase with the strain rate, respectively. Hence η'(ω), the so called dynamic viscosity, reflects the viscous contribution to η* (ω), while η''(ω) is related to the elastic contribution. Another important parameter characterizing the relation between the viscosity and elasticity of polymer is the ratio between the components of the complex modulus or viscosity.

$$\text{Tan}\,\delta = \frac{G''(\omega)}{G'(\omega)} = \frac{\eta'(\omega)}{\eta''(\omega)} \tag{1.28}$$

It is conventionally termed as loss-tangent (tan δ). Depending on the time (or frequency) the stress measured under well controlled oscillatory deformation, all the quantities defined above can be calculated. Thus probing spectroscopic information of polymer dynamics can then be obtained through analysis of the results.

1.10 Time-temperature superposition principle

For polymers the spectroscopic information is spread over a wide range, but the time and frequency range on which strain and stress can practically be measured is very narrow. To solve this problem time-temperature-superposition (TTS) principle is used. According to this principle for viscoelastic polymers, time and temperature are equivalent to the extent that dynamic data at one temperature can be superposed on data at another temperature by shifting the curves along the time axis. By shifting the mechanical spectra measured at different temperatures to overlap with each other, a composite spectrum over a much wider scale of reduced frequency $a_T(T)$ is the shift factor of the data measured at the temperature T_0. Construction of this composite spectrum, illustrated in Figure 1.13 is usually called as 'Master curve' of a polymer. It is evident that temperature dependence of the shift factor allows one to get some insight into the polymer dynamics.

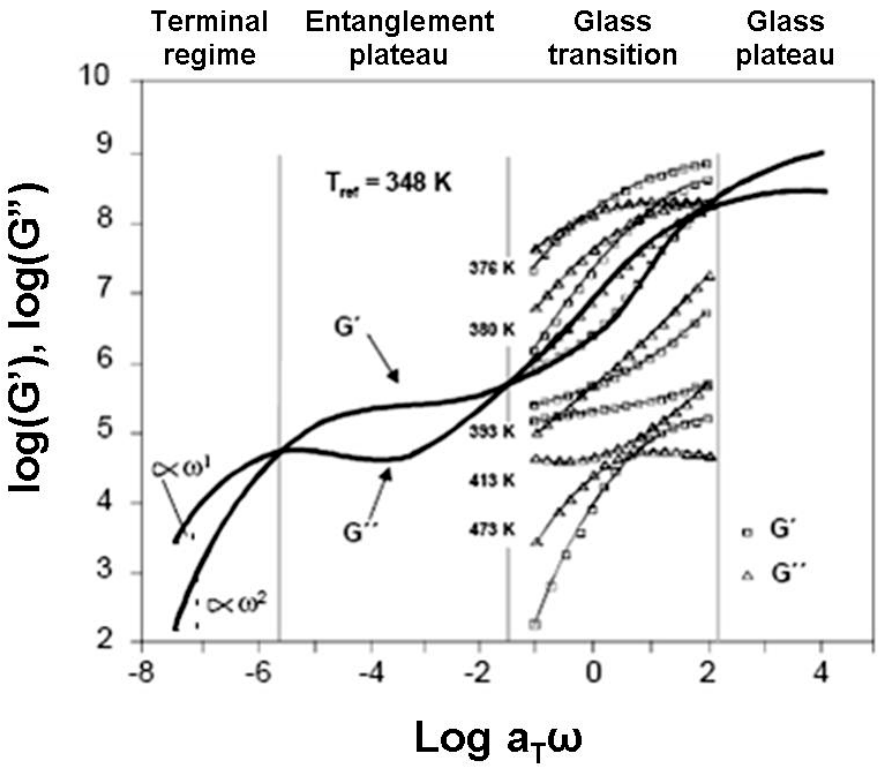

Figure 1.13 Master curve of Polystyrene – taken from Fig 2.9 of Ref. 24

The $a_T(T)$ curve can usually be fitted to two types of equations; The WLF equation and the Arrhenius equation. The WLF equation is related to the free-volume theory of polymer dynamics above the glass transition and is expressed as

$$\log[a_T(T)] = -\frac{C_1(T-T_o)}{C_2+(T-T_o)} \quad (1.29)$$

where T_o is the reference temperature and C_1 and C_2 are two fitting constants.

The Arrhenius temperature dependence of $a_T(T)$ originated from the Boltzmann activation of the relaxation modes and expressed as

$$a_T(T) = A_0 \exp(-Ea/RT), \quad (1.30)$$

where both, amplitude A_o and activation energy E_a, serve as fitting parameters. The prerequisite for the applicability of the time-temperature superposition is that, all the relaxation processes involved with in the measured temperature and frequency have the same (or similar) temperature dependence. However, polymers with heterogeneous nature coming either from blend components or from the inherent chain architecture possess complexity in their rheological response. On the other hand, existence of unusual relaxations in such systems results in failure of the time temperature superposition.

1.11 Linear viscoelasticity of block copolymers

The linear viscoelastic properties of the block copolymers involved in the present work are studied using their master curves. These master curves were obtained based on the time-temperature superposition principle discussed above. To get some primary impression of the overall features of the master curves of a block copolymer the master curves for G', G'', η* and tan δ for a polystyrene-b-polyisoprene (PS-b-PI) diblock copolymer which has been studied by Yuanming Zhang et al. [25] is schematically illustrated in Figure 1.14 and 1.13. The three regimes which are usually observed in a homopolymer, i.e. the glass plateau, the transition regime and the entanglement regime, are also observed in the master curves of block copolymers and shown in Figure 1.14. In both, the glass regime and the entanglement plateau regime, the storage-modulus G'(ω) is larger than the loss-modulus G''(ω). The elasticity dominates the response with the deformation field in these two frequency regimes. In between these regimes a transition regime where the loss-modulus G''(ω) is larger than the storage-modulus G'(ω). Another feature of this transition zone is the complex viscosity (η*) which has a more moderate slope relative to that in the glass and the entanglement plateau regimes in (Figure 1.15). At the same time the loss-tangent (tanδ) presents a

maximum. All this features indicate the domination of the viscous flow over the linear viscoelasticity of the block copolymer in the transition frequency regime.

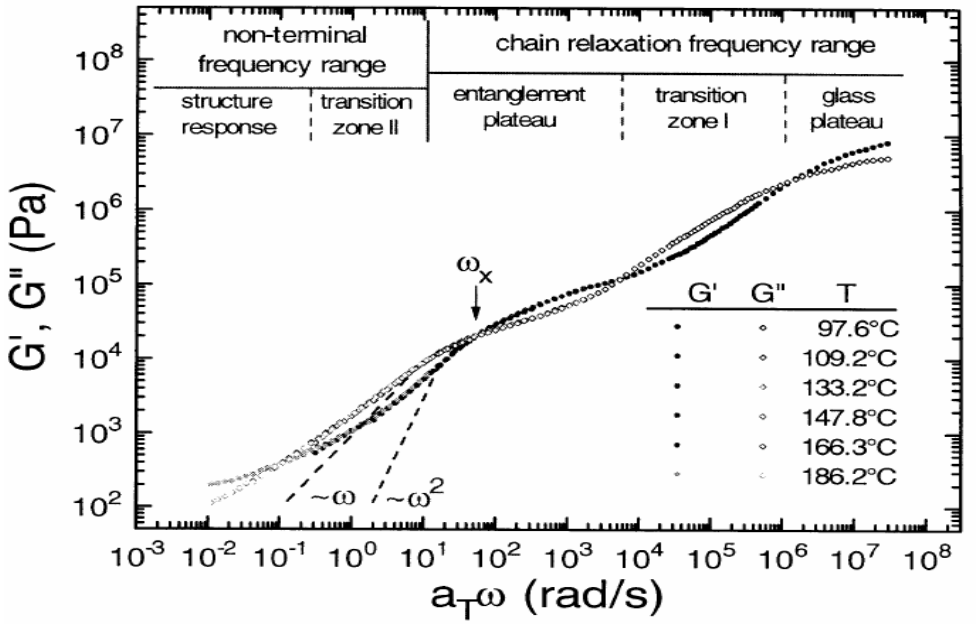

Figure 1.14 Master curves for G', and G'' at reference temperature of T_0 = 160°C

Since the glass plateau, the transition zone, and the entanglement plateau in a homopolymer are related to different molecular chain relaxation modes, the frequency range spanned by the similar regimes observed in the block copolymers will be termed as chain relaxation frequency range.

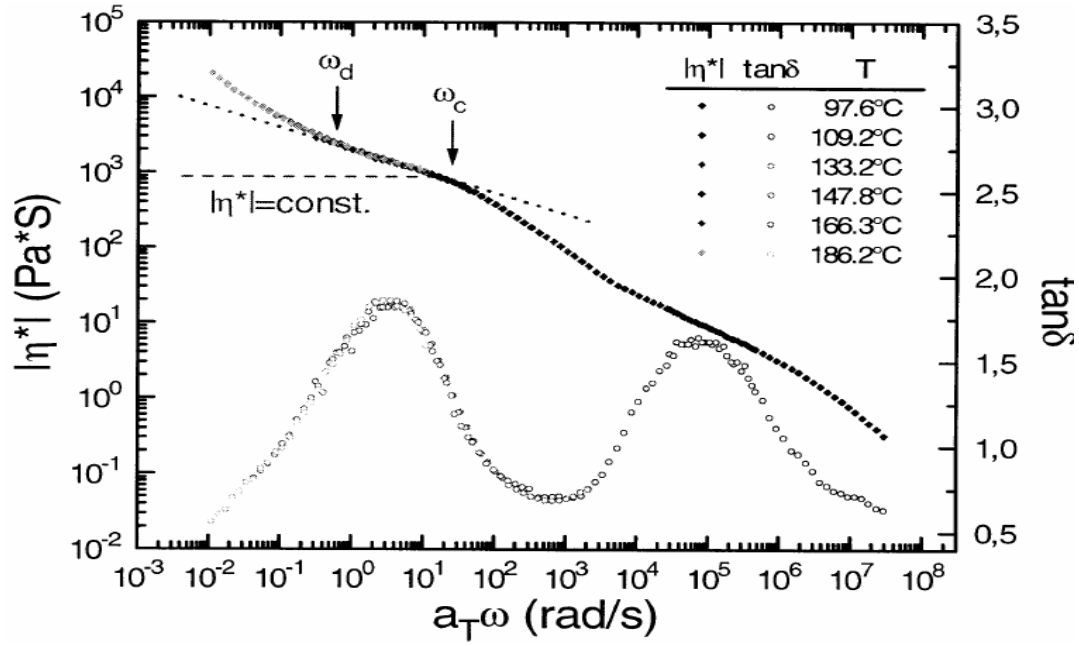

Figure 1.15 Master curves for η*, and tanδ at reference temperature of T_0 = 160°C

The most striking features of the linear viscoelasticity of block copolymers appear below the end of the entanglement plateau. In this frequency range a homopolymer usually behaves like an ideal Newtonian fluid with the viscosity being independent of shear frequency, i.e $\eta^*(\omega)$ = const. This frequency dependence for the linear viscoelasticity of a homopolymer is conventionally termed as the terminal behaviour and is indicated in Figure 1.14 using dashed lines. The frequency dependency of the moduli G' and G'' can then be described by equations 1.31. However, the moduli and the magnitude of the complex viscosity in this frequency regime are much higher than those of a homopolymer in the terminal regime. Thus this frequency range can be termed as non-terminal frequency range as shown in Figure 1.14.

$G' \propto \omega^2$ and $G'' \propto \omega$ (1.31)

At low frequencies in Figure 1.15 there is an onset of another plateau regime at which probably structure elements prevent relaxation of the stress and the elasticity dominates the linear viscoelasticity of the block copolymer. This plateau regime is indicated by a doted line in Figure 1.15. In order to further investigate the origin of the unusual relaxation behaviour at low frequencies, a master curve of a block copolymer which is having molecular weight lower than the entanglement molecular weight and having an order disorder transition temperature within the experimental accessible temperature is studied by Rosedale et al. [26] and is illustrated in Figure 1.16. The failure of time temperature superposition in Figure 1.16 allows one to deduce the existence of some unusual relaxation processes in the samples.

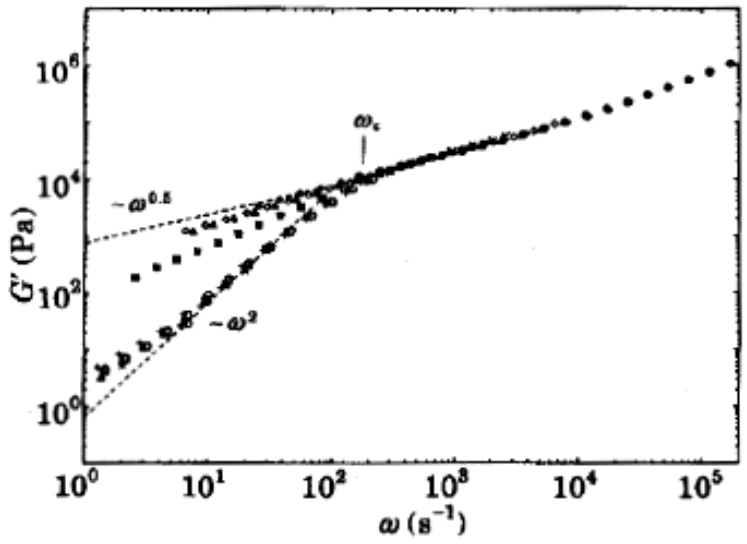

Figure 1.16 Failure of time temperature superposition in Block copolymer showing unusual relaxation

1.12 Mechanical Properties in block copolymer

The triblock copolymers with glass-rubber-glassy chain architecture are observed to have high tensile strength when compared to diblock copolymers which is due to immobilizing the elastomer segments in between non-elastomeric segments [27]. Studies on the morphological and mechanical behaviour of different styrene/butadiene triblock copolymer systems gave deeper insight in the characteristics of various molecular architectures [28,29]. As reported by Holden et al. [27] the mechanical behaviour of PS-PB block copolymers is mainly governed by the ordering of microphases with periodic arrangement of PS and PB segments but not only due to the segregation of blocks in distinct microphases. Such ordering is highly prominent in lamellar morphology compared to disordered or weakly segregated morphologies. The soft rubbery SB middle block bridges the two PS glassy domains due to the presence of ordered phase separated structure, resulting in enhancing the effect of physical cross-linking. As a consequence of such physical cross-links, the collective distribution of the stress between PS and PB phases take place in a more efficient manner, which results in enhanced toughness. From the practical point of view, these materials represent an excellent class of heterogeneous polymers allowing the adjustment of mechanical behaviour via a change in composition and in varying the molecular parameters [33].

Domain theory was proposed to describe the mechanical properties of SBS TPEs in early sixties [30,31] which postulates that the TPEs consist of glassy domains dispersed in rubbery matrix holding the elastomeric network together by means of physical crosslinks. Styrene/butadiene block copolymers provide model systems for the study of structure-property correlations of phase separated block copolymers. Figure 1.17 illustrates the stress-strain behaviour of SBS triblock copolymers with different morphologies [32]. At the composition range f_{PS} = 0.10 - 0.15, where spherical polystyrene (PS) domains are formed in a polybutadiene (PB) matrix, the block copolymer behaves as a weakly cross-linked rubber due to relatively large inter-domain spacing. Increasing the PS content to about f_{PS} = 0.30 results in the formation of spheres in a bcc lattice with relatively smaller inter-domain distance, and the copolymer behaves as a cross-linked elastomer showing a steep increase in tensile strength. Further increase in PS content to about f_{PS} = 0.40 causes an increase in strength where the PS cylinders are expected to form in side PB matrix. Most commercial TPEs have the composition in the range of f_{PS} = 0.20-0.40. As the block copolymer approaches a compositional symmetry, alternating layers of PS and PB phases are formed, and the macroscopic neck formation prevails during tensile deformation.

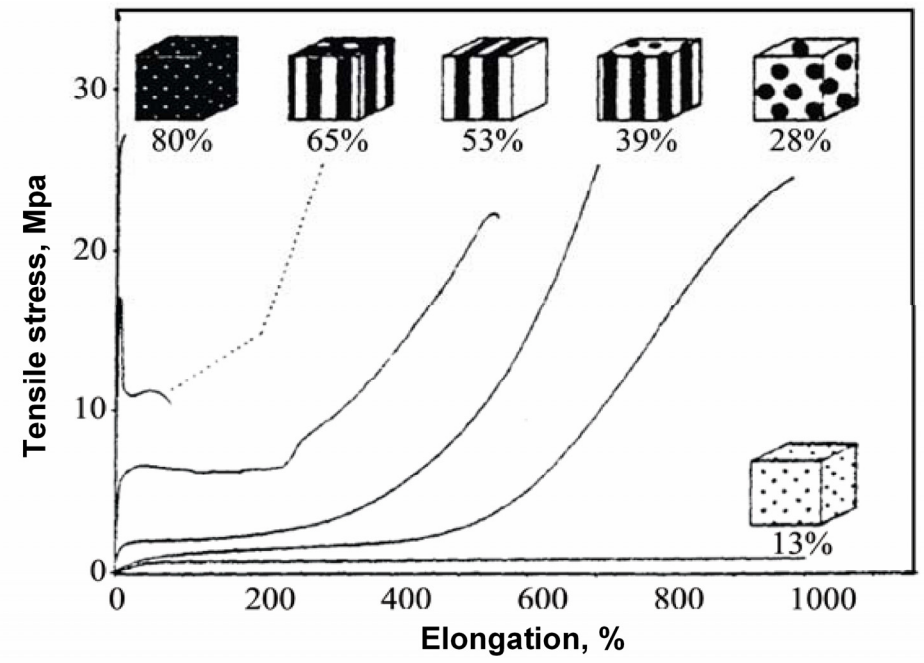

Figure 1.17 Stress-strain behaviour of SBS triblock copolymers as a function of styrene content; styrene domains are black

With increasing PS content, as the morphology reverses, yield stress increases and strain at break decreases due to localisation of deformation. Block copolymers with dispersed cylindrical PB domains break in a quite brittle manner.

The architectural parameters in triblock copolymers play a decisive role in determining mechanical behaviour. In some of our recent studies [33] it was observed that enhancement of mechanical properties of S-B-S triblock copolymers can be attained by replacing the butadiene phase with a styrene-butadiene middle block. Despite of enhancing the strength of elastomeric block copolymer (TPEs) by varying the wt.-% of PS, as shown in Figure 1.17, the mechanical properties of block copolymers with thermoplastic nature (TPs) above 65 wt.-% of PS content was exclusively studied [33]. As shown in Figure 1.18, LN4 is showing an elastomeric nature due to its inherent micro phase separated structure that is coming from high miscibility between PS and PB phases. However it is interesting to observe that at nearly same M_w and wt.-% of PS the morphology of LN-172 was changed to an ordered lamellar structure when compared to LN4. Further, a transition from elastomeric to tough plastic behaviour can be observed. With the increase of PS wt.-% to 70% and 75% at similar chain architecture the triblock copolymers are showing a thermoplastic behaviour where the stiffness in terms of yield strength and tensile strength prior to failure was observed to be strongly depending on the over all PS content. Thus the strength of TPs from block copolymers can be tailored by varying the over all PS content as well as the composition of the SB middle block in case of S-(S/B)-S type triblock copolymers.

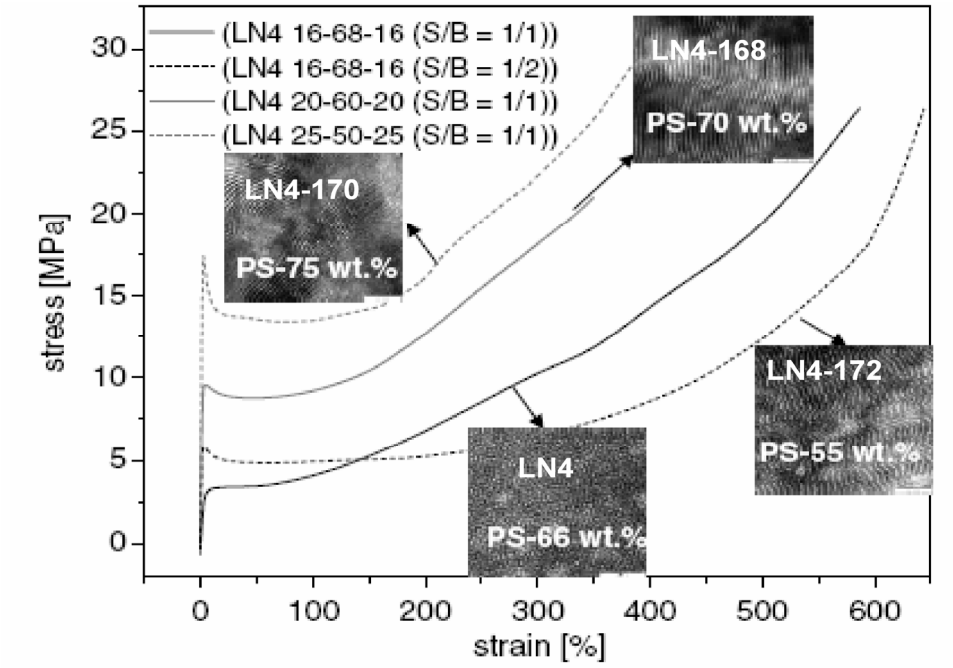

Figure 1.18 Mechanical properties of S-(S/B)-S triblock copolymers: Stress-strain behaviour with respect to chane in molecular chain architecture and PS wt.-%

Additionally, despite of high PS content of 55-75 wt.-% these S-(S/B)-S triblock copolymers reveal high strain at break values between 650% and 350% which is a striking contrast to the conventional SBS as shown in Figure 1.17. Such an unusually high enhancement in the mechanical properties is also in congruence with the morphology and phase miscibility interpretation [33]. However the architectural modification is dependent on many parameters and their optimisation demands a deep understanding of the phase behaviour of these block copolymers.

The elastomeric segment constrained between the two glassy PS outer blocks was varied and their influence on the deformation behaviour was investigated [27, 34]. The stress strain behaviour of three triblock copolymers with different elastomeric middle block is shown in Figure 1.19. The major reason for distinct variation in the deformation behaviour was attributed to the M_w difference between the chain entanglements [30]. The stiffness of the block copolymer is mainly coming from the high entanglement nature. In case of S-EB-S triblock copolymers with ethylene-propylene as an elastomeric middle block is having high M_w when compared to S-B-S (with butadiene middle block) and S-iB-S (with isobutylene middle block). The difference in the M_w of the middle blocks can be seen in the Figure 1.19. Accordingly, the stress-strain curve of S-iB-S copolymer lies well below that of S-B-S. Thus, other than f_{PS} content, the molecular parameters of the chain architecture is also showing a strong influence on the mechanical properties of block copolymers.

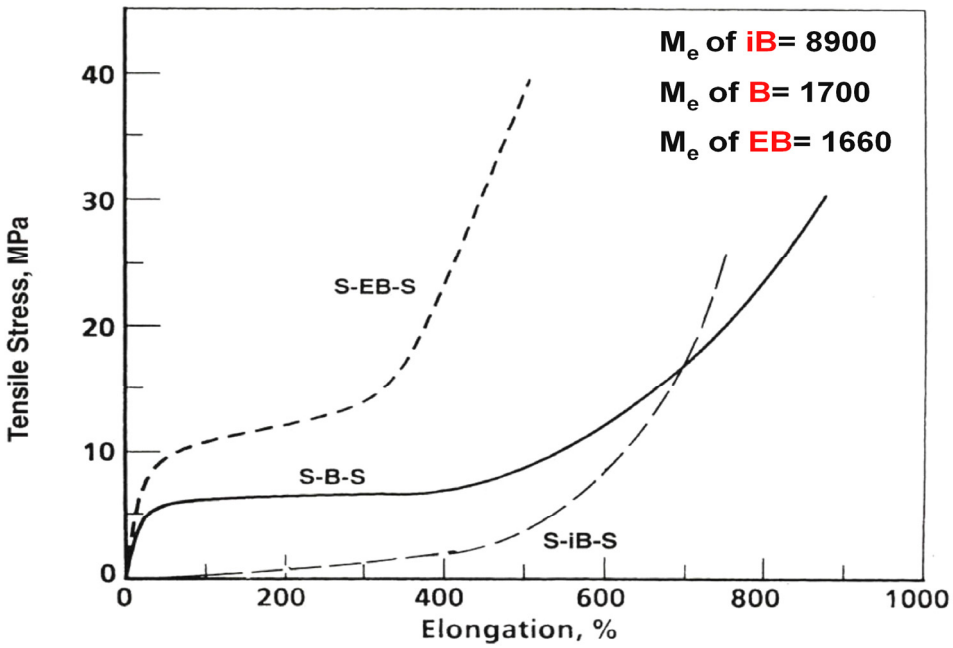

Figure 1.19 Stress-strain behaviour of styrene block copolymers having different elastomeric mid-blocks

1.13 Multigraft copolymers: Structure-property correlation

The interrelation between structure and properties in multigraft copolymers resemble similar to those of block copolymers. Other than block copolymers, multigraft copolymers are also considered as potential routes for developing high performance thermoplastic elastomers. In most of the graft copolymers a soft elastomeric backbone is grafted either regularly or randomly with a hard segment. Previous studies on multigraft copolymers based on polystyrene-g-polyisoprene (PS-g-PI) have showed an exceptional elasticity when compared to commercial Thermo plastic elastomers (TPE) [35,36]. Development of new synthesis techniques to synthesize graft copolymers provide a route for attaining well defined molecular architecture which allows the control of the molecular weight of the backbone and the graft arm, the arm polydispersity, the placement of number of branch points and the number of grafts at each branch point. For example graft copolymers with PI backbone which is regularly grafted with PS block with varying functionality and number of graft points is illustrated in Figure 1.20. From the earlier investigations it has been shown that the graft copolymers with complex architecture can be studied morphologically by considering as the fundamental building blocks which defines the average structure per junction point. The fundamental component of a large graft molecular architecture is referred as a constituting block copolymer [37,38].

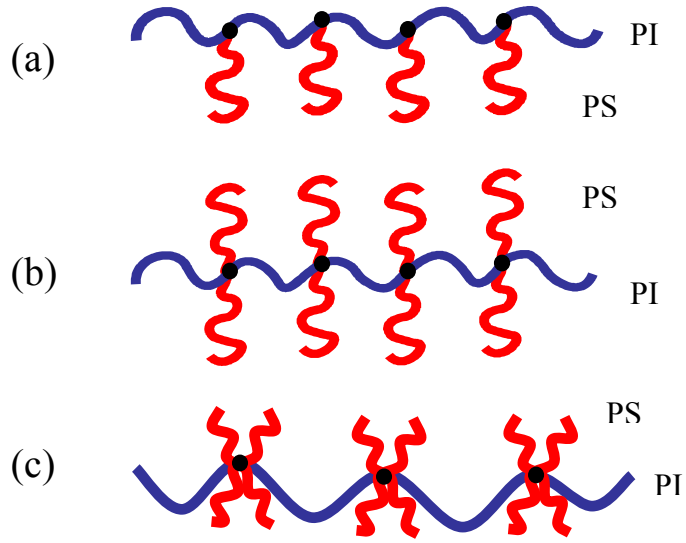

Figure 1.20 Illustration of MG copolymers based on PI backbone and PS branches with regularly spaced junction points. (a)trifunctional, (b)tetrafunctional (c) hexafunctional MG copolymer.

Further the morphological behavior of these multigraft copolymers with different molecular parameters can be predicted by the model of Milner [39] on the basis of the constituting block copolymer concept. Milner calculated the phase diagram of asymmetric miktoarm star block copolymer and demonstrated that stability window for a particular morphology is dramatically shifted as a function of copolymer chain architecture [39]. The influence of asymmetry was analysed by taking into consideration the molecular asymmetry parameter "ε" which constitutes both molecular architecture and conformational asymmetry. This theory predicts the morphology as a function of composition ϕ and molecular asymmetry parameter, $\varepsilon = (n_A/n_B)(I_A/I_B)^{1/2}$, where n_A and n_B are the number of arms of the block materials A and B linked at the junction point and $I_i = V_i/R_i$ (V_i and R_i are the volume and radius of gyration of one arm of polymer i. The theory has successfully predicted the phase behaviour for the investigated multigraft copolymers.

The mechanical properties of these superelastic materials were investigated by Weidisch et al. [36]. They described that multigraft copolymers show a surprisingly high strain at break far exceeding the commercial TPEs as shown in Figure 1.21. The Stress-strain behaviour of the two multigraft copolymers which are compared with the commercial TPEs like Styroflex and Kraton 1102 are denoted as MG-4-22-10 and MG-4-14-3.5 in Figure 1.21. A combination of high strain at break with a reasonable tensile strength of about 21 MPa revealed an exceptional property profile for tetrafunctional multigraft copolymers. Further, it

was observed that muligraft copolymers are showing exceptional elasticity with very low residual strain. From the hysteresis experiment as shown in Figure 1.22.

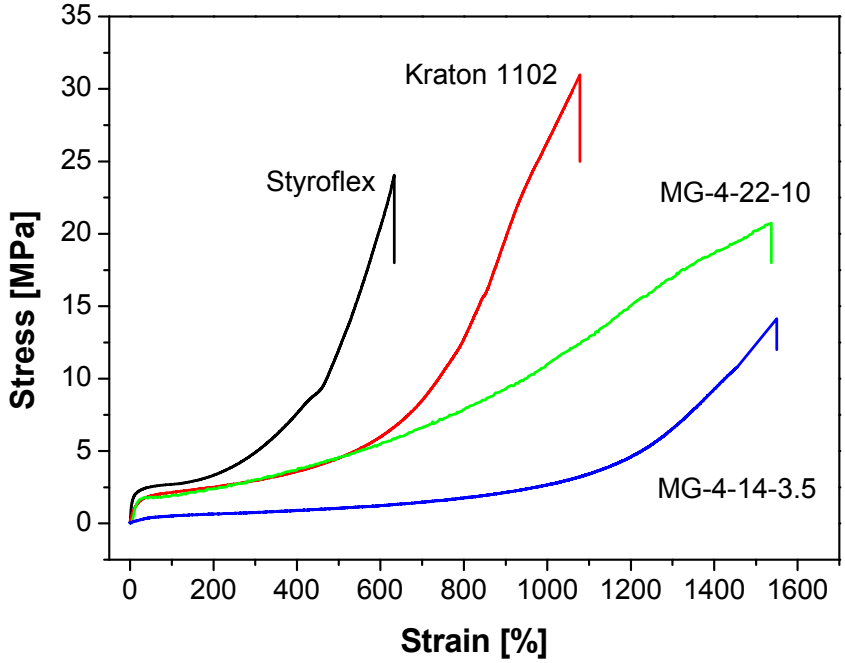

Figure 1.21 Stress-strain behaviour of tetrafunctional multigraft copolymers compared to commercial TPEs

Further it was observed that the high elastic nature was accompanied with very low hysteresis even after extending to extremely high strains. As shown in Figure 1.22, the tetra functional multigraft copolymers are demonstrating a residual strain of only 40% even after deforming to 1400% [40].

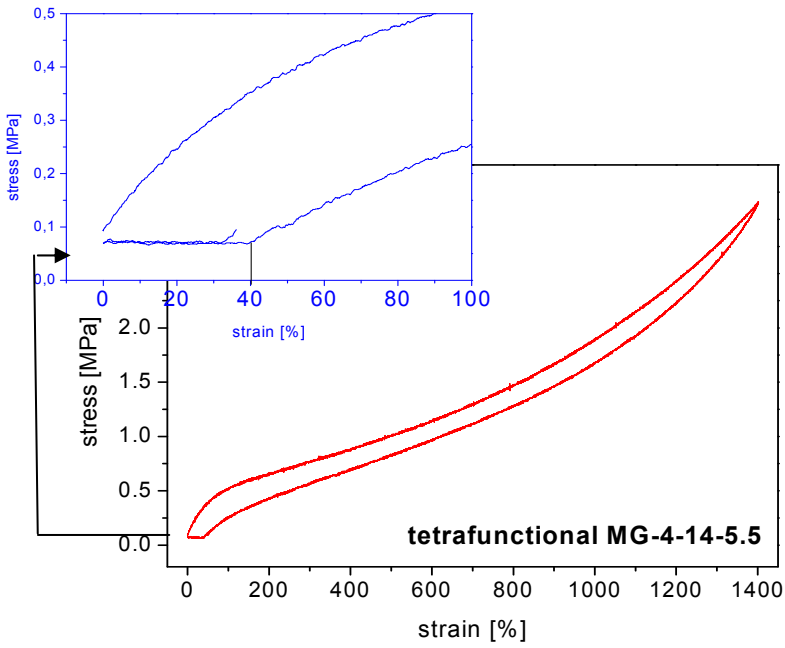

Figure 1.22 Hysteresis behaviour of tetrafunctional multigraft copolymer MG-4-14-5.5.

From the architectural point of view, it was observed that the Stress-strain behaviour and the hysteresis losses are strongly depending on the number of branch point, functionality and the wt.-% of PS content in the over all molecular chain architecture. The PS segments that are grafter regularly to the PI backbone can segregate to form PS microdomains in side soft PI matrix. Thus the reason behind the super elasticity in multigraft copolymers was mainly due to effective stress transfer between the rubbery matrix and polystyrene domains arising from strong coupling formed during phase separation process.

1.14 Electron beam cross-linking

Electron beam curing of dien based elastomers is an emerging technology which has the potential to provide significant advantages for rapid manufacturing of a variety of components for aerospace, automotive and consumer applications. A traditional thermal curing method demands varieties of toxic curing ingredients, long cure times, high energy consumption, where as EB curing is a fast non-thermal process which utilizes highly energetic electrons at controlled doses to polymerize and crosslink polymeric materials. EB is an electromagnetic radiation with high frequencies and very short wavelengths. The major advantages of electron beam cross-linking are listed below.

1. The high penetrating power and high energy of the electron beams allow efficient curing of thick polymeric articles and coatings
2. It gives large throughputs compared to other radiation processes.
3. It is practically free of waste products and hence environmentally safe.
4. It is very fast and versatile technique
5. It gives better improvement in properties compared to other thermo chemical means.

A comparison between EB curing to that of conventional Sulphur/ Peroxide curing system is summarized in Table 1.2. Radiation cross-linking of polymers by EB is a continuous process, which accomplishes a variety of reactions in a fraction of a second. It results in the formation of a three-dimensional network structure through union of macro radicals generated [41-43]. As shown in the Figure 1.23 the electrons emitted from the cathode are then accelerated in an electrostatic field applied between cathode and anode. The acceleration takes place from the cathode that is on negative high voltage potential to the grounded vessel as anode. The accelerated electrons are often focused by an optical system to the window plane of the accelerator [44].

The basic electrical parameters of an electron beam processing equipment are its acceleration voltage, the electron beam current and the electron beam power. The process

parameters are line speed, penetration range and dose rate. When the line speed and dose rate are combined, the total delivered dose can be calculated.

Table 1.2 Comparing EB curing with that of sulphur and peroxide curing

Electron Beam Curing System	Conventional Sulphur/ Peroxide Curing System
C-C linkage	C – S x – C or C – O x – C linkage (x = 1, 2, 3….)
Extremely Strong Bonds	Comparatively weaker bonds
Extremely short curing cycles	Comparably curing time is quite high
Perfect for thin products	Good for bigger products

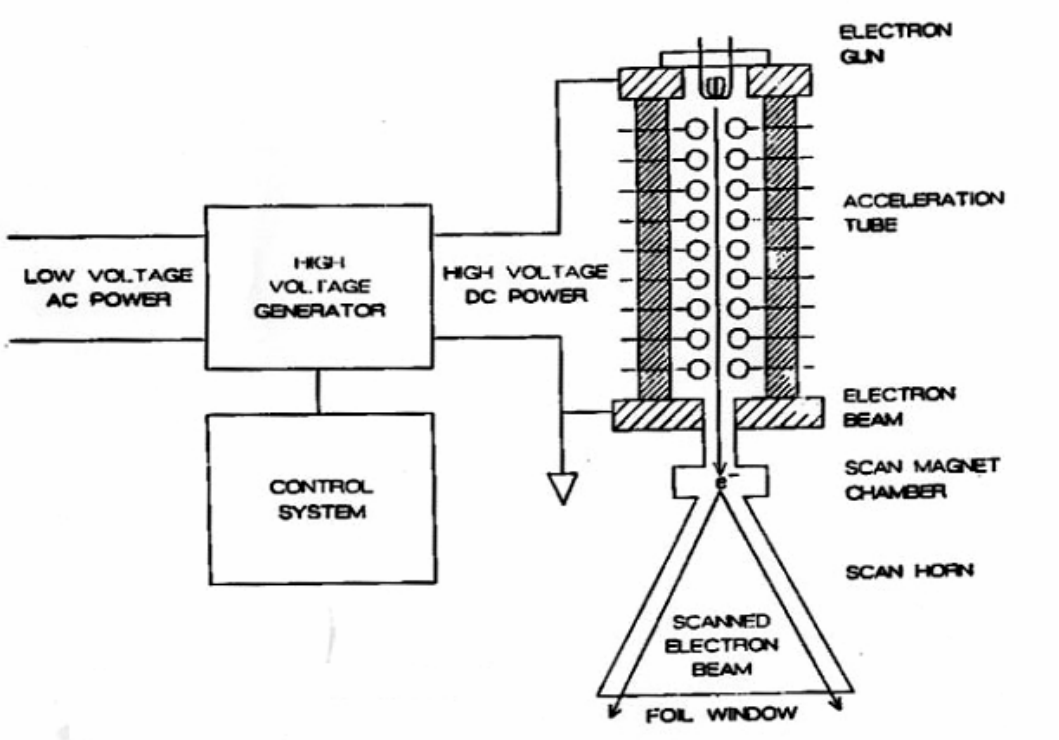

Figure 1.23 Schematic representation of Electron beam processor [44]

1.15 Electron beam cross-linking in block copolymers

Stiffness in combination with high extensibility is the major reason for cross-linking filled elastomers. However, cross-linking of elastomers requires high processing energy and it's an irreversible process. Since the block copolymers are essentially thermoplastic, on heating, the mechanical characteristics coming from the inherent phase separated structure will be easily lost. But at service temperature block copolymers are having excellent mechanical properties, such as controllable modulus, elongation, and tensile strength as discussed in the previous sections, the block copolymers are having high potential in controlling the property

profiles for the end use application. In order to restore this excellent property profile at high temperature, cross-linking by electron beam irradiation is commonly used, because it doesn't need an initiator. Recent studies have shown that cross-linking can be used to restore the ordered arrays of block copolymer mesophases [45,46]. In addition, the cross-linking reaction by electron beam proceeds at a lower temperature than that of thermal or UV exposure. In this context, E.L.Thomas et al. [47] has studied the micromechanical deformation in block copolymers by freezing the deformed microstructure by cross-linking with the aid of Electron beam cross-linking. Further, they illustrated the deformation process of a single grain from the nano phase orientation by comparing the results from SAXS and TEM during stretching. Thus, cross-linking with electron beams in block copolymer based TPEs is used to enhance the material behaviour by selective cross-linking the soft phase and restoring the microphase separated structure to improve their thermal properties for industrial applications.

1.16 Nanocomposites from block copolymers and Sol-gel technique

Nanocomposites are having extensive scientific interest as a special class of materials both in terms of fundamental interest and practical applications. Controlling the material at nanometer scale is one of the greatest challenges for current nanocomposite research. The hybrid nanocomposites with organic and inorganic components exhibit a superior property profile and the interactions between those heterogeneous components at molecular level can lead to a synergistic combination of properties. An increase in the surface area of such molecular level interactions can be attained through a super fine dispersion of inorganic nanoparticles in organic matrix. In elastomeric materials it is very prominent to fill the rubber matrix either with carbon or silica for enhancing the material properties. Other than carbon, silica is important and economical reinforcing filler since it provides a unique combination of transparency tear resistance, abrasion resistance and additional properties [48]. Moreover, in recent years significant attention has been given to the use of precipitated silica as filler in tyre industry in order to gain access of high performance materials [49-51]. In general, silica is filled in the rubbers through mechanical mixing. However, due to the presence of strong inter particle hydrogen bonding a fine dispersion of silica particles is strongly hindered [52]. In order to overcome such difficulties a silane coupling agent is used for attaining fine dispersion of silicon particles within the elastomer matrix.

Other than using coupling agents in mechanical mixing, sol–gel processing is a versatile technique, making it possible to produce a wide variety of materials and to provide existing materials with novel properties. The main advantage of this technique lies in formation of

metal oxide frameworks starting from molecular precursors at ambient temperature. In this method polymerization of alkoxysilanes, and the molecular precursor will take place in side the polymer matrix. The subsequent hydrolysis and condensation reaction of the inorganic precursor results in the formation of well dispersed inorganic silica particles in polymer network. The applicability of this method is observed to be quite simple and it was used as a direct method for modifying many commercially available polymers [53-57]. However, controlling the interaction between the silica particles with the polymer chains, which play a crucial role in governing the material behaviour, was observed to be critical. The reinforcement effect in the nanocomposite resulting from enhanced interaction between silica particle and polymer chains can be attained either by selective functionalising or by increasing the interacting surface of the nano particles through reducing the size at constant wt.% of the filler. In the vicinity of controlling the size of nano particle, it was reported by Yuan et al.[58] that the pH level of the reaction medium also plays an important role on the hydrolysis and the condensation process of the alkoxysilanes. Further it was also observed that the size of the particle can be reduced in polydimethylsiloxane (PDMS) matrix if the sol-gel reaction was carried out in acidic medium. In another work it was described that the sizes and size distributions of *in-situ* precipitated silica fillers can be controlled by the concentration of base catalyst (more specifically, diethylamine) in a single-step or multi-step procedure [58].

Concerning the elastomer matrix, the material behaviour in TPE's from block copolymers are observed to be governed by the persisting microphase separated structure. Such microstructures are mainly controlled by the molecular weight M_w, composition of block constituents and molecular architecture of block copolymer chain [59]. Inclusion of nano particles within this microstructure can further provide a tool for scaling the material properties at nanometer scales. A synergetic interactions between the nano particles and self-assembled nano structure in block copolymer matrix in thin films was reported earlier [60,61]. However, the mechanical properties are determined mainly by the molecular parameters as well as the structural details of the polymer and their response to the applied load. In this context, in the recent years, there has been a rapid growing trend for the incorporation of inorganic filler into the polymer matrix to enhance the material behaviour. The main objective of most of these applications is to achieve a large effect with the aid of small particles.

1.17 References

1. U. Eisele, Introduction to Polymer Physics, Springer Verlag, Heidelberg, 1990.
2. N. R. Lagge, Ed. Thermoplastic elastomers-A comprehensive review, New York, 1987.
3. I. Goodman, Ed. Developments in block copolymers-2 Applied science, New York, 1982.
4. M. W. Matsen, F. S. Bates, Macromolecules, 1996, 29, 1091.
5. L. Leibler, Macromolecules, 1980, 13, 1602.
6. G. H. Fredrickson, E. Helfand, J. Chem. Phys 1987, 87, 697.
7. F. S. Bates, J. H. Rosedale, G. H. Fredrickson, J. Chem. Phys 1990, 92, 6255
8. N. Sakamoto, T. Hashimoto, Macromolecules, 1995, 28, 6825
9. I.W. Hamley, The Physics of Block copolymers, Oxford Science Publications, Oxford, 1998.
10. C.M. Papadakis, K. Almdal, K. Mortensen, D. Posselt, J. Phys., II France., 1997, 7, 1829.
11. M. W. Matsen, M. Schick, Macromolecules, 1994, 27, 187.
12. A.M. Mayes, M. Oliver de la Cruz, J. Chem. Phys.,1989, 91, 7228.
13. M. W. Matsen, J. Chem. Phys**.,** 1995, 1022, 3884.
14. T. Hashimoto, H. Tanaka, H. Hasegawa, Macromolecules, 1990, 23, 4378.
15. H. Tanaka, T. Hashimoto, Macromolecules, 1991, 24, 5713.
16. C. D. Han, D. M. Baek, J. Kim, K. Kimishima, T. Hashimoto, Macromolecules, 1992, 25, 3052.
17. R. J. Spontak, N. P. Patel, In Developments in Block Copolymer Science and Technology. edited by I. W. Hamley, Wiley, New York, 2004
18. M. W. Matsen, F. S. Bates, Macromolecules, 1995, 2, 7298.
19. T. Hashimoto, S. Koizumi, H. Hasegawa, Macromolecules, 1994, 27, 1562
20. D. Yamaguchi, S. Shiratke, T. Hashimoto, Macromolecules, 2000, 33, 8258.
21. F. Court, T. Hashimoto, Macromolecules, 2001, 34, 2536
22. I. D. Sakurai, S. Okamoto, S. J. Nomura, Macromol. Sci.-Phys., 2002, 41, 387.
23. C. W. Macosko, Rheology, Principles, Measurements and Applications, VCH Publishers, New York, 1994.
24. M. Langela, Struktur und rheologische Eigenschaften von PS-PI und PS-PB Blockcopolymeren, Johannes-Gutenberg-Universität Mainz, PhD thesis, 2001.
25. Y. Zhang, U. Wiesner, Macromol. Chem. Phys., 199, 1771, 1998.

26. J.H. Rosedale, F.S. Bates, Macromolecules, 1990, 23, 2329
27. G. Holden, E. T. Bishop, N. R. Ledge, J. Polym. Sci. C: Polym. Lett. 1969, 26, 37.
28. T. A. Huy, L. H. Hai, R. Adhikari, R. Weidisch, G. H. Michler, K. Knoll, Polymer, 2003, 44, 1237.
29. R. Adhikari, R. Lach, G. H. Michler, R. Weidisch, K. Knoll, Macromol. Mater. Eng, 2003, 288, 432.
30. G. Holden, Understanding Thermoplastic Elastomers; p. 15-35, Carl Hanser Verlag, Munich, 2000.
31. G. Holden, Applications of Thermoplastic Elastomers; In G. Holden, N.R. Legge, R.P. Quirk and H.E. Schroeder (Eds.), Thermoplastic Elastomers, 2nd Edition, Chapter 16, p. 574-601, Hanser Publishers, Munich, 1998.
32. H. J. Elias, Makromoleküle - Band 1: Grundlagen, 5. Ausg., Hüthig&Wepf Verlag Basel, Heidelberg, New York, 1990, 962.
33. U. Staudinger, B. K. Satapathy, M. Thunga, R. Weidisch, A. Janke and K. Knoll, Eur Polym J 2007, 43 , 2750.
34. H.A. Vaughn, J.Poly. Sci., 1969, B7, 569
35. J. W. Mays, D. Uhrig, S. P. Gido, Y. Q. Zhu, R. Weidisch, H. Iatrou, N. Hadjichristidis, K. Hong, F. L. Beyer, R. Lach, M. Buschnalowski, Macromol. Symp., 2004, 215, 111.
36. R. Weidisch, S. P. Gido, D. Uhrig, H. Iatrou, J. W. Mays, N. Hadjichristidis, Macromolecules, 2001, 34, 6333.
37. M. Xenidou, F. L. Beyer, M. Hadjichristidis, S. P. Gido, N. Beck Tan, Macromolecules, 1998, 31, 7659.
38. F. Beyer, S. P. Gido, C. Buschl, H. Iatrou, D.Uhrig, J. W. Mays, M. Chang, B. A. Garetz, N. Balsara, N. Beck Tan, N. Hadjichristidis, Macromolecules, 2000, 33, 2039.
39. S.T. Milner, Macromolecules, 1994, 27, 2333.
40. Y. Zhu, E. Burgaz, S. P. Gido, U. Staudinger, R. Weidisch, D. Uhrig, J. W. Mays, Macromolecules, 39, 2006, 4428.
41. M. A. Hillmyer, P. M. Lipic, D. A. Hajduk, K. Almdal, F.S. Bates, J. Am. Chem. Soc. 1997, 119, 2749.
42. S. Sakurai, K. Iwane, S. Nomura, Macromolecules, 1993, 26, 5479.
43. R. Clough, “Radiation Resistant Polymers,” Encyclopaedia of Polymer Science and Technology, Wiley, New York, 1989, 15, 666.

44. J. G. Drobny, presented in 167th spring Technical meeting of Rubber division, ACS, Paper-29, 2005.
45. Charlesby, "Atomic Radiation and Polymers," Pergamon, London, 1960, 162.
46. G.G.A. Bohm, J.O.Tveekrem, Rubber Chem. Technol. 1982, 55, 575.
47. C.C.Honeker, E. L. Thomas, Macromolecules 2000, 33, 940.
48. M.P. Wagner, Rubber technology, Morton M, Van Nostrand Reinhold, New York, 1987, 86.
49. J.M.W. Noordermeer, Macromol. Symp. 1998, 127, 131.
50. J.T. Byers, Rub. Chem. Technol. 2002, 75, 527.
51. T.A. Okel, W.H. Waddell, Rub. Chem. Technol., 1994, 67, 217.
52. S. Kohjiya, Y. Ikeda, Rubber Chem. Technol. 2000, 73, 534.
53. S. Wang, P., J. Xu, E. Mark, Rubber Chem Technol 1991, 64, 746.
54. Y. Ikeda, Y. J. Kameda, Sol-Gel. Sci. Technol. 2004, 31, 137.
55. Y. Ikeda, S. Kohjiya, Polymer, 1997, 38, 4417.
56. K. Murakami, S. Osanai, M. Shigekuni, S. Ito, H. Tanahashi, S. Kohjiya, Y. Ikeda, Rubber Chem. Technol. 1999, 72, 119.
57. D. Sun, R. Zhang, Z. Liu, Y. Huang, Y. Wang, J. He, B. Han, G. Yang, Macromolecules, 2005, 38, 5617.
58. Q.W. Yuan, J.E. Mark, Macromol. Chem. Phys., 1999, 200, 206.
59. I. W. Hamley, in The Physics of Block Copolymers, Oxford, Oxford University Press, 1996.
60. Y. Lin, A. Böker, J. He, K. Sill, H. Xiang, C. Abetz, X. Li, J. Wang, T. Emrick, S. Long, Q. Wang, A. C. Balazs, T. Russell, Nature 2005, 434, 55.
61. S. C. Park, B. J. Kim, C. J. Hawker, E. J. Kramer, J. Bang, J. S. Ha, Macromolecules, 2007, 40, 8119.

2. Experimental

2.1 Sample Preparation

2.1.1 Compounding and compression moulding

A series of blends covering the whole composition range of the two triblock copolymers (LN3/LN4) varying in a step of 20 wt% were extruded using a Micron 27 twin screw compounder (Leistritz). The blends are extruded with a relative mean torque of 70 % , at a screw speed of 110 rpm and a pressure of 40 bar is maintained at the extruder die, And the output is set to 10 kg/h. The temperature ranges from 160 to 170 °C is maintained in the compounding cylinder. The extradite from the extruder is palletized and then dried at 80 °C for 24 h. Neat polymers are also processed under the same conditions to remove the effect of processing on the mechanical properties of blends and pure components.

The block copolymers were prepared as plates with 1mm thickness by rolling and subsequent compression moulding at 200 °C in BASF Co. This compression moulded plates are used for observing morphology, rheological measurements, dynamic mechanical analysis (DMA) and for tensile testing.

2.1.2 Solution casting

Solution cast films of these multigraft copolymers are prepared from a non-selective solvent (toluene). The solvent was allowed to evaporate slowly over 7-14 days at room temperature. The films were then dried to constant weight in a vacuum oven at 120 °C for three days. The resulting films are about 0.2 to 0.3 mm thick. These cast films are used for dynamic mechanical analysis, tensile testing and cross-linking investigations

2.2 Physical characterization

2.2.1 Morphology

2.2.1.1 TEM

Morphology studies of block copolymers and multigraft copolymers were performed by transmission electron microscopy (TEM) using a JEOL 2000 200 kV microscope. Ultrathin sections (~60 nm) were cut at –100 °C with diamond knives from Diatom in a Leica ultramicrotome, and the fresh cut samples were stained by keeping them in osmium tetroxide (O_sO_4) chamber for 24 hours. The poly-butadiene (PB)-rich phase was selectively stained with osmium tetroxide (O_sO_4) during the staining period in order to obtain a phase contrast.

2.2.1.2 SAXS

Small angle X-ray scattering (SAXS) are capable to give information on the structural features of block copolymer microstructure as well as their spatial correlation. Hence, they are very suitable for a comprehensive analysis of block copolymers. A schematic description of scattering principle is shown in Figure 2.1. The incident X-rays are formed into a fine beam, often by slits, and strike the samples. A small fraction of this beam is scattered at an

angle θ with the direction of the incoming beam. A 2D-detector is used to record the scattering intensity which dependence on the scattering angle. Information about the structure of the sample can often be obtained from the analysis of the scattering intensity at a sequence of scattering angles.

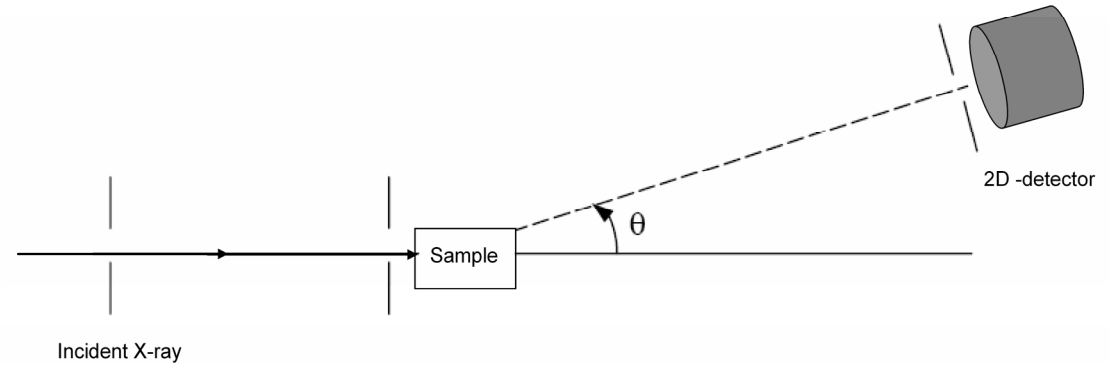

Figure 2.1 Experimental scheme of small angle X-ray scattering (SAXS).

From the Figure 2.1 it is quit obvious to obtain the following relation.

$$|\vec{q}| = \frac{4\pi}{\lambda}\sin\left(\frac{\theta}{2}\right)$$

The small angle X-ray scattering (SAXS) measurements were performed using an indigenous three pinhole collimation system with a Rigaku 2D rotating anode generator (Cu Kα radiation, k = 0.1542 nm), an Osmic multilayer mirror and a MARCCD detector with a sample-to-detector distance of 1581.7 mm. In the SAXS experiment the intensity I(q) of the scattering X-rays can be expressed as [1].

$$I(q) = I_e.|A(q)|^2$$

Where I_e is the scattering intensity from one electron and A(q) is the amplitude. A detailed description about the SAXS principle is given in reference [1]. The temperature dependent SAXS measurements were made within the temperature range of 373 to 473 K with the stability better than ±0.2 K. Between successive temperatures a 20 minute waiting time was preset for equilibration. The data was corrected for absorption and background scattering obtained in transmission geometry at room temperature.

2.2.1.3 AFM

The AFM specimens were prepared from the bulk sample at 1 mm thickness. The fresh cut samples were made with Leica RM 2155 microtome (Leica, Nussloch, Germany) equipped with a diamond knife at a cryo-temperature below the glass transition temperature of PB phase in the block copolymer. The AFM measurements were performed in tapping mode by

a Dimension 3100 NanoScope IIIa (Veeco, USA). We used Pointprobe silicon-SPM-sensors (Nanosensors, Germany) with a spring constant of approx. 3 Nm^{-1} and resonance frequency of ~75 kHz with the tip radius lower than 10 nm. The scan conditions are chosen according to Magonov et al. [2] (free amplitude > 100 nm, set-point amplitude ratio 0.5) in order to get stiffness contrast in the phase image, which means bright features in the phase image are stiffer than dark areas.

2.2.2 Rheological characterization

An Advanced Rheometric Expansion system (ARES) is used for the oscillatory shear experiments, isochronal temperature scans and for the dynamic mechanical measurements on the samples. The experimental temperature is controlled by vaporized liquid nitrogen (N_2) convection. The precision of temperature control is within ±5 °C. Samples are punched out at a dimension of 25 mm from a 1 mm thickness compression moulded plate. These samples are used for the tests. The measurable modulus limits for Φ25 and 1mm thickness plates are 1.02E+01 to 2.22E+06 Pa. This measurable modulus limits can be selected online by changing the transducer based the limits of modulus. More instrumental specifications are available in the Rheometric's manual of ARES.

For constructing master curves, the measurements were performed at temperatures ranging from 120 to 220°C as a function of frequency in the dynamic mode on a parallel plate geometry (diameter: 25 mm) with set-gap of about 1 mm. The frequency was varied between 10^{-1} and 10^{2} rad/s. The strain amplitude was kept to be at 2 % in the whole frequency range to ensure linearity. The data measured at different temperatures were superimposed to construct reduced frequency plots as master curves following time-temperature superposition (TTS) principle based on Williams-Landel-Ferry (WLF) equation [3] at a reference temperature (T_0) by introducing a shift factor (a_T), where, $\log a_T = -C_1 (T-T_0) /(C_2+(T-T_0))$. The constants C_1 and C_2 are slightly material specific.

2.2.3 Dynamic mechanical analysis

Dynamic mechanical analysis (DMA) has been done using an ARES-LS2 rheometer. Measurements have been carried out on test specimens with dimensions of $30\times8\times1$ mm^3 in torsion mode using torsion rectangular geometry tools to characterize the glass transition temperature of the triblock copolymers. The temperature sweep test was carried out between -80 and 120 °C at a frequency of 1.0 rad/s and 0.01 % strain amplitude. Elastic modulus (G') and viscous modulus (G") as a function of temperature have been measured.

2.2.4 Tensile testing

Tensile tests were performed with a ZWICK 1456 universal testing machine according to ISO 527 (specimen type 5A) at a crosshead speed of 15 mm/min. To ensure good measurement statistics, 5 to 6 dog bone shape specimens from each material were prepared by stamping from the annealed films. Due to limited availability of trifunctional multigraft copolymers, the tensilse testes are conducted on small size dog bone shape specimens with a over all sample length of 20 mm and a crosshead speed of 50 mm/min was employed for the test. The crosshead displacement and strain from optical devices are compared in order to evaluate the strain of these small samples.

2.2.5 Thermogravimetric analysis

The TGA was conducted with Q500, TA Instruments, under nitrogen atmospheres from 40 °C to 750 °C. A heating rate of 10 K/min was employed.

2.3 Crosslinking and chemical test methods

2.3.1 Electron beam irradiation

The compression moulded plates with dimension of 80*80*1 mm samples were irradiated in the air at room temperature with absorbed doses of 0, 50, 100, 150, 300, and 500 kGy by an electron beam accelerator ELV-2 from Budker Institute of Nuclear Physics, Novosibirsk, Russia, installed at the Leibniz Institute of Polymer Research Dresden. The beam parameters are maintained at an absorbed dose of 2 kGy per pass with an average dose rate of about 10 kGy/h. Further information about the electron accelerator (ELV-2) facility can be found in [4].

2.3.2 Sol-gel extraction

The sol-gel extraction is carried out in an extractor-container with uninterrupted reflux (Soxhlet apparatus). The solvent used is toluene and the temperature is maintained above the boiling point of solvent. After every nine minutes, the solvent overflows and the whole extraction takes 15 hours to complete. The gel is dried in a vacuum drier at 50 ^{0}C for 24 hours.

2.3.3 Preparation of in-situ silica by sol-gel method

During the sol-gel process, the inorganic glass particles are generated in side the organic polymer matrix through two steps. As shown in Figure 2.2, in the first step hydrolysis of TESO in presence of aqueous medium results in formation of Si particles in the form of gels with SiO_2 network and these gels are condensed during heating in the second step. In order to prepare such organic-inorganic hybrid composites from LN4 and Si particles, LN4 plates

which are cross-linked at 50, 150 and 500 kGy are swollen in TEOS at room temperature for 48 hours, followed by soaking in 10 wt.-% aqueous solution of n-butylamine for 24 hours. The excess TEOS on the surface of the gels was wiped out before soaking them in aqueous solution. The samples are then dried in vacuum oven for 48 hours continued by drying to a constant weight at 80 °C for several days [5].

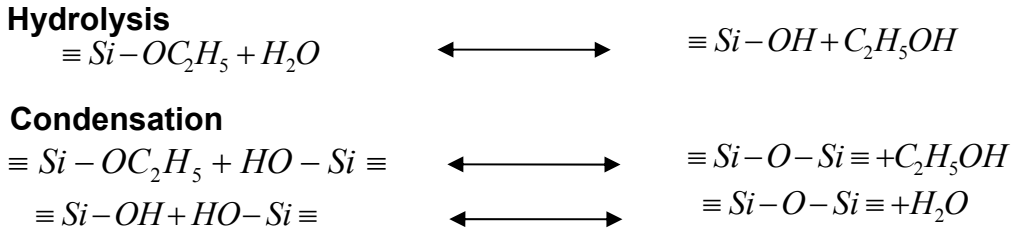

Figure 2.2 Sol-gel reaction in TEOS to form silica

2.4 References

1. Y.Zhang, Dissertation, Johannes Gutenberg-University, Mainz 1996
2. S. N. Magonov, V. Elings, M.-H. Whangbo, Surface Science, 1997, 375, 385.
3. C.W. Macosko, Rheology: Principles, Measurements and Applications, VCH Publishers, New York,1994.
4. H. Dorschner, U. Lappan, K. Lunkwitz, Nuclear Instruments and Methods In Physics Research, Section B, 1998, 139, 495.
5. Y. Ikeda, A. Tanakaa, S. Kohjiya, J. Mater. Chem., 1997, 7, 1497.

3. Influence of chain architecture on phase behaviour of styrene-(styrene/butadiene)-styrene triblock copolymers and their binary blends

The results of this chapter have been communicated to

Journal of Polymer Science Part B: Polymer Physics, 2008, 46, 329 – 343
&
European Polymer Journal, 2009, 44, 3790-3796

3.1 Investigated Materials

The synthesis of the S-(S/B)-S copolymers provided by BASF AG Co. is described by Knoll and Niessner [1]. Both block copolymers, LN3 and LN4, that were blended are linear triblock copolymers with PS in the outer blocks and a SB random copolymer in the middle block. While LN4 has a symmetric architecture with short outer PS blocks, LN3 is asymmetric with respect to the outer PS blocks. The molecular characterization is summarized in Table 3.1.

Table 3.1 Molecular characterization of the blend components LN3 and LN4

Material	M_n (kg/mol)	M_w/M_n	Total PS content (wt.-%)	PS_1/(S/B)/PS (wt.-%)	S/B ratio in the random copolymer block	Morphology
LN3	111	1.21	75	12/49/39	1:1	Lamellae
LN4	119	1.30	66	16/68/16	1:1	Wormlike

Blends of these two block copolymers were prepared in twin screw compounder. Plates of 1 mm thickness were prepared by compression moulding at 200°C for 5 minutes followed by annealing the sample to room temperature prior to the release of the pressed plates. In order to attain equilibrium morphologies, the bulk samples were annealed for two days in vacuum at a temperature slightly above the T_g of PS phase.

3.2 Morphology and phase behaviour

The morphologies of two triblock copolymers (LN3 and LN4) and their blends were investigated by TEM and are shown in Figure 3.1(a-f). The bright and dark phases correspond to the PS and PB phases respectively which are caused by selective staining of PB phase with OsO_4. It can be observed from Table 3.1 that the molecular architecture of LN4 is symmetric with two small outer PS-blocks showing a wormlike structure where styrene domains are dispersed in butadiene matrix. On the other hand LN3, with an asymmetric architecture with one small and one long outer PS-block, reveals a lamellar structure. In case of their blends, a systematic change in the morphologies can be observed with the increase of LN3 content in LN4, which could be attributed to the influence of the molecular architecture. It is observed from the TEM micrographs that the binary blends are fully miscible at molecular level over the whole range of composition. The transparency of 1 mm thick plates is the primary observation which reveals that blends are micro- and not macrophase separated. The significant factors which control phase separation process are the

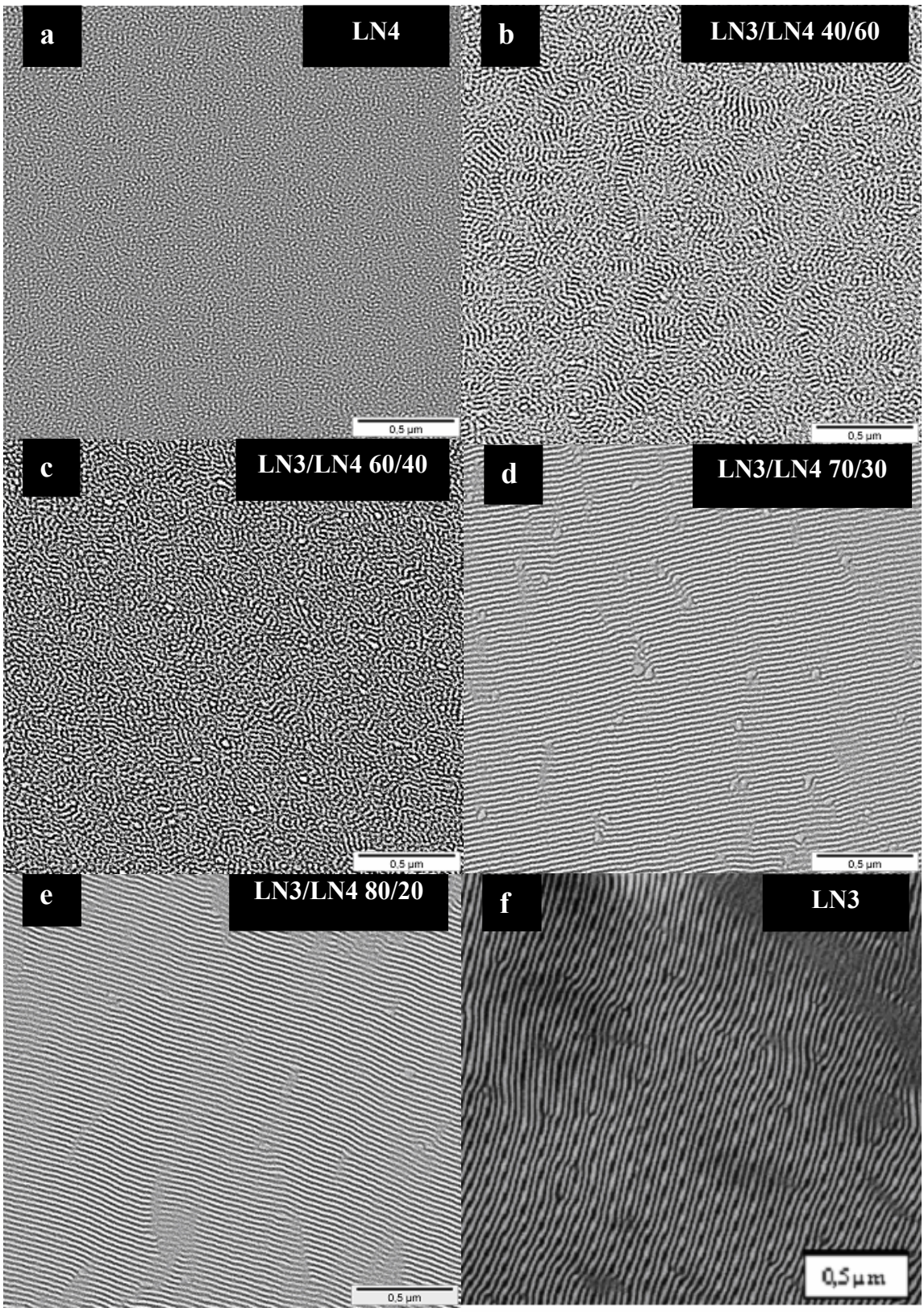

Figure 3.1 Morphology from TEM of a) LN4 – weakly phase separated wormlike, b) LN3/LN4 40/60 – locally ordered short cylinders, c) LN3/LN4 60/40 – locally ordered short cylinders d) LN3/LN4 70/30 – lamellar, e) LN3/LN4 80/20 – lamellar, f) LN3 – lamellar.

ratio of the molecular weights i.e. $\delta = N_1/N_2$ should theoretically be less than 5 (N_1 and N_2 are the degrees of polymerization of the two base block copolymers) and the block fractions in both the blend components should be comparable i.e. $f_1\text{-}f_2 \leq 0.1$ (f_1, f_2 are the wt. -% of PS or PB in the copolymer) [2,3]. From Table 3.1 it could be observed that the material parameters of LN3 and LN4 are in accordance with both conditions for microphase separation instead of macrophase separation. The morphologies of LN3, LN4 and their blends on solution-cast films have already been discussed [4]. They show equilibrium morphologies varying from wormlike (0-20wt.-% LN3) to cylindrical (30-60 wt.-% LN3) to bicontinuous (70-80 wt.-% LN3) and to lamellar (90-100 wt.-% LN3). However, From Figure 3.1(a-f) it could be observed that the compression moulded plates show a change in morphology from wormlike (0-20 wt.% LN3) to cylindrical structure (30-60 wt.% LN3) to lamellar (70-100 wt.% LN3). The structural variations of these blends (compression moulded plates) were also reconfirmed by small-angle X-ray scattering (SAXS) studies and were discussed in our recent article [5]. The wormlike morphology in case of LN4 is contradicting the equilibrium morphologies, where a cylindrical morphology is expected to form, so the observed morphology can be either an equilibrium morphology or a meta-stable morphology. Thus, by comparing the observed morphology of LN4 with the early study on solution cast films reveals that, if the morphology of LN4 is not truly in equilibrium state then its meta-stable form is highly persistent.

In order to explain the morphological variation with increase in LN3 content, it is essential to study the chain organisation during the formation of such microphase separated structure. All the blend compositions have been observed to exhibit single microdomain morphology depending on blend compositions (Fig 3.1b-e). In such a phase separation process the possible chain conformations of LN3, LN4 and their blends which can organize in a common microdomain space is schematically shown in Figure 3.2(a-c). In case of LN3, due to the asymmetric architecture the shorter-PS end-block can either get pinned down in the PS-rich phase along with the longer-PS end-block or it can get miscible in the PB-rich phase as shown in Figure 3.2a. In the former case, when both the PS end-blocks get pinned down into the PS-rich phase, the two ends of the soft middle block will be constrained to the interface lowering the chain-entropy and thereby causing an unfavourable chain conformation leading to packing frustration. Therefore, the feasibility of such a conformation can thermodynamically be unfavourable. In order to relax from such constraints the SB-random middle block will pull the smaller PS end-block inside the PB-rich phase. Once the chain pulling of the short PS end-block occurs, the short PS-chains are

forced to mix with the SB rich phase resulting in an increase in the PS content in the PB-rich phase. This chain pulling phenomenon which arises from the influence of architecture can be ascribed to be a complete entropic action which in turn is due to the difference in M_w between the PS end blocks in the chain architecture of LN3.

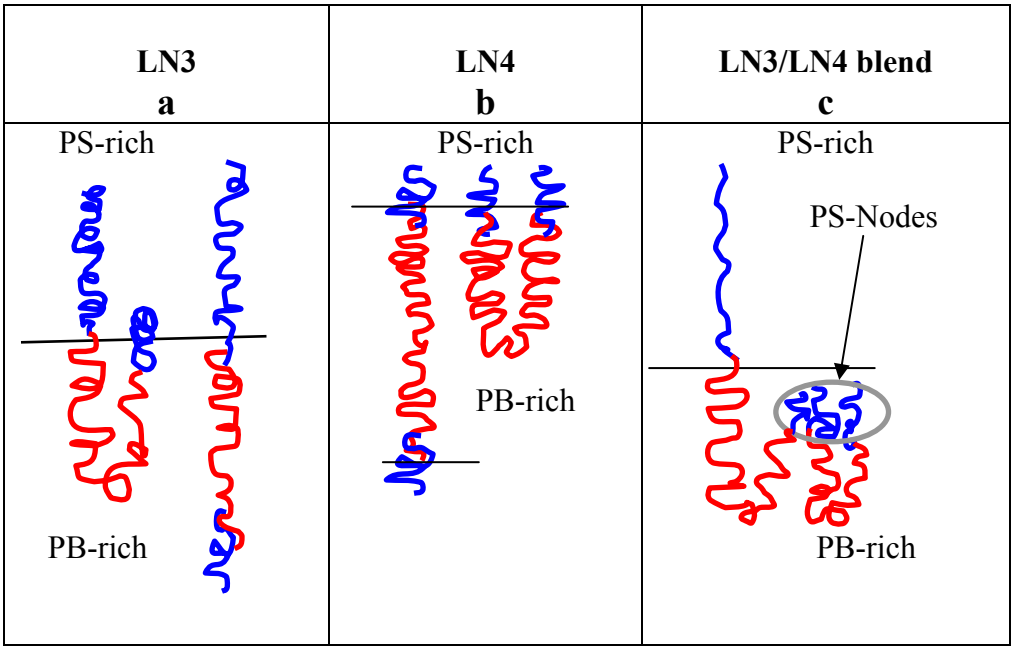

Figure 3.2 Schematic illustration depicting the chain conformation of a) LN3, b) LN4, c) LN3/LN4 50/50 blend

However, after complete miscibility of short-PS end-block in PB-rich phase the longer-PS end-block contributes to the elastic free energy of stretching resulting in formation of lamellar structure with reduced interfacial curvature. The weight fraction of PS in the form of long-PS block promoting the formation of ordered lamellar structure in LN3 is in accordance with the literature reported by Matsen which was shown in Figure 3 of reference [6]. On the other hand, in case of LN4 with symmetric architecture the PB chains can either form loop or bridge type conformations as shown in Figure 3.2b. In both the situations it is entropically less favourable for the SB middle block to confine the two PS end-blocks into PS-rich phase and hence in order to compensate such a packing frustration, partial miscibility of PS end-block with the PB middle-block near the interface can be expected. However, such miscibility further depends on the chain length of PS end-blocks. The short PS outer-blocks in LN4 will exhibit higher translational entropy due to their size which is considerably small when compared to the random SB middle block. Hence, high translational entropy for the PS end blocks could enhance the miscibility between PS end-blocks with SB random middle block resulting in weak phase segregation.

The change in miscibility between PS end-blocks and random SB middle-block due to architectural differences between LN3 and LN4 was already studied experimentally by dynamic mechanical analysis (DMA) in our earlier reported work [5]. An enhanced miscibility of PS end-blocks with PB middle block will significantly reduce the effective weight fraction of PS for phase separation. The weight fraction of this effective PS content can be calculated by comparing the experimental and theoretical T_g values as obtained from DMA and Fox equation respectively. Based on these studies Figure 3.3 was constructed which shows the change in the effective weight fraction of PS from LN3 and LN4 in the blend system with respect to LN3 content.

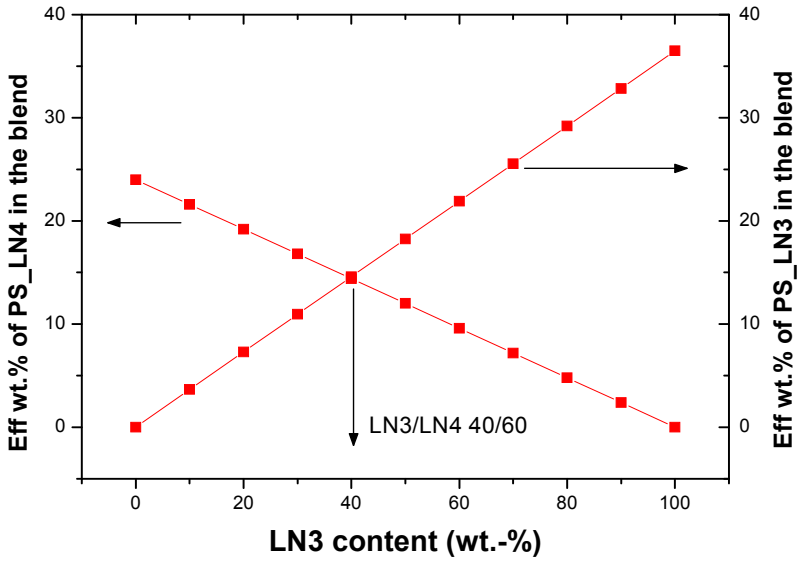

Figure 3.3 Effective weight fraction of PS content in LN3/LN4 blends with respect to LN3 content

It could be observed from Figure 3.3 that a crossover between the effective PS contents in LN3 and LN4 occurred at LN3/LN4 (40:60) composition. This crossover point indicates the significant influence of the chain conformations of LN3 and LN4 on the ultimate morphologies of the blends, i.e. below 40 wt.% of LN3 the blend morphology is controlled by LN4 chain conformations and above 40 wt.% of LN3 the chain conformation of LN3 will predominantly control the phase separation. It is also quite interesting to note that a change in morphology from cylindrical structure to locally ordered lamellar structures starts exactly above this critical blend composition, i.e. at 40 wt.% of PS. From the TEM (in Figure 3.1) a single microdomain structure has been observed in which LN3 and LN4 are uniformly mixed at all compositions indicating that the chains of LN3 and LN4 are organized in a common microdomain space. A schematic representation of chain organisation during the phase separation process of LN3/ LN4 blend compositions is shown

in Figure 3.2c. When equal number of LN3 and LN4 chains are mixed at molecular level i.e. at LN3/LN4 50:50, a bi-dispersed PS-rich phase can be expected during the phase separation process, i.e. in the PS-rich phase, for every long PS end-block from LN3 there exists two short outer blocks from LN4. This will influence the phase separation process in two ways. Firstly, the bi-dispersed nature of the chains in the PS-rich phase in the vicinity of the interface will reduce the stretching energy of LN3 long chains [7] and secondly, the short PS end-blocks in LN4 behave as a neutrally good solvent and thereby resulting in the apparent reduction in the segregation strength that prevents the formation of an ordered morphology by the fraction of LN3 component [8]. Thus, it reveals that the morphology is largely governed by the balance between the conformations of long-PS chains of LN3 in between two short-PS end-blocks of LN4. However, this balance in the blends can also be influenced by the shorter PS outer block of LN3, i.e. the shorter PS-chain in the outer block which is completely miscible in the random SB middle block. When LN3 is blended with LN4, as the M_w of the PS-chains of LN4 is similar to that of short PS-chains in LN3, the intermixing is easily promoted forming node-like PS-microdomains in the SB-matrix, without causing tremendous frustration of the rubbery middle SB-block chains. Such a mixing situation is schematically represented in Figure 3.2c. As a matter of fact, from the TEM images of the blends with 40-70 wt. % of LN3 content (Fig 3.1(b-d)), PS-nodes are identified as bright patches and these nodes are observed to be larger than the surrounding regular PS-microdomains. These unusual morphologies with PS-nodes in the cylindrical morphology have been observed for the first time in this work and thus offer new insights regarding the significant influence of short PS outer blocks in triblock architecture in controlling the ultimate morphologies.

3.3 ODT from SAXS

The order-to-disorder transition temperature (ODT) of LN4 has been determined using temperature dependent SAXS (T-SAXS). The plot of the measured scattering intensity *I(q)* vs. scattering vector *q* at different temperatures during heating process for LN4 is shown in Figure 3.4. The ODT is determined by recording the parameters of SAXS pattern as a function of temperature. The SAXS pattern for the weakly segregated microphase-separated LN4 shows a narrow peak with quite constant intensity in the range of 110 to 130 °C which originates from the correlation between PS and PB microdomains of the micro structure. On further increase in temperature, i.e. > 130 °C a slight decrease in the scattering peak intensity without any appreciable change in shape of the peak is observed leading to the conclusion that the copolymer tends to approach a disordered state with increasing temperature. The

microphase separation from ordered structure to isotopic melt is connected with a pronounced discontinuity in the shape and intensity of the peak above 140 °C.

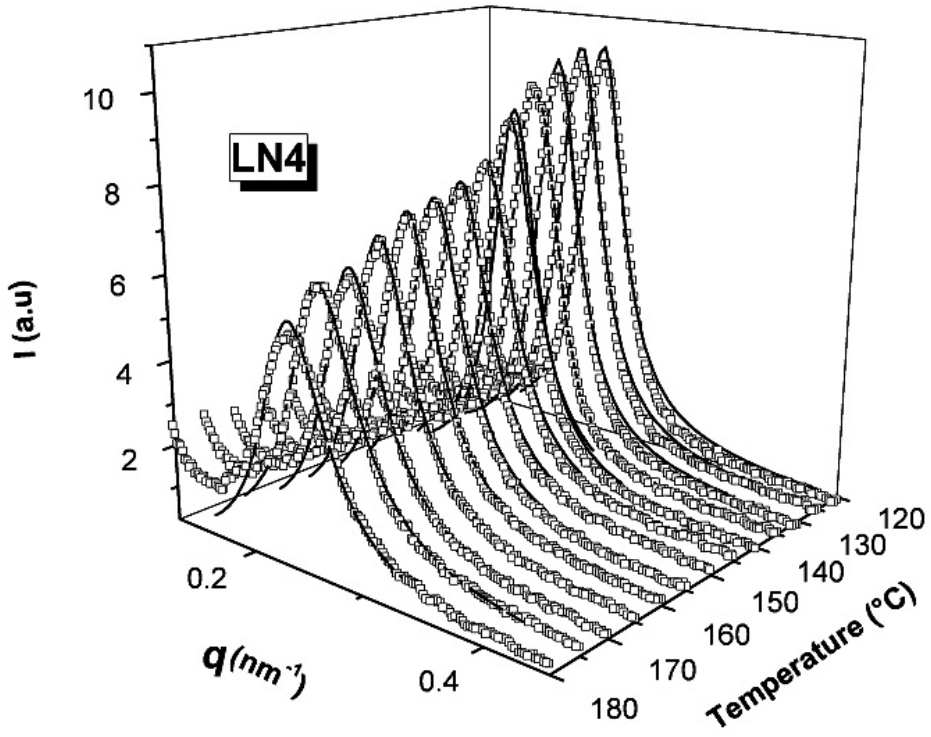

Figure 3.4 SAXS profiles for LN4 in between 120 - 180 °C: Comparison of theoretical structure factor from Leibler theory (Eqs. (1)) with experimental scattering profile form LN4.

Such discontinuity was also observed in reverse direction while cooling the sample from 180 to 110 °C. To characterize the change in the SAXS profile across the ODT, the inverse of peak intensity (I_m^{-1}) is plotted as a function of inverse absolute temperature (T^{-1}) as shown in Figure 3.5a, which is in accordance with mean-field theory predictions [9]. The position and width of the first order peaks are plotted as function of absolute temperature *(T)* in Figure 3.5b and c respectively. All these three plots in Figure 3.5 show a change at around 140 °C, which apparently ascertains the ODT. Further it can be observed from Figure 3.5a that nearly linear dependence of I_m^{-1} vs. T^{-1} at high temperature indicates a homogeneous state of the triblock copolymers and the deviation of the linear extrapolation from the experimental data occurs at approximately 139°C, which could be taken as the order disorder transition temperature (ODT).

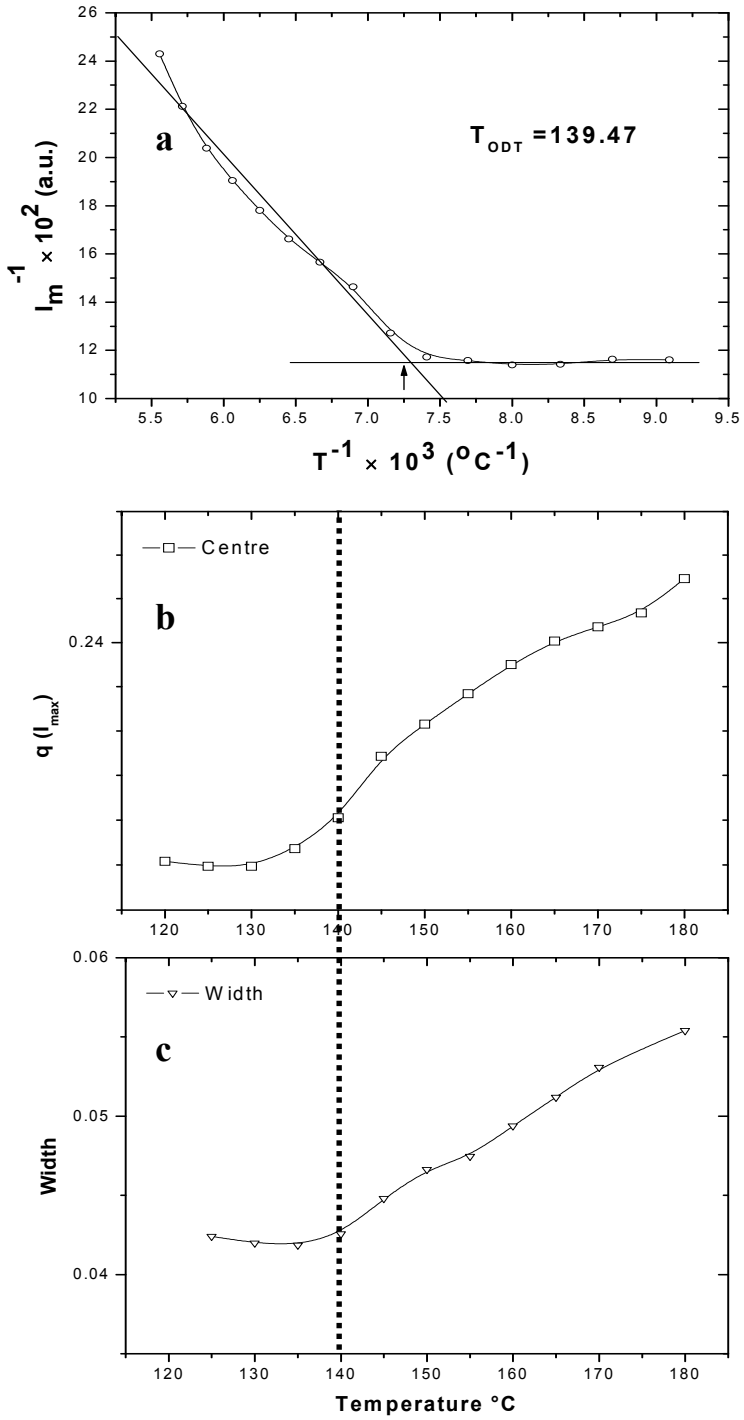

Figure 3.5 SAXS profile characteristics a) Inverse peak intensity I^{-1} (q^*) plotted versus inverse temperature T^{-1}, b) Temperature dependency of peak position q^* Vs T, c) Temperature dependency of peak width is shown.

The ODT of LN4 is observed to be broad when compared to the phase transition of triblock copolymers in the previous studies [10,11]. Such a distinct change in ODT behaviour is attributed to the influence of the structural ordering of chains in LN4. The enhanced miscibility of PS end blocks with the SB random middle block considerably

reduces the segregation strength between the PS and PB phases leading to a weak phase transition near ODT. Thus the broad and continuous transition in LN4 reconfirms the weak phase segregation in LN4.

In the disordered state above ODT, the spacing in the disordered structure $D=2\pi/q^*$ (domain size) has been observed to decrease constantly with increase in temperature which is in contrast to the theoretical predictions (according to which above ODT the domain size D should remain nearly constant) for homogeneous block copolymers. As the segregation in the block copolymers is restricted to the molecular dimensions, the unfavorable segment–segment interactions in the disordered state near ODT are expected to be relieved through the development of composition fluctuations. Such fluctuation effects should theoretically be high in triblock copolymers as compared to diblocks because of the architectural complexity in the triblock copolymers where the blocks are connected covalently in an unlinking sequence [10]. However, in the present situation the middle block consisting of PS-PB random copolymer with 50 wt. % of PS which is coupled with two short PS outer blocks has a great effect in reducing such unbearable interactions and thereby significantly influences the transition from extended conformation in the ordered state to Gaussian conformation in the disordered state of the triblocks.

Scattering from triblock copolymers in the disordered state is similar to that of homogeneous diblock copolymers i.e., due to concentration fluctuations there exists a maximum in the scattering profile in the homogeneous state. Such peaks in the scattering profile in the disordered state are caused by the correlation-hole effect. However, as the triblocks are observed to have higher concentration fluctuations when compared to diblocks, the peak parameters are expected to be more pronounced in this class of block copolymer materials. The static structure factor of two-component system in the disordered state was presented by theory of Leibler [9] in the context of random phase approximation (RPA). According to the proposed theory, the structure factor $\widetilde{S}(q)$ is derived as following

$$\widetilde{S}(q) = \frac{W(q)}{\left[S(q) - 2\chi W(q)\right]} \tag{3.1}$$

Where q is the wave vector, χ is the interaction parameter and

$S(q)$ and $W(q)$ are represented as

$$S(q) = S_{11}(q) + S_{22}(q) + 2S_{12}(q) \tag{3.2}$$

$$W(q) = S_{11}(q)S_{22}(q) - 2S_{12}{}^{2}(q) \tag{3.3}$$The

composition correlation functions $S_{11}(q), S_{22}(q)$ and $S_{12}(q)$ for diblock copolymers are given

in equation IV-2 to IV-6 of reference 2a. However these correlation functions are extended for ABA triblock copolymers by Mori et al. [12] and are expressed by

$$S_{11}(q) = N\left[g_1(f_1,x) + g_1(f_2,x) + g_1(f_3,x) + g_1(1,x) - g_1(1-f_3,x) - g_1(1-f_1,x)\right] \quad (3.4)$$

$$S_{22}(q) = Ng_1(f_2,x) \quad (3.5)$$

$$S_{12}(q) = (N/2)\left[g_1(1-f_1,x) + g_1(1-f_3,x) - g_1(f_1,x) - g_1(f_3,x) - 2g_1(f_2,x)\right] \quad (3.6)$$

Where $g(f,x) = \frac{2}{x^2}\left[fx - e^{-fx} - 1\right]$ and $x = \frac{q^2 Na^2}{6}$

The scattering profiles at different temperatures between 150°C and 180°C which is well above the ODT are observed to fit very well with the structure factor $\tilde{S}(q)$ for triblock copolymer as shown in Figure 3.4. However, at low value of q, there appears a slight deviation from the fit, this deviation could be due to finite compressibility of the copolymer melt which is beyond the scope of the theory. The temperature dependency of χ is extracted from the fits and plotted in Figure 3.6. The composition in the middle block was maintained constant as with PS to PB ratio as 1:1. Therefore, the value of χ corresponds to the interaction between SB random middle block with the PS end blocks.

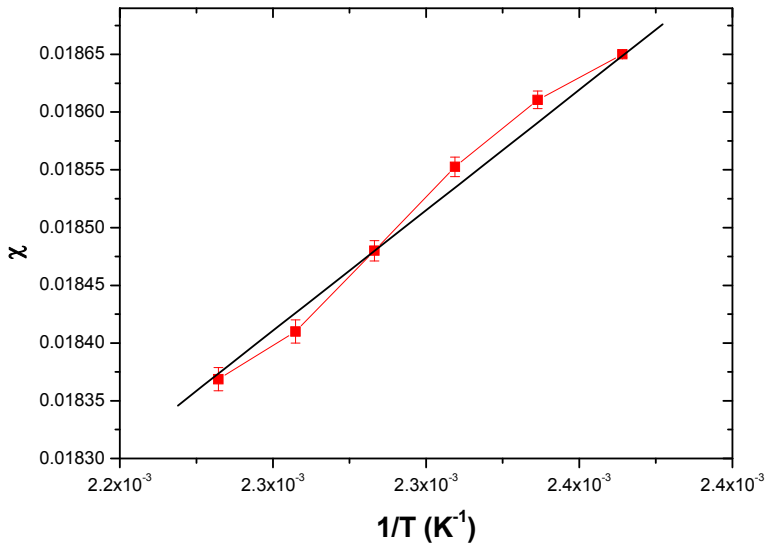

Figure 3.6 Temperature dependency χ parameter obtained by fitting SAXS profiles for LN4 in between 120 - 180 °C

A fit in accordance to equation 3.7 reveals a very weak temperature dependency in the disordered state. Wolff et al. [11] have observed the phase behaviour of PS-PB diblock copolymer where the temperature dependence of χ was given by equation 3.8.

$$\chi = 0.01372 + \frac{3.577}{T} \tag{3.7}$$

$$\chi = -9.6e^{-4} + \frac{18.73}{T} \tag{3.8}$$

The temperature dependence of χ is represented as $\chi = A + B/T$ where A and B are the entropic and enthalpic terms respectively. From equation 3.7 and 3.8 it could be observed that the enthalpic term is much less for LN4 as compared to PS-PB diblock copolymers. The decrease in the enthalpic term with the increase in the complexity in the block copolymer architecture reveals that the phase behaviour is mainly governed by the entropic term in block copolymers and this is particularly imperative in case of block copolymers with complex architectures. The phase behaviour is mainly described by the compatibility between heterogeneous phases which is quantitatively represented in terms of product of χ and N. With smaller χ the entropic term in Flory-Huggins theory, which is inversely proportional to N, will have increasing influence in controlling the phase behaviour of block copolymers with complex architectures.

3.4 Rheological behaviour from Master curves

3.4.1 Master Curves of LN3 and LN4

The rheological properties of the asymmetric (LN3) and symmetric (LN4) triblock copolymers and their blends were studied with the aid of their master curves. The master curve of the storage modulus (G') of LN3 and LN4 are shown in Figure 3.7. The dynamic mechanical spectra are constructed based on Time-Temperature-Superposition (TTS) principle. The response of the samples (LN3 and LN4) over a broad frequency window is obtained by deforming the sample within the linear viscoelastic regime. As the frequency sweeps are conducted far above the T_g of PS phase, so the entanglement regime followed by a terminal flow regime can be observed for both LN3 and LN4 in Figure 3.7. From Table 3.1, it can be observed that the over all M_w of LN3 and LN4 are far above the entanglement M_w of PS, M_e, which is about 19000 g/mol. As the M_w of the random middle block in LN4 is larger than LN3, a high modules value in the entanglement plateau is expected. However, from Figure 3.7 it can be observed that both LN3 and LN4 are showing similar modules in the entanglement plateau, which reveals that the entanglement effect in LN4 is compensated

by the persistent phase separation in LN3. However, in the vicinity of phase behaviour and phase transitions the master curves of the blend components are briefly discussed here.

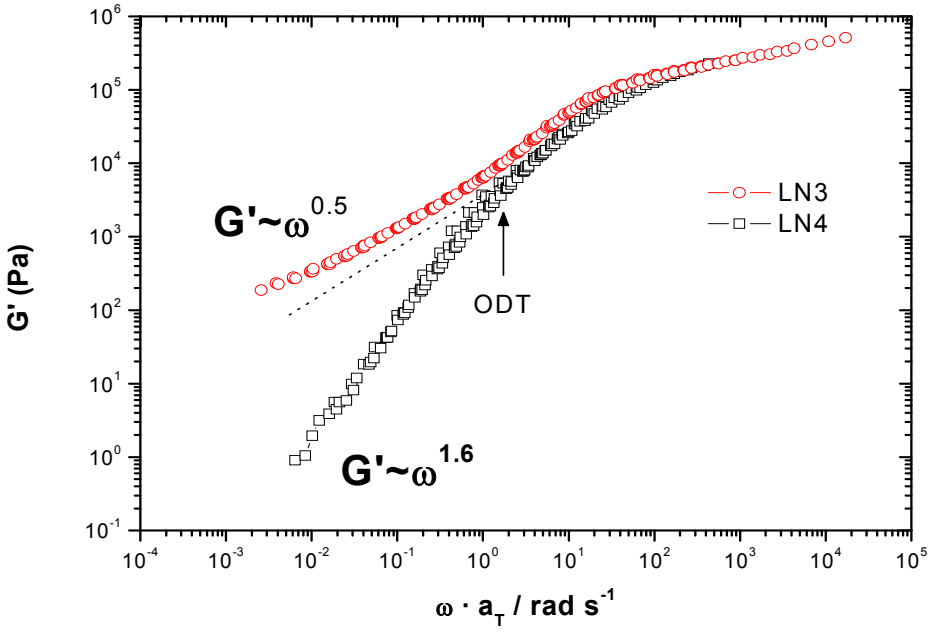

Figure 3.7 Master curves of G' as a function of ω for LN3and LN4 at T_0=130 °C. The ODT in master curve of LN4 is indicated by an arrow and the dotted line.

The most important features that could be observed from the master curves of LN3 and LN4 were in the low frequency regime. In this frequency range, conventionally for homopolymers, the frequency dependence of G' and G'' are described by the equation G' ~ ω^2 and G'' ~ ω as ω→0 and it is termed as terminal flow regime. Interestingly, the terminal slopes of G' for LN3 and LN4 are observed to be 0.5 and 1.6 respectively. It was reported by Kossuth et al. [13] that the variation in the terminal slopes in block copolymers is mainly attributed to their persisting morphology. Due to the presence of phase separated structure there exists some tethered junctions across the interface, which constrains the deformation of the nanodomains as individual units, causing a longer relaxation time. These topological constraints due to tethered junctions act as physical cross-linking points that restrict the PS chain dynamics on much larger length scale than the local segment size. Thus by comparing the slope of G' in the terminal regime for LN3 and LN4 it could be confirmed that a phase separated structure is existing in LN3 within the measured temperature range i.e. up to 220°C, whereas a nearly homogeneous disordered structure can be expected in LN4. The observed terminal slope value of 0.5 for LN3 is in accordance with the observation of Kossuth et al. [13] for block copolymers having lamellar morphology.

However, in case of LN4 a different terminal flow behaviour is observed i.e. the terminal slope of G' is 1.6 which has been observed to be less than the terminal slope of

conventional homopolymers. This slight difference in the values of the slopes is attributed to the composition fluctuations present in the one-phase region for LN4 [15]. As discussed above from the T-SAXS results, the architectural complexity in the triblock copolymers, due to the presence of a random middle block, results in extending the temperature limit for the block copolymer chain to attain a conformation similar to homopolymers with a terminal slope of 2. Thus it could be observed from the master curve of LN4 that such fluctuations are existing until 220 °C in LN4. The ODT from T-SAXS measurements can be reconfirmed from the master curves by carefully noticing the presence of deviations in the master curve, which is marked with an arrow in Figure 3.7. This inconsistent superposition indicates the presence of T_{ODT} within the measured temperature range and it is observed that deviations are observed around 140 °C, which is well in agreement with T-SAXS results. However, below T_{ODT} the frequency dependence of G' has been observed to be more modest like that in cross-linked polymers i.e. $G' \sim \omega^{0.5}$ (indicated by dotted line in Figure 3.7), which is due to the presence of phase separated structure. Above T_{ODT} the block copolymers show a homogeneous disordered nature with a liquid like conventional terminal flow behaviour i.e. $G' \sim \omega^2$ at low frequency regime. The nature of such deviations further complies with the state of ordering in the block copolymers. It was observed by Rosedale et al. [14] that the amplitude of the concentration fluctuation near ODT is dependent on the long period size which shows a strong influence on the nature of deviations in the master curve. As the branching is observed to be less pronounced in LN4 it could be considered that LN4 is weakly ordered. Such transitions in LN4 and non terminal behaviour in LN3 can further be illustrated by using Han plots.

3.4.2 Han plot for LN3 and LN4

Han et al. [15] have described that the frequency dependency of the moduli (G' and G'') are not sensitive enough for determining the T_{ODT} for block copolymers and suggested that based on equation 5 of ref. 8, G' vs. G'' plots can be used to determine the T_{ODT}. Accordingly, Figure 3.8 was constructed for both LN3 and LN4 at different temperatures in the range of 130 °C to 200 °C. As it was observed previously that, the state of segregation and the persistence of phase separated structure in the experimental temperature range influence the superimposability of the data from frequency sweeps. The precision of TTS is hence examined by using Han plot which involve the elimination of the effects due to shifting along frequency axis. From Figure 3.8 it can be observed that G' and G'' are following a single line with a slope of 0.56 within the measured temperature range (130-200 °C). However, a significant variation in G' at a fixed G'' with respect to temperature can

be observed for N4. G' shows a significant decrease with respect to temperature in the range of 130 °C to 160 °C followed by a tendency to remain independent of temperature above 160 °C.

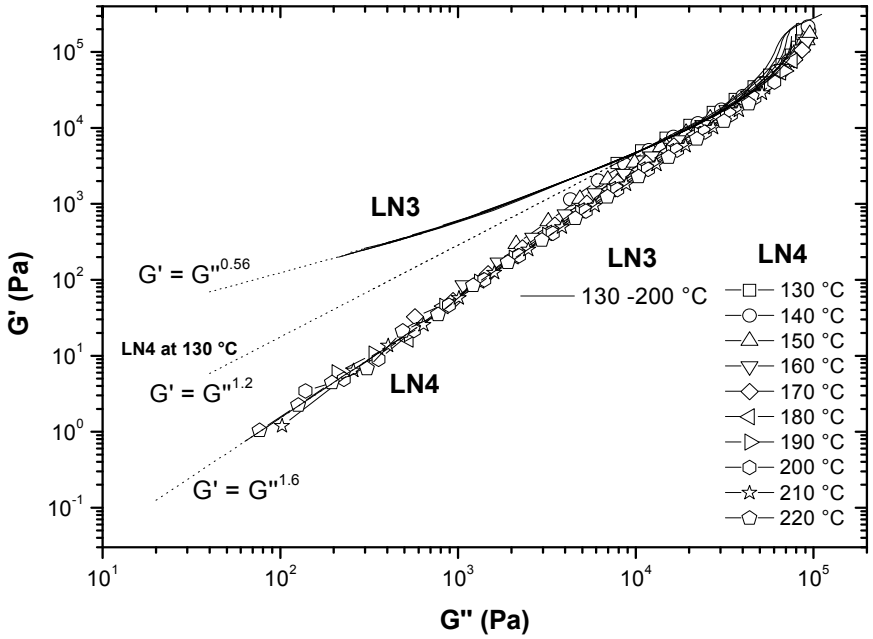

Figure 3.8 G' vs. G'' plot for LN3 and LN4 (The isotherms are shown without shift).

On the basis of the theoretical prediction by equation 5 of ref. 21, the G' and G'' for a monodispersed homopolymer melt has a weak temperature dependence with a gradient of 2 in the terminal region. Thus we could conclude form Figure 3.8 that the variation of log G' vs log G'' in between 130-160 °C from a slope of 1.2 at 130 °C to 1.6 at 160 °C is attributed to the temperature dependent transition from ordered microphase separated structure to a fluctuation state. However, the nature of variation of G' at constant G'' in between 130-160 °C further implies that the transition is extended over a broad temperature range with a gradual change from phase-separated structure to homogeneous phase with increase in temperature. In contrast, absence of such variations in G' and G'' with respect to temperature along with a slope of 0.56 for G' dependency on G'' for LN3 can be attributed to the persistence of solid-like rheological behaviour i.e. the material exists in the ordered state within the measured temperature range.

3.4.3 Master curve of LN3/LN4 60:40 blend

DMA and morphological investigations reveal that with the increase of LN3 content the phase dynamics of the blends gradually shift from a weak segregation limit (WSL) to strong segregation limit (SSL). Further SAXS studies which details the information concerning increase in long period size with the increase in LN3 content has been discussed in one of our earlier communication [16]. As stated above, the slight branching in the master

curve of LN4 was observed to be less pronounced in LN4 and this is attributed to the weakly ordered structure in LN4. As the amplitude of the concentration fluctuation near ODT is dependent on the long period size of the micro structure. Thus the complex thermo-rheological behaviour accordingly can be observed in a more pronounced manner for blends with higher LN3 content. In order to further investigate the origin of this behaviour, such as ODT, the linear visco-elasticity of the blend with 60 wt.-% of LN3 at low frequencies has been examined. This blend composition was selected keeping in view of the TTS curves of storage modulus (*G'*) which shows a pronounced branching when compared to the other blend compositions which are having less than 60 wt.-% of LN3. The TTS curves of *G'* derived from these measurements are shown in Figure 3.9.

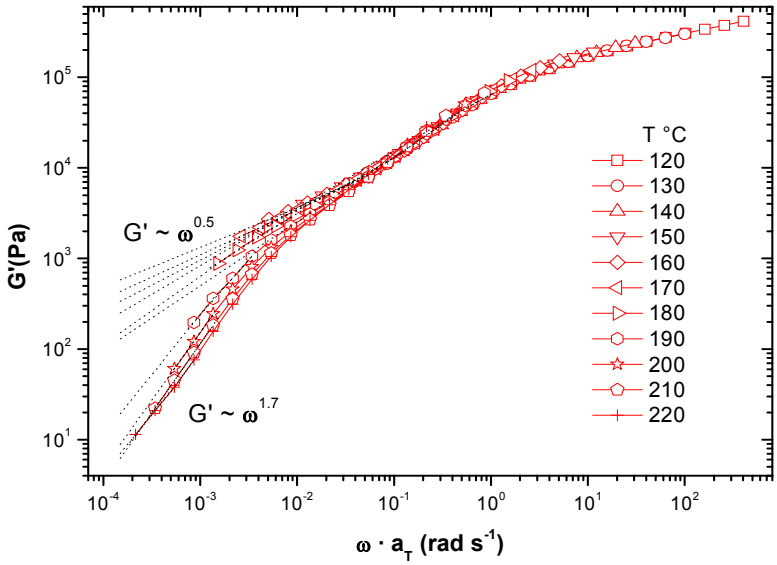

Figure 3.9 TTS master curve of storage-modulus G'of LN3/LN4-60/40.

The presence of branching (inconsistent superposition as indicated by a pronounced shoulder starting at 180 °C) in the master curve of the blend with 60 wt.-% of LN3 indicates that the T_{ODT} remain in the measured temperature range as observed earlier for LN4. However, below 180 °C the frequency dependency of G' is observed to be more modest like in cross-linked polymers (i.e., $G' \sim \omega^{0.5}$ and $G'' \sim \omega^{0.5}$ as $\omega \rightarrow 0$) as shown in Figure 3.9 with dashed lines. As the temperature was raised above T_{ODT} i.e., $T > 180$ °C, no phase separated structure was observed and hence behaves like a liquid at sufficiently lower frequency. Thus the moduli decreased abruptly with a conventional terminal behaviour (i.e., $G' \sim \omega^2$ and $G'' \sim \omega$ as $\omega \rightarrow 0$). However, the pronounced shoulder at low frequency (T ≥ 180 °C) is derived from the relaxation of the microstructure. The results from the master curves of LN3, LN4 and 60 wt.-% LN3 suggest a detailed investigation of the effect of blend composition on the linear visco-elastic properties of S-(S/B)-S triblock copolymers especially in the non-

terminal frequency range it becomes even more important. Hence the following section exclusively focuses on the influence of blend compositions on their rheological and ODT behaviours.

3.5 Influence of blend composition on rheological properties

The increase in the G' and |η*| with the increase in LN3 content are clearly observed in the low frequency regime in the blends as shown in Figure 3.10 and 3.11. Since the TTS curves for loss modulus (G'') is having a similar frequency dependence like that of storage modulus (G') it is not shown here. The increase in the dynamic modulus of the blends with the increase in LN3 content is mainly attributed to the gradual change in the morphology from more homogeneously phase separated structures to more strongly segregated structures. In case of highly ordered structures like lamellar morphology as in LN3, an extended entanglement regime towards low frequencies with higher terminal relaxation time can be observed when compared to LN4. This extension of entanglement plateau is attributed to the slow diffusion of the individual polymer chains into the melt due to the confinement of the polymer chain mobility (as in lamellar structure). The terminal relaxation time depends on the diffusion time and molecular weight of the polymer. On the other hand in case of weakly segregated structures e.g., in the wormlike morphologies (0-20 wt.-% of LN3) a complete relaxation can be observed at shorter time scales with a sharp decay in the modulus as illustrated in Figure 3.10.

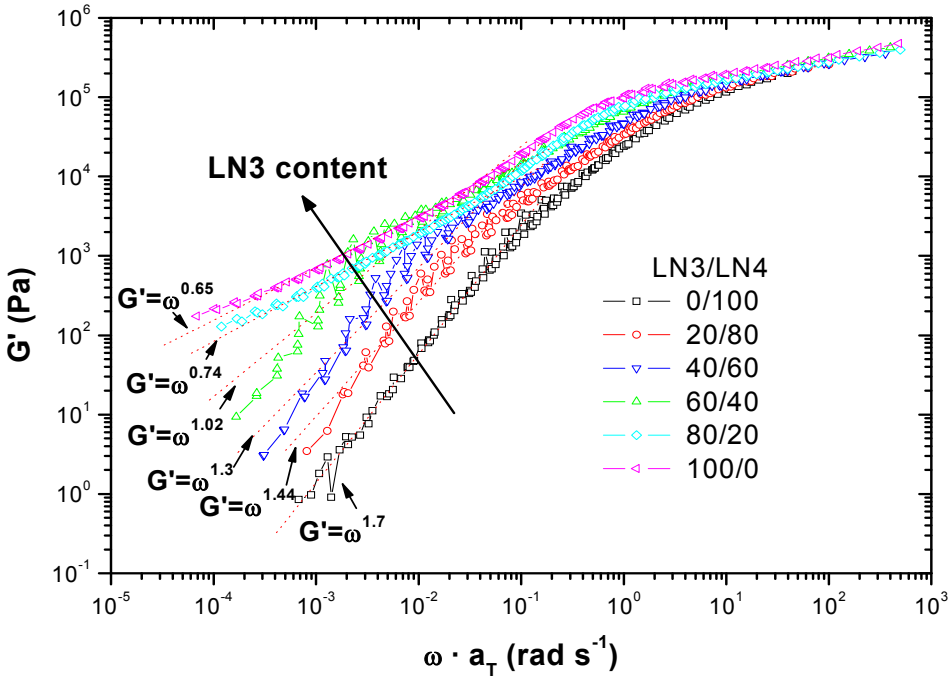

Figure 3.10 Master curves of the storage modulus of pure and blends of LN3 and LN4 as a function of frequency at T_o=130 °C

As discussed earlier, LN4 shows a typical terminal behaviour and LN3 shows a non terminal behaviour in the low frequency regime. A transition from typical terminal behaviour with G' ~ ω^2 and G"~ ω to a non-terminal behaviour with the moduli scaling as G' ~ G" ~ $\omega^{0.5}$ can be observed. This transition in the rheological behaviour occurring in the structural response regime with the increase in LN3 content can also be observed from the master curves of complex viscosity ($|\eta^*|$) as shown in Figure 3.11. At low frequency regime, $|\eta^*|$ of pure LN4 reveals Newtonian behaviour resulting in a plateau. This behaviour changes gradually to non-Newtonian behaviour with an increasing trend in shear-thinning exponent *n* ($|\eta^*| \sim \omega^n$). In order to identify the point of transition the shear-thinning exponent (*n*) was plotted against LN3 content (Figure 3.12), which indicated the occurrence of a clear transition (from terminal to non-terminal behaviour) in the rheological behaviour at 60 wt.-% of LN3 content. This transition in the rheological response can apparently be attributed to the change in the morphologies from cylindrical structure (WSL) to lamellar structure (SSL). Thus microphase separated lamellar structure, corresponding to blends with 70-100 wt.-% LN3 content is able to remain in the ordered state within the experimental temperatures range. Hence, the rheologicla properties of the ordered block copolymers change drastically when compared to disordered block copolymers showing typical visco-elastic liquid like behaviour [17,18,19]. The microphase separation characteristics influence the low frequency rheological properties of these blends.

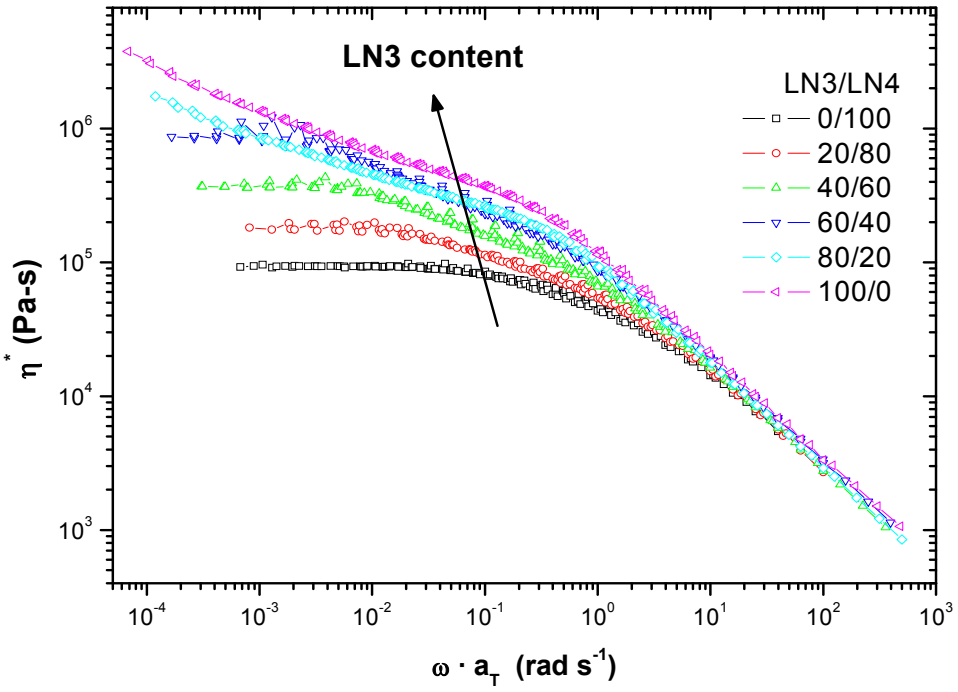

Figure 3.11 Master curves of the complex viscosity of LN3/LN4 blends as a function of frequency at T_o=130 °C

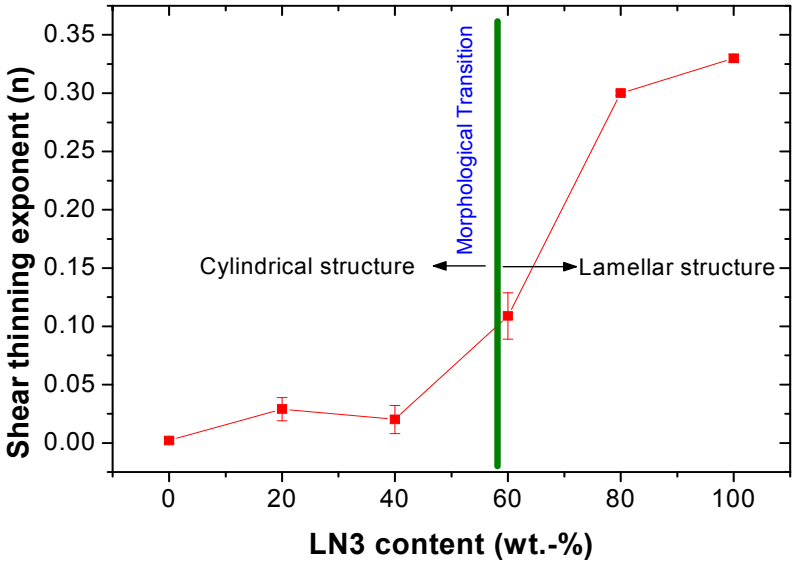

Figure 3.12 Shear-thinning exponent *n* from master curves of |η*| vs LN3-content

3.6 van Gurp-Palmen plot

The van Gurp and Palmer method is based on the analysis of the behaviour of the phase angle (tanδ = G"/G') versus the absolute value of the complex modulus of the blends (|G*|). The method entails the elimination of the effects due to the shifting along the frequency axis. The phase angle (δ) is plotted against the absolute value of complex modulus (|G*|) for all the blend compositions and is shown in Figure 3.13. It could be observed that LN4 shows a

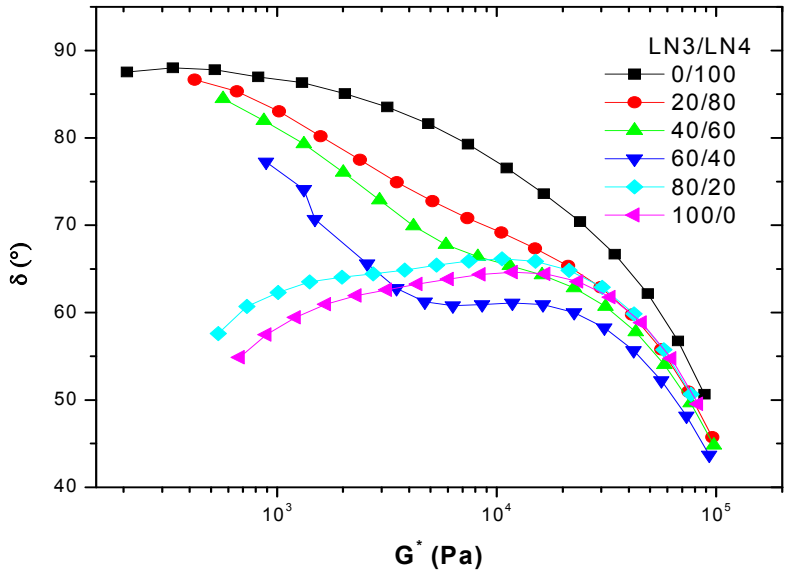

Figure 3.13 van Gurp Palmen plot for LN3/LN4 triblock copolymers and their blends at 190°C.

homopolymer like behaviour with a plateau at low |G*| and then decreases gradually at higher |G*|. The curve approaches a phase angle of ~90° at lower complex modulus indicating the flow behaviour like that of a viscous fluid [19,20]. In contrast, the blends with

80-100 wt.-% of LN3 content having a lamellar structure resemble the behaviour of an elastic solid. A transition from solid to liquid like behaviour can be clearly observed in the case of blends with 20-60 wt.-% of LN3 content. This transition from viscous fluid to an elastic solid like behaviour can be well correlated with the composition dependent morphological transitions as discussed above.

3.7 Terminal slopes of G' as a function of temperature

To compare the temperature dependence of the relaxation behaviour of these blends at low frequencies, terminal slopes of *G*' at different temperatures were determined as shown in Figure 3.14. Generally, the terminal slopes show an increasing trend with the increase in temperature due to the ease in polymer chain mobility at higher temperatures. However, pure LN3 and blend with 80 wt.-% of LN3 content show an increasing trend in their respective terminal slopes with the increase in the temperature till ~ 140 °C followed by a subsequent decreasing trend by several orders of magnitude. On the other hand when the temperature is increased further the terminal slope tends to be temperature independent which is clearly seen from the values of the slopes at high temperatures for LN3 and the blend with 80 wt.-% of LN3. Appearance of such a peak in the terminal slope curves for the samples having highly ordered lamellar structures could be attributed to phase transitions resulting from super-molecular structural relaxation. However, the presence of an order-to-disorder phase transition (ODT) in this temperature range and the characterization of the order-disorder transition temperature needs to be investigated further.

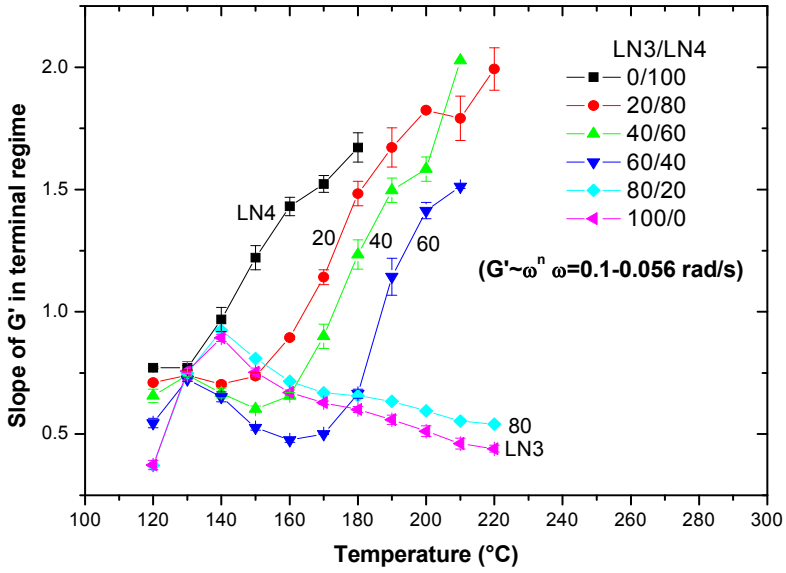

Figure 3.14 Terminal slope of G' versus temperature of the triblock copolymer blends

The existence of a phase transition (ODT) in S-B-S triblock copolymers was already reported in the literature, lying well above the glass transition temperature of PS [21]. Partly it could be confirmed from the temperature independent terminal slope values in the range of 140-220 °C that the ODT of LN3 and the blend with 80 wt.-% of LN3 remain well above the measured temperature range i.e., 220 °C. Thus the blend compositions with ≥ 60 wt.-% of LN3 content are well ordered within the experimental range.

In case of LN4 the terminal slopes tend to increase sharply with the increase in temperature indicating the complete relaxation of the material within a shorter time scale confirming the liquid like behaviour attributed to weakly segregated structures. However, in the blends with 20, 40 and 60 wt.-% of LN3 contents the terminal slopes remained nearly temperature independent till 155, 160 and 180 °C respectively followed by a sharp increase in the magnitude of the slopes like that of LN4. Such a change in the terminal slope behaviour at a specific temperature can be considered as the order-to-disorder transition temperature, i.e. below this temperature range the material shows a solid like behaviour due to ordered microphase separated structures. However, above this critical temperature the structure disappears leading to a strongly temperature dependent liquid-like flow behaviour. Further it is also observed from Figure 3.14 that this phase transition temperature shows an increasing trend with the increase of LN3 content and thus reaffirms that with the increase of LN3 content the resistance of the material to withstand temperature also increases without any structural alterations. Since slopes are taken for every 10 °C step it is difficult to identify ODT more accurately and hence ODT behaviour is studied further by conducting temperature ramp experiments and is discussed elaborately in the next section.

3.8 ODT from Rheology

The determination of order-to-disorder transition temperature is rheologically scrutinised based on the procedure that was established in the previous studies [22]. Based on this phenomenon characterisation of the temperature dependence of moduli around the order-to-disorder transition is widely used as a method to determine the phase transition temperature (T_{ODT}). At ODT G' and G'' drop discontinuously as a consequence of disordering. This discontinuity in rheological properties is reported to be a natural consequence of first order nature of the ODT [14]. In order to precisely identify the ODT range, low frequency isochronal dynamic shear measurements as a function of temperature have been carried out and the elastic moduli have been measured at a frequency lying well below the critical frequency, ω_c (which is observed from TTS). The elastic modulus was

found to decrease discontinuously which could be clearly observed in the plot of *G' versus T* in Figure 3.15.

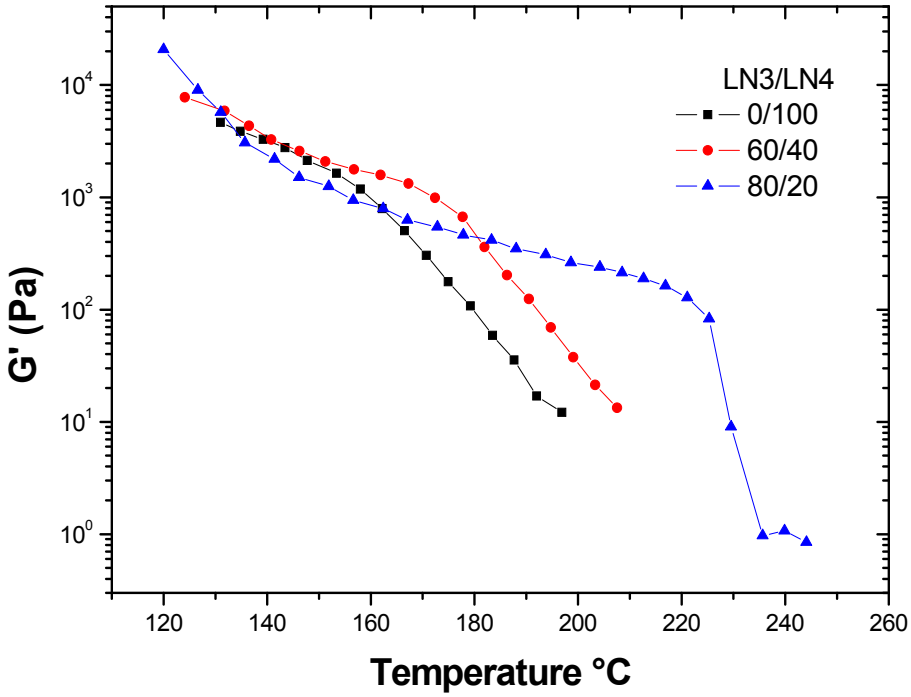

Figure 3.15 Temperature dependency of G' showing ODT temperature for LN3, LN4 blends

An abrupt change in elastic modulus over a narrow temperature range can be observed for the blend with 80 wt.-% of LN3 content which is attributed to the disappearance of microdomain structure of the block copolymer sample. A similar behaviour is reported in several studies involving SBS and SIS triblock copolymers, which are well ordered below ODT [23]. In the blend composition with 60 wt.-% of LN3 and pure LN4 the change in the slope of G' below which the apparent elastic modulus dropped significantly has been taken as the ODT range. The ODT transition was also observed to be reversible, however as the present work is not focused on discussion about the hysterisis in phase transitions, so the reversible transitions was not included. In general as the temperature approaches ODT a sharp drop in the G' is expected. Nevertheless, in the present scenario the sharp drop in the G' at ODT is influenced by the state of order below ODT. LN4 with weak phase segregation shows this drop in modulus with hardly any change in the slope. However, this change in slope is more significant in blend with 60 wt.-% of LN3 which is having the phase separated structure in between weakly phase separated LN4 and strongly phase separated LN3. Thus the order-to-disorder transition (ODT) behavior provides the information about phase segregation state far below T_{ODT}.

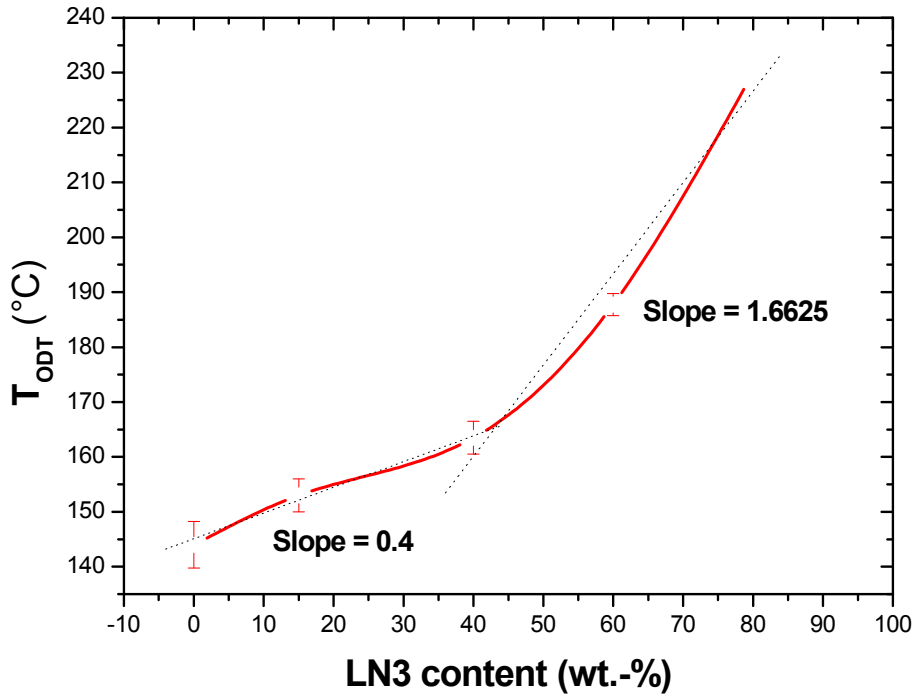

Figure 3.16 ODT of the blends with respect to LN3 content in the blend composition.

Transition temperatures are plotted against composition in Figure 3.16, it was observed that the ODT increased with the increase in the LN3 content in the blends. The ODT is observed at ~ 140 °C for pure LN4 and at ~ 230 °C for blends with 80 wt.-% of LN3.However, an increase or decrease in the ODT in block copolymers can generally be observed by blending with a corresponding homopolymer or a block copolymer with large difference in M_w between the blend components. Interestingly, in the studied blend system, the two components inspite of having similar molecular weights, an increase in ODT of blends with increase in LN3 content has been observed. Such a variation in ODT can be attributed firstly to the interplay between the PS end blocks of LN3 and LN4 and secondly to the presence of random middle block which influence the chain stretching during phase separation in the blends. We have observed from TEM, SAXS and rheological studies that all the blends are miscible at molecular level across the entire composition range. Hence it is worth noting the co-surfactant effect to study the chain organization in the blend systems that leads to an increase in the ODT with increase in the LN3 content [14]. The co-surfactant effect influencing the chain organization of PS end blocks in LN3, LN4 and their blends are schematically shown in Figure 3.17. Even though the M_w of LN3 and LN4 are nearly the same a difference in the M_w of PS end blocks is very pronounced due to the difference in the chain architecture [Table 3.1].

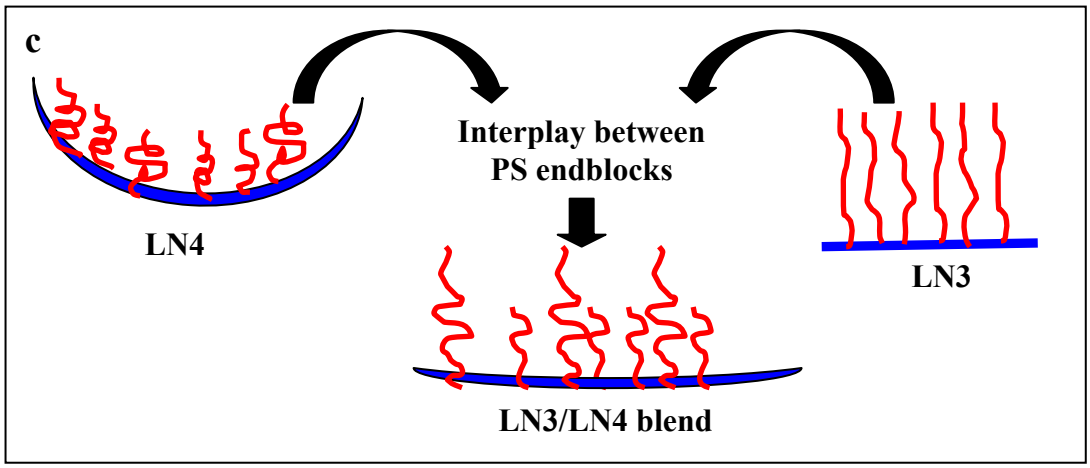

Figure 3.17 Schematic illustration depicting the chain organization of PS end blocks confined to the PS rich phase.

In case of LN3, as discussed above, the long PS end block exhibits a high elastic stretching energy resulting in the formation of highly ordered lamellar structure at higher temperatures. By extrapolating the ODT values above 40 wt.-% of LN3 content viz. 100 wt.-%, it could be observed that the ODT of pure LN3 can be expected at ~ 250 °C. However, due to the influence of degradation in the sample above 240°C (observed from TGA) the accessible experimental temperature range is below the ODT of LN3. The ODT of LN3 stays at higher temperature due to its strong stretching energy of long-PS end blocks which arise from (a) high M_w and (b) asymmetric architecture. On the other hand, the ODT of LN4 remains at lower values (a) due to its weak stretching energy of short PS end blocks which arise mainly from high miscibility between PS end blocks and random SB middle block and (b) due to the large content of the statistical middle block. In the blend compositions when chains of LN3 and LN4 are organized on a common interface the shorter PS end blocks in the symmetric architecture of LN4 will considerably reduce the stretching energy of longer PS outer blocks of LN3, which is due to the co-surfactant effect. The co-surfactant effect is mainly due to the difference in M_w between the PS end blocks of LN3 and LN4 in the PS-rich phase. Such a reduction in the stretching energy leads to simultaneous reduction in the segregation strength as well as the ODT with the increase of LN4 in LN3.

A visible change in ODT has been noticed in the blends as the composition exceeds 40 wt.-% of LN3, i.e. an increase in ODT with different slope in blends with 40 wt.-% of LN3, reaffirms the presence of an intermediate segregated structure above this critical composition. Thus a high slope of 1.66 above 40 wt.-% of LN3 shows that the influence of phase behaviour of LN3 is predominant showing high segregation strength. On the other hand a

low slope of 0.4 i.e., at low LN3 contents indicates that the phase behaviour of LN4 is predominant remaining in a weak segregation state. In one of our recent publication we have also showed that the transition in the state of ordering occurs in the range of 40 to 60 wt.-% of LN3 content in their binary blends. Such transitions in the state of ordering are also in congruence with the observed morphologies.

3.9 Mechanical properties of LN3/LN4 blends

The most interesting futures of these blends lie in their mechanical properties. In our earlier works [5] the mechanical properties of these blend systems were studied by using tensile testing and fracture mechanical behaviour. The transition range of the blend composition that is observed in the present work from rheological response was also strongly reflected in their ultimate mechanical properties. The weakly segregated LN4 is observed to show an elastomeric nature, whereas LN3 with lamellar structure is showing thermoplastic properties. With the increase of LN3 in LN4, the enhancement in the mechanical properties in terms of yield stress and ultimate tensile strength are increasing with out loosing its elastomeric nature. With respect to phase behaviour and morphologies, the investigated block copolymers show two kinds of behaviour. Firstly, high impact behaviour – low yield stress, very high elongation at break, strain hardening, large plastic deformation (for LN3 and samples having LN4 content up to 30 wt.-%) and secondly, Thermoplastic elastomeric behaviour – no pronounced yield point, high elongation at break, excellent recovery (for LN4 and samples having LN3 content up to 30 wt.-%). Therefore, a distinct improvement of tensile properties was observed while maintaining the elastomeric behaviour, corresponding to the cylindrical morphology of the blends up to 70 wt.-% LN3. Beyond 70 wt.-% LN3 the stress-strain-behaviour changes up to significant higher stress values. Similar type of conclusions was also revealed from the fracture mechanical behaviour of these blends system [5]. The study demonstrates that the crack initiation is highly composition dependent, and the resistance to crack propagation is controlled by morphology.

3.10 References

1. K. Knoll, N. Niessner, Macromol Symp, 1998, 132, 231.
2. M. W. Matsen, F. S. Bates, Macromolecules, 1995, 28, 7298.
3. T. Hashimoto, K. Yamasaki, S. Koizumi, H. Hasegawa, Macromolecules, 1993, 26, 2895.
4. R. Lach, R. Weidisch, K. Knoll, J Polym Sci, Part B: Polym Phys 2005,43,429
5. U. Staudinger, B. K. Satapathy, M. Thunga, R. Lach, R. Weidisch, K. Knoll, Acta Materialia 2007, 55, 5844.
6. M. W. Matsen, J.Chem.Phys 2000, 113,5539.
7. S. T. Milner, T. A. Wintter, J.Phys (Paris) 1988, 49, 1951.
8. H. Tanaka, T. Hashimoto. Macromolecules 1991, 24, 5713.
9. L. Leibler, Macromolecules, 1980,13, 1602.
10. J. T. Koberstein, T. P. Russell, D. J. Walsh, L. Pottick, Macromolecules, 1990, 23, 877.
11. T. Wolff, C. Burger, W. Ruland, Macromolecules, 1993, 26, 1707.
12. K. Mori, H. Tanaka, T. Hashimoto, Macromolecules, 1987, 20, 381.
13. M. B. Kossuth, D. C. Morse, FS. Bates, J. Rheo, 1999, 43, 167.
14. J. H. Rosedale, F. S. Bates, Macromolecules, 1990, 23, 2329.
15. C. D. Han, J. Kim, J. K. Kim, Macromolecules, 1989, 22, 383.
16. B. K. Satapathy, U. Staudinger, M. Thunga, R. Lach, R. Weidisch, Macromol. Rapid Commun., 2006 , 27, 1814.
17. M. Thunga, U. Staudinger, B. K. Satapathy, R. Weidisch, M. Abdel-Goad, A. Janke, K. Knoll , J. Polym. Sci Part B Polym. Phy, 2006, 44, 2776.
18. Y. Zhang, U. Wiesner, H. W. Spiess, Macromolecules, 1995, 28, 778.
19. M. Pitsikalis, S. Pispas, J.W. Mays, N. Hadjichristidis, In Advances in Polymer Science, Springer-Verlag, Berlin, 1998, 135,1-137.
20. J. D. Tong, Ph. Lecle`re, A. Rasmont, J. L. Bre´das, R. Lazzaroni, R. Je´rome, Macromol. Chem. Phys., 2000, 201, 12, 1250
21. N. R. Lagge, Ed. Thermoplastic elastomers-A comprehensive review, New York 1987.
22. C. I. Chung, M. I. Lin, J. Polym Sci, Part B, Polym Phys 1978, 16, 545.
23. J. M. Widmaier, G. C. Meyer, J. Polym. Sci, Part B, Polym Phys 1980, 18, 2217.

4. Influence of molecular weight on physical and mechanical properties of linear symmetric S-(S/B)-S triblock copolymers

The results of this chapter have been communicated to

Macromolecular Chemistry and Physics, 2009, 210, 179-188.

4.1 Investigated Materials

The synthesis of the S-(S/B)-S copolymers provided by BASF AG Co. is described by Knoll and Nießner [1]. All the block copolymers LN-41 to LN-44 are linear triblock copolymers with symmetric architecture having outer PS blocks and a middle block composed of a S/B random copolymer. The samples are named based on the type of chain architecture and $M_{w,}$ where LN stands for the linear triblock architecture and the numbers 41 to 44 corresponds to the increase in the value of M_w. The molecular characterization is summarized in Table 4.1. These block copolymers were prepared as plates with 1 mm thickness by compression moulding at 200 °C for 5 minutes followed by annealing the sample to room temperature prior to the release of the pressed plates. In order to attain equilibrium morphologies, the bulk samples were annealed for several days in vacuum at a temperature slightly above the T_g of PS phase.

a

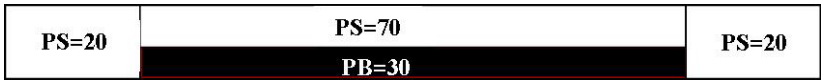

Table 4.1 Molecular characterization of the S-(S/B)-S triblock copolymers with an 80 wt.-% PS content and a S/B ratio in the random middle block of 70/30.

Material	M_w (kg/mol)	M_w/M_n	N	$\chi_{eff}N$	$T_{g\text{-soft}}$ (°C, Fox-equation)	T_g's from DSC (°C)		
						$T_{g\text{-MIX}}$	$T_{g\text{-PB}}$	$T_{g\text{-PS}}$
LN- 41[a]	140	1.1	1256	16.5	35	42	-	-
LN- 42[a]	149	1.09	1341	17.7	35	36	-	-
LN- 43[a]	187	1.11	1611	21.3	-	-	-	-
LN- 44[a]	288	1.23	2306	30.5	4	-	4	82

4.2 Influence of M_w on Phase behaviour and Morphology of triblock copolymers

The morphology of the investigated triblock copolymers LN-41 to LN-44 was studied by TEM and SAXS and is shown in Figure 4.1a-d respectively. The corresponding SAXS profiles are shown in the Figure 4.2. From Figure 4.1 it can be observed that the overall M_w of triblock copolymers is significantly influencing the microphase separation. The triblock copolymer LN-41 having low M_w shows a morphology without phase separation, whereas with the increase of the M_w from 140 kg/mol to 288 kg/mol results in the formation of a phase separation with lamellar structure for LN-44. However, in the intermediate range of M_w i.e. in case of LN-42 and LN-43 the morphology was appeared to be weakly phase separated.

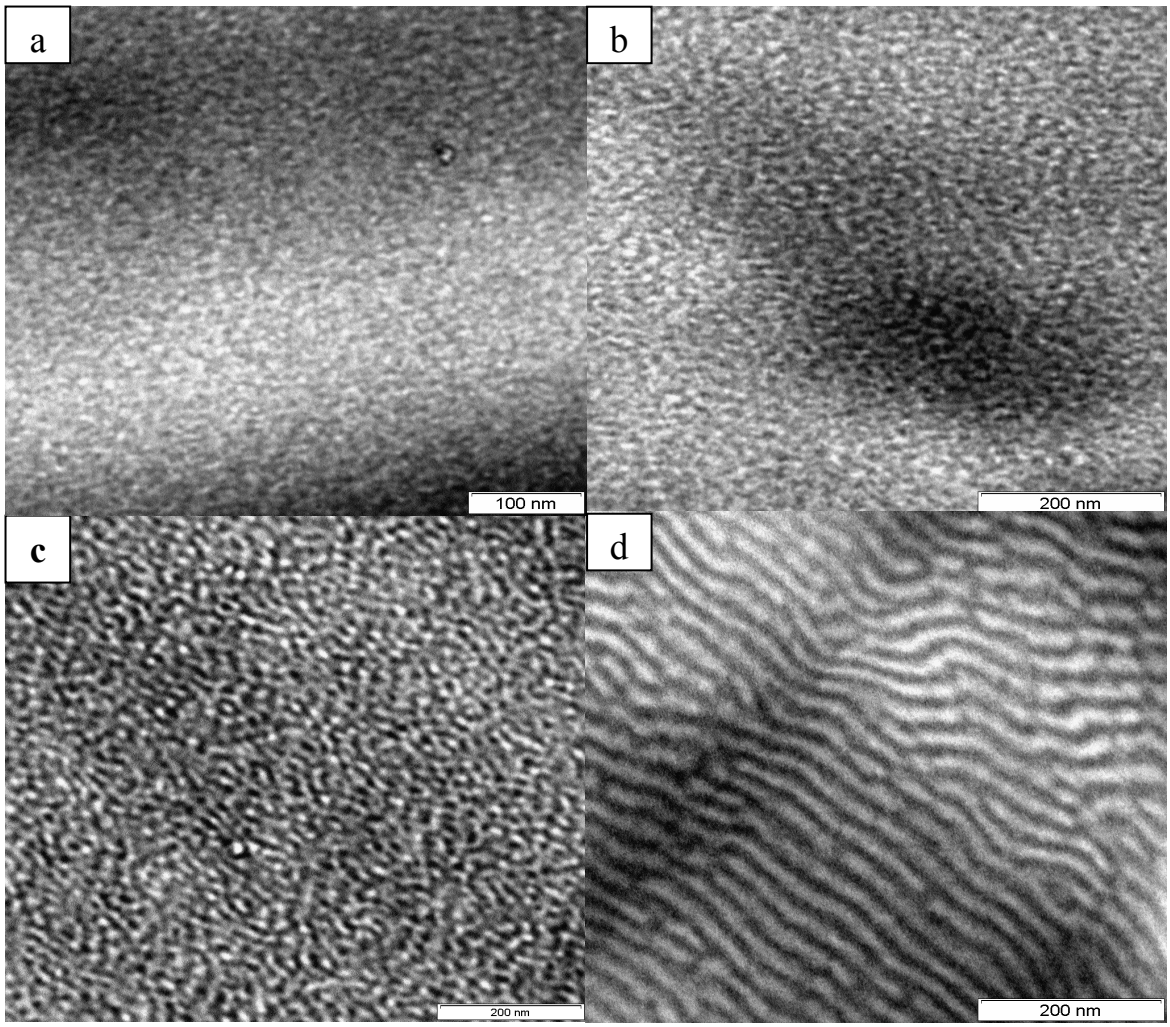

Figure 4.1 Morphology from TEM of a) LN-41 – Disordered structure, b) LN-42 – weakly ordered structure, c) weakly ordered with enhanced phase separation d) LN-44 – phase separated with lamellar structure.

The SAXS profile for LN-44 exhibits two Bragg reflections at integral multiple of q* which resembles the lamellar structure. The absence of additional higher order peaks could be due to the influence of processing of samples. As the samples are compression moulded at 1 mm, formation of lamellar morphology with long-range order was expected to be hindered even after annealing for considerable time. On decrease of M_w from 288 kg/mol to 187 kg/mol a single Bragg reflection is observed for LN-43, which is an indicative of phase separation with microdomain structure. Such broad maximum in the SAXS profile in block copolymers are generally regarded as "correlation hole" which comes from the local segmental density fluctuations [2]. However, at low M_w i.e. in LN-41 in spite of having heterogeneity in the chain architecture the SAXS profile did not show a pronounced Bragg reflection. The nature of such SAXS profile ascribes the absence of phase separation in the block copolymer. Thus it could be observed that the investigated triblock copolymers are showing a transition from

disordered nature to phase separation with lamellar structure with the increase of M_w from 140 kg/mol to 288 kg/mol.

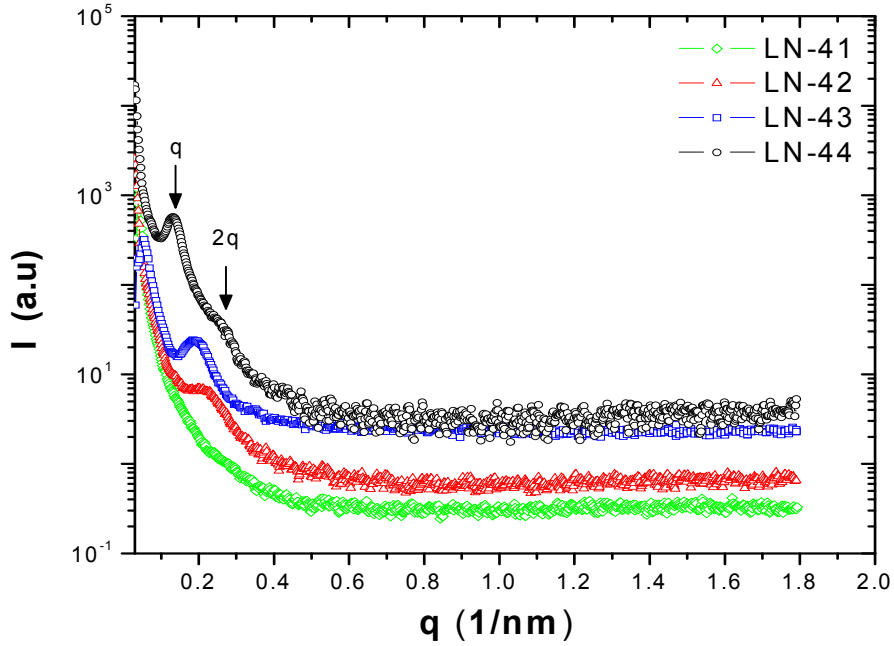

Figure 4.2 SAXS Patterns obtained from LN-41, LN-42 and LN-43 triblock Copolymers

These variations in the phase separation can be explained by comparing the observed results with the phase diagram of triblock copolymers [3]. In block copolymers the state of ordering is mainly controlled by the combined parameter χN andϕ. As in the present case, all the investigated triblock copolymers are having PS and PB as the constituent blocks with similar chain architecture, the χ value is expected to be identical in all the samples. On the other hand the wt.-% of PS was also kept constant at 80 wt.-%, implying the insignificance of PS content (ϕ). However, with the increase of M_w, the block copolymer chain length that corresponds to N (shown in Table 1) increases which ultimately results in an increasing value of the combined parameter χN. In general an increase in the M_w favours phase separation due to high loss in translation entropy at higher N values. On the other hand the phase separation is also partially aided by the repulsive enthalpic interaction χ parameter between PS and PB segments. In some of our recent articles, similar types of triblock copolymers were investigated and it was observed that the ratio of PS and PB in the random middle block was described as crucial parameter in governing the state of ordering in triblock copolymers [4,5]. It was shown that the variation of S/B ratio in the random middle block from 1:1 to 1:2 results in a transition from disordered to ordered lamellar structure. The phase separation is favoured due to enhancement in the χ parameter between outer PS end blocks with the random middle block by increasing the PB content in the S/B random

middle block. In the present case the PS content in the S/B random middle block is kept larger than the PB content (S/B 70/30) which could considerably reduce the repulsive interaction between PS outer blocks and the S/B random middle block. Hence, in order to overcome the influence of χ parameter on phase separation, N is increased. Thus through tuning the M_w of the block copolymer chains an ordered lamellar structure was achieved even at 80 wt.-% of PS.

However, in order to estimate the threshold M_w for attaining transitions from weakly ordered (LN-42) to a ordered lamellar structure (LN-44) it is necessary to calculate the critical $(\chi N)_c$ value required for phase separation. It was illustrated by Leibler's weak segregation theory that, diblock copolymers would order at χN=10.5 (at f=0.5 where f refers to the volume fraction of PS) [2]. Later Mayes and Olvera de la Cruz [6] extended this treatment to triblock copolymers and showed that by coupling of two symmetric diblocks results in increasing the χN=18 near the order-to-disorder transition (ODT). In the present scenario, the middle block constitutes a certain fraction of PS content in the form of a random middle block; this could reduce the influence of χ in the phase separation process. Hence the effective interaction parameter χ_{eff} should be considered. The relation for χ_{eff} is given in equation (1) where f_{PS} is the mole% of PS in the random middle block [7].

$$\chi_{eff} = \chi.(1 - f_{PS})^2 \qquad (4.1)$$

However, recently the temperature dependency of the interaction parameter (χ) for a similar type of triblock copolymers with the mol% of S/B in the middle block as 55:45, was extracted by fitting the SAXS patterns at temperatures well above the ODT and is given in equation (2) [equation 3.7 in chapter 3].

$$\chi = 0.0276 + \frac{3.577}{T(K)} \qquad (4.2)$$

As the segmental relaxation at low temperatures near $T_{g\text{-}PS}$ could show a significant influence in interaction between heterogeneous blocks, the χ from equation (4.2) is calculated above the T_g of PS phase i.e. at 393 K. The χ attained from equation (4.2) for triblock copolymers with a S/B ration of 55:45 is normalised with the mole% of PS (55%) in the random middle block. Thus, the χ_{eff} for the present triblock copolymers can be obtained by substituting χ from equation (4.2) in equation (4.1) with f_{ps}=0.66 which corresponds to the mole% of PS in the random middle block. The final product of χ_{eff} and N is listed in Table 1. From Table 1 it can be affirmed that the combined parameter $\chi_{eff}N$ for LN-41 and LN-42 are staying below the critical value for attaining a transition from disordered to ordered structures ($\chi_{eff}N$ =18), whereas it stays slightly above and well above the critical $\chi_{eff}N$ in case of LN-43 and LN-44

respectively. In the context of crude analysis we have neglected the influence of fluctuation effect, which should be considered in block copolymers. Thus the quantitative results obtained by studying the phase behaviour in triblock copolymers illustrate a trend in showing a transition from a disordered to an ordered microphase separation nature. At low M_w the entropy term is dominating the repulsive enthalpy interactions between PS and PB within the chain architecture i.e. in case of LN-41 when compared to LN-44, which results in the absence of phase separation. However, the presence of weakly ordered structure in LN-42 and LN-43 describe the fact that with the increase in M_w the chain length is increasing which results in a decrease of influence of entropy term during the phase separation. A balance between the enthalpic and entropic interactions was observed to be reaching very close in between LN-42 and LN-43. Thus the critical value of N that should be considered for attaining phase separation in similar tribock copolymers can be easily estimated from Table 1 by calculating N at $\chi_{eff}N_S$ =18 and the molecular parameters can be adjusted accordingly.

4.3 Dynamic Mechanical Analysis (DMA)

Figure 4.3 depicts the temperature dependency of storage modulus (G') and loss modulus (G'') curves for the investigated triblock coplymers which are studied for quantifying the phase behaviour in the triblock copolymers with respect to variation in M_w. The ordered microphase separated structure and the disordered homogeneous structure were characterized by their glass transition (T_g) behaviours. From the dynamic loss modulus (G'') it could be observed that in spite of heterogeneity in the molecular architecture LN-41 and LN-42 are showing a single glass transition temperature, whereas LN-43 and LN-44 are showing two distinct glass transition temperatures which correspond to $T_{g\text{-}PS}$ and $T_{g\text{-}PB}$ for PS and PB-rich phases respectively. Thus the existence of two distinct T_g's for LN-43 and LN-44 reveals the persistence of phase separation in the bulk samples. The nature of the T_g peaks and the distance between the $T_{g\text{-}PS}$ and $T_{g\text{-}PB}$ peaks in LN-44 are more pronounced when compared to LN-43. Such observations are attributed to enhanced phase separation in LN-44 when compared to LN-43 and this is confirming the observed local morphological in TEM in terms of bulk material behaviour. However, in both LN-42 and LN-43 the $T_{g\text{-}PB}$ is shifted to high temperature when compared to the T_g of pure PB phase (-95 °C) and at the same time the T_g of the PS phase is shifted to lower temperature when compared to T_g of pure PS phase (100 °C). Such shifting in T_g peaks reveals the miscibility between the heterogeneous phases [8]. The miscibility between PS and PB phases in LN-43 and LN-44 could be influenced by

two factors i.e. either from the S/B random middle block or from the partial miscibility of the PS end blocks in the S/B random middle block [4,5].

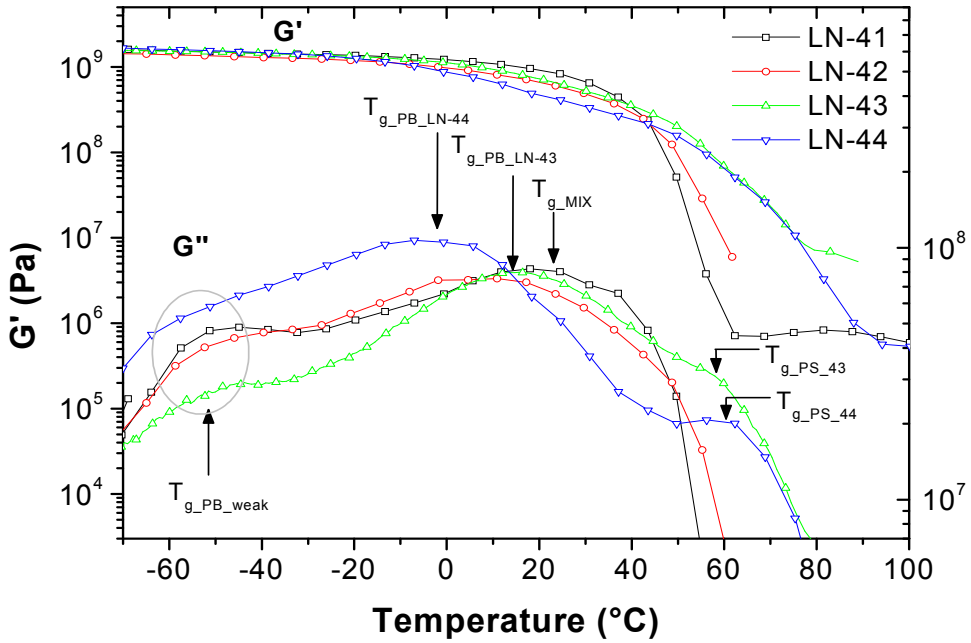

Figure 4.3 Dynamic mechanical analysis of the triblock copolymers

The T_g behaviour observed from DMA is reconfirmed by DSC-measurements and the T_g values are listed in Table 1. Due to the limitation in the measurement time, the DSC of LN-43 was not measured, but the significance in the peak positions can be clearly seen in Figure 4.3 as indicated by arrow marks. The Fox equation was used to identify the factors influencing the shift in T_g's in a quantitative manner. The experimental T_g's from DSC measurements are compared with the theoretical values from Fox equation and are summarized in Table 1. The mathematical representation of Fox equation is shown below.

$$\frac{1}{T_{g-soft}} = \frac{w_{PS}}{T_{g-PS}} + \frac{w_{PB}}{T_{g-PB}} \qquad (4.3)$$

Where (w_{PS}, $T_{g\text{-}PS}$) and (w_{PB}, $T_{g\text{-}PB}$) represent the weight fraction and glass transition temperatures of pure PS and PB phases respectively. In case of LN-44 the Fox equation is applied only for the random middle block by considering w_{PS} and w_{PB} as 0.7 and 0.3 wt.-% (as the ratio between S/B in the random middle block is 70 :30) respectively, which accounts that the random SB middle block alone is influencing the shift in $T_{g\text{-}soft}$. As expected, the experimentally observed $T_{g\text{-}PB}$ at 4 °C is in exact accordance with the theoretical $T_{g\text{-}soft}$ obtained from Fox equation. Hence, the partial miscibility of PS outer blocks in the SB random middle block is expected to be completely absent. However, the immiscible outer PS blocks which constitute 40 wt.-% of PS, could act as the effective PS content for phase

separation in LN-44. According to the theoretical phase diagram constructed by Matsen, (shown in Figure 3 of ref. 9) in symmetric ABA type triblock copolymers where the asymmetric parameter τ = 0.5, a lamellar morphology can be observed at 40 wt.-% of fraction A, both in case of χN=30 and χN=40. Thus, by comparing the observed lamellar morphology of LN-44 from TEM micrographs with the theoretical phase diagram, it reveals the fact that, 40 wt.-% of PS from the end blocks in the triblock copolymer chain architecture is completely contributing in formation of lamellar structure. On the other hand in case of LN-41 and LN-42, the observed single broad T_g is closely in accordance with the theoretical $T_{g\text{-soft}}$ only when the overall composition of PS and PB wt.-% in the triblock chain architecture are accounted (i.e. 80 wt.-% PS and 20 wt.-% PB). Therefore the T_g's for LN-41 and LN-42 which are in the range of 36 to 42 °C are named as $T_{g\text{-MIX}}$, which arise due to complete miscibility of PS blocks with the random middle block. From Figure 4.3 it can be also observed that, in the low temperature range i.e. in between -40 to 60 °C appears a weak T_g peaks for both LN-41 and LN-42. Such $T_{g\text{-weak}}$ peaks inspite of disordered structures could be arising due to the presence of some uncoupled diblock copolymers along with the triblock copolymer chains during synthesis process. Thus a comparative study of the experimental results with the theoretical facts reveal that LN-41 and LN-42 are staying in disorder state, whereas LN-43 and LN-44 forms a phase separated structure.

On the other hand the variation of storage modulus G' with respect to temperature for all the triblock copolymers can be readily studied from Figure 4.3. It can be observed that in the glass zone i.e. below the $T_{g\text{-PB}}$, the G' for all the samples remains at a constant value. The constant modulus in the glass zone is due to the similar wt.-% of PS (80 wt.-%) and same chain architecture. Further, the G' of LN-43 is showing a nonlinear decrease in the modulus with respect to temperature and this can be seen more prominently in LN-44. Whereas a sharp drop in G' above T_g is observed for LN-41 and LN-42. Thus the nonlinear decrease in G' along with weak temperature dependency in LN-43 and LN-44 could be due to the elastic nature which arises from the collective deformation of PS and PB phases due to the presence of phase separated structure. On the other hand, in case of LN-41 and LN-42 the samples failed to respond to the applied torque and start flowing above the T_g which reaffirms the absence of phase separation in the bulk samples.

4.4 Rheology

The influence of the overall M_w in triblock copolymers on rheological properties was studied with the aid of their master curves. The master curves of storage modulus (G'), complex viscosity ($|\eta^*|$) and loss-tangent (tan δ) for LN-41 to LN-44 are shown in Figure 4.4a to 4.4c

respectively. The dynamic mechanical spectra are constructed within the linear viscoelastic regime using Time-Temperature-Superposition (TTS) principle. Since the TTS curves for loss modulus (G'') have a similar frequency dependence like that of storage modulus (G') they are not shown here. The extended frequency window obtained by constructing master curves can be broadly divided into two regions, the chain relaxation frequency range and the non-terminal frequency range [10] as shown in Fig. 4a. The chain relaxation frequency range is similar to the entanglement regime, which is commonly observed in homopolymers. At high frequencies within the chain relaxation regime, the variation in the M_w is observed to be insignificant on storage modulus. However, with the decrease in frequency, a gradually decrease in G' is observed for LN-41 and LN-42, whereas a plateau like behaviour which is extended towards low frequency regions is observed in case of LN-43 and LN-44. On further reduction in the frequency, i.e. the frequency range which is usually considered as terminal frequency regime for homoplymers was also reflected in case of LN-41 and LN-42. In this frequency range, due to the homogeneous nature in the polymer melt the frequency dependency of G' and G'' are described by the equation $G' \sim \omega^2$ and $G'' \sim \omega$ as $\omega \to 0$ [10]. Interestingly the terminal slopes for LN-41 and LN-42 were observed to be 1.9, which is very close to that of the homopolymer melt. The slight deviation in the terminal slope could be due to the composition fluctuations present in one-phase region of LN-41 and LN-42. However, a non-terminal response with a slope of 0.73 is recognised in case of LN-44. A transition from terminal to non-terminal response can be observed in case of LN-43 with a terminal slope of 1.67. It was reported by Kossuth et al. [11] that the variation in the terminal slopes in block copolymers is mainly attributed to their persisting morphology. Due to the presence of a phase separated structure some tethered junctions exists across the interface which constrain the deformation of the nanodomains as individual units, causing a longer relaxation time. These topological constraints due to tethered junctions act as physical cross-linking points restricting the PS chain dynamics on much larger scale than the local segment size. Thus by comparing the slope of G' in the terminal regime of LN-44 and LN-43 with LN-41 and LN-42 it could be reconfirmed that with the increase in M_w the triblock copolymers are phase separating and the phase separation is gradually going from a disordered structure to an phase separated structure in between the M_w of LN-42 and LN-43. Thus the low frequency rheological response is strongly influenced by the phase separation in the triblock copolymers.

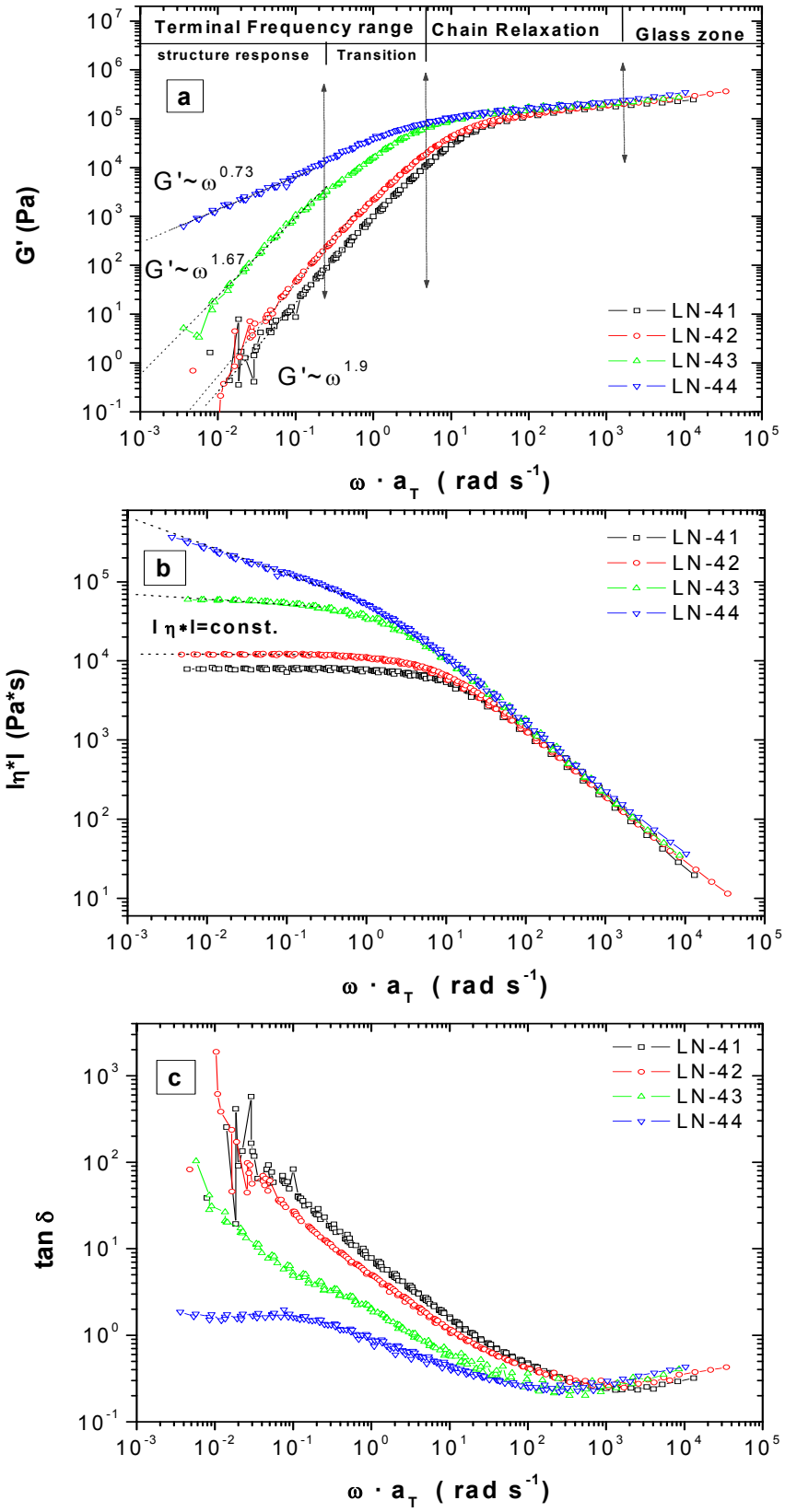

Figure 4.4 Master curves for (a) storage modulus G', (b) complex viscosity |η*| and (c) tan δ of measured triblock copolymers at T_o=160 °C

The significance of M_w on the frequency dependence of complex viscosity (|η*|) and loss tangent (tan δ) is revealed from figure 4.4b and c. At the high frequency regime, |η*| is

increasing sharply with the decrease in frequency for all the samples. However, on further decrease of the frequency the |η*| of LN-41 and LN-42 is remaining independent of frequency, which is an indicative of complete relaxation of copolymer chains at low angular frequency. Whereas in case of LN-43, it is still remaining independent of frequency but with an enhanced zero shear viscosity. However, in LN-44 it is increasing with a reduced slope. Such an increasing trend in |η*| at reduced frequency is attributed to the shear thinning behaviour. Morrison et al. [12] have studied the rheological behaviour of SBS triblock copolymers at low frequency regime and reported that, the unusual shear thinning behaviour in block copolymers is due to the persistent phase separated micro domains in the form of grains, where the tethered junctions between these grain boundaries could contribute in extending the time for complete relaxation of the block copolymer chains. Similarly, the phase separation in LN-44 is significant in showing yield behaviour at low frequency due to the collective deformation of heterogeneous phases within the measured temperature and frequency range. On the other hand the master curve of tan δ (Fig 4.4c) which represents the ratio between viscous to elastic components is strongly increasing in both LN-41 and LN-42 with the decrease in frequency and the increase is nominal in case of LN-43. Whereas in LN-44 the tan δ is increasing until intermediate frequency range followed by a plateau like behaviour at reduced frequencies. The strong increase of tan δ for LN-41 and LN-42 is attributed to the liquid-like flow behaviour which arises from the increased energy dissipation per cycle in the melt through enhanced viscous modulus at reduced frequency. The absence of such behaviour in LN-44 indicates highly elastic solid-like melt, as evident from the plateau like behaviour in the master curve of tan δ in the low frequency regime. A transition from liquid-like to solid-like behaviour can be observed with the increase in the over all M_w as seen from the terminal response of tan δ in LN-43 and LN-44.

4.5 Relaxation spectra

The influence of the microstructure on the relaxation behaviour of the polymer chains was studied from their relaxation spectra constructed from the corresponding master curves at 160 °C. The master curves are transformed into relaxation spectra by employing nonlinear regression method with the aid of Rheometric scientific Instrument software (RIS). Figure 4.5 depicts the relaxation spectra for the investigated block copolymers and the data characterizing the spectra are shown in between the dotted lines. Within the characteristic range the relaxation spectra of LN-41 is observed to be typical for a mono dispersed homogeneous polymer system. The prominence of peak within the relaxation time in LN-41 corresponds to the terminal relaxation strength. In LN-42 and LN-43 this terminal relaxation

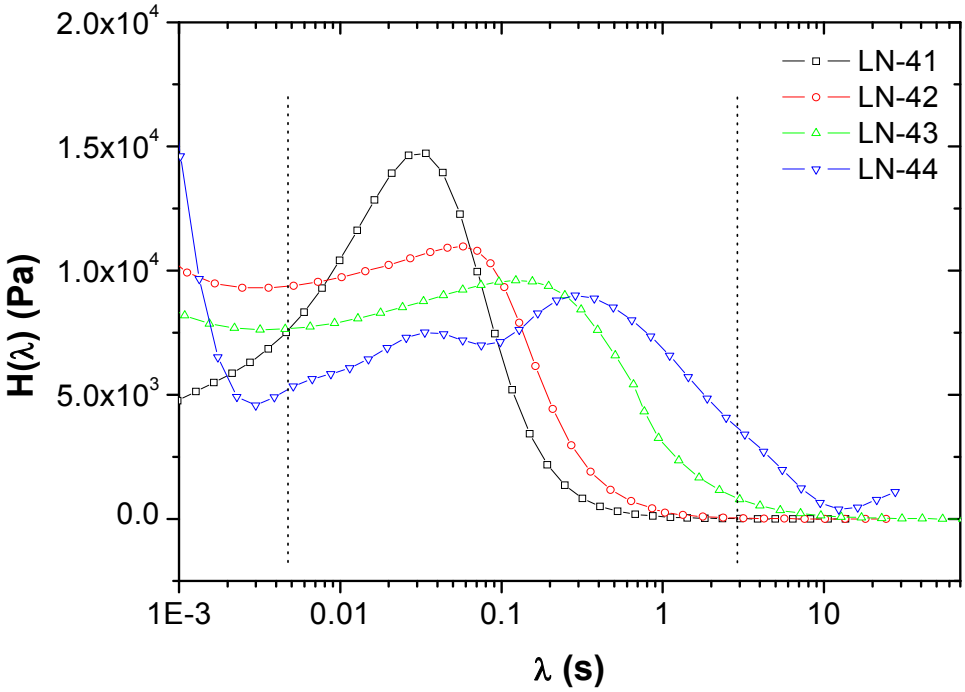

Figure 4.5 Relaxation spectra for the three triblock copolymers calculated with nonlinear regularization method. The data characterizing the spectra are shown within the doted lines.

peak is observed to shift towards longer relaxation times along with simultaneous decrease in H(λ) with the increase in M_w. The hindrance in terminal relaxation time along with the reduced relaxation strength in LN-42 and LN-43 are attributed to the presence of a weakly microphase separated structure which lies very close to the spinodal decomposition point as seen in the phase diagram of triblock copolymers [3]. However, a considerable difference in the relaxation behaviour of LN-44 compared to other triblock copolymers with low M_w can be observed from Figure 4.5. The differences are attributed to the presence of characteristic relaxation regime after the glass zone. Due to the persistence of phase separation within the measured temperature range, the relaxation process in LN-44 could take place in two ways, firstly by the contribution from the diffusion of the outer block out of the microdomains and secondly by the subsequent diffusion of the released chains through entangled mid-block chains. Such extended relaxation process results in showing two distinct relaxation zones, which could be due to the hindrance in PS chain relaxation by the tethered junctions along the lamellar structure in LN-44 [13]. Thus the phase separation occurred due to high M_w in triblock copolymers is showing a predominant influence on the relaxation behaviour.

4.6 Mechanical properties

The mechanical properties of the investigated triblock copolymers were characterized from their tensile behaviour and Figure 4.6 depicts their stress-strain curves at room temperature. The tensile properties are observed to be strongly influenced by the M_w and the phase

separation in block copolymers. At low M_w i.e. in case of LN-41 the material undergoes a brittle failure (strain at break ~ 3 %) with a tensile strength of ~ 48 MPa which is attributed to the predominance of 80 wt.-% of PS in the disordered structure. An increase in M_w from 140 kg/mol to 149 kg/mol results in a weakly segregated microphase structure leading to a reduction in tensile strength up to 11 % and Young's modules up to 19 % (Fig. 4.7) with a slight increase of strain at break to ~20 %. Interestingly, at high M_w i.e. at 187 kg/mol, a dramatic influence of M_w on the tensile behaviour can be observed, i.e. LN-43 shows a ductile behaviour with high strain at break of 200 % followed by a nearly constant stress which resembles the cold drawing process until 200 % strain. Whereas in case of LN-44, above this regime, the stress is increasing i.e. strain hardening is taking place until 340 % of strain followed by the failure of the sample with a tensile strength of ~30 MPa. Further the deformation behaviour in both LN-43 and LN-44 is observed to be embossed by a distinct yield point with a yield strength of ~ 29 and ~ 21 MPa respectively (yield stress of LN-42, LN-43 and LN-44 is shown with an arrow mark in Figure 4.7). Within the cold drawing process, the gradual orientation of the PS chains along with a pronounced orientation of soft SB middle block chains bridging between glassy PS domains can be expected.

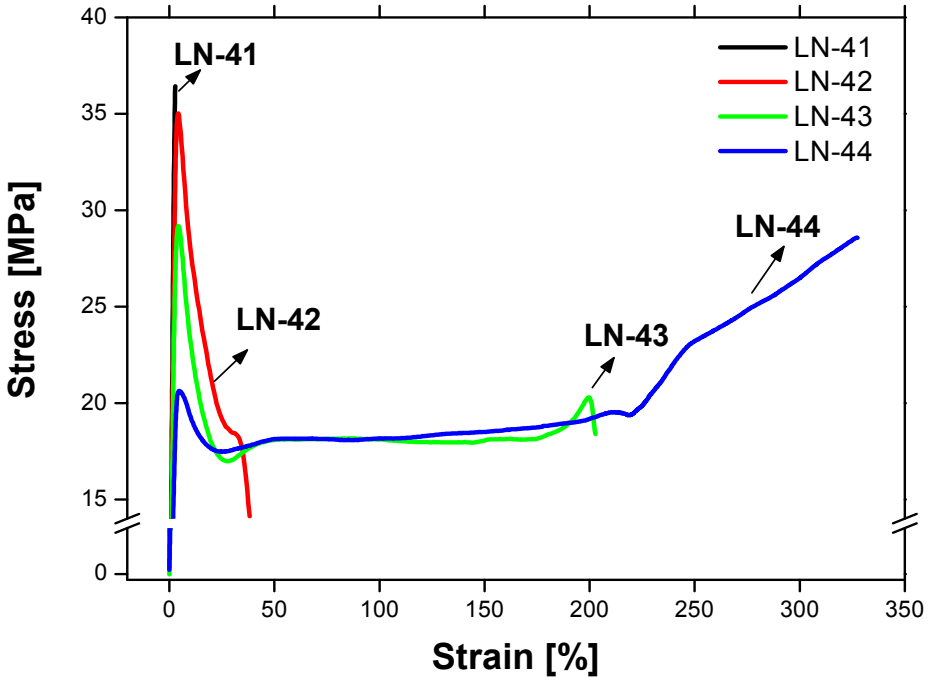

Figure 4.6 Mechanical properties of the triblock copolymers as a function of M_w: Stress strain behaviour of the S-(S/B)-S triblock copolymers influenced by variation in the M_W

Such orientation behaviour in S-B-S triblock copolymers was studied earlier by Sakurai et al. [14] by means of FT-IR measurements. The observed strain hardening is attributed to the plastic deformation of the PS microdomains. An enormous increase in strain

at break even at 80 wt.-% of overall PS-content is attributed to the presence of periodically ordered lamellar structure in LN-44.

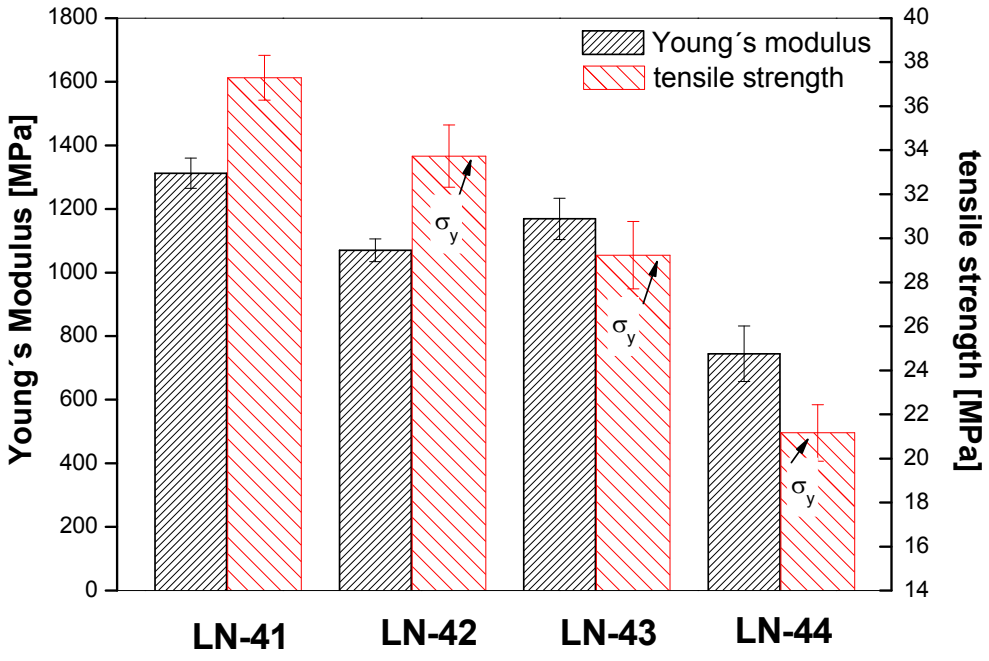

Figure 4.7 Mechanical properties of the triblock copolymers as a function of M_w: Young's modulus and tensile strength of the triblock copolymers.

As reported by Holden et al. [15] the mechanical behaviour in of PS-PB block copolymers is mainly governed by the ordering of microphases with periodic arrangement of PS and PB segments but not only due to the segregation of blocks in distinct microphases. Such ordering is prominent in LN-44 with lamellar morphology compared to LN-43. In LN-44 the soft rubbery SB middle block bridges the two PS glassy domains due to the presence of lamellar structure, resulting in enhancing the effect of physical cross-linking [15]. As a result of such physical cross-links, the collective distribution of the stress between PS and PB phases take place in a more efficient manner, which results in the observed toughness in LN-44. In our early communications, the tensile properties of similar type of triblock copolymers were studied [16]. It was observed that the cold drawing process and the strain hardening in S-(S/B)-S type triblock copolymers possessing lamellar structure is mainly governed by the balance between the M_w of the PS outer block and the SB middle block. Hence, the M_w of the SB middle block in the triblock architecture governs the extension of the cold drawing process towards high strains. On the other hand the PS/PB ratio in the random middle block controls the tensile strength of the material with in cold drawing process. The specific molecular architecture combined with high M_w leads to the formation of a lamellar-like structure and thus to the observed tough mechanical property profile for LN-44.

4.7 References

1. K. Knoll, N. Nießner, Macromol. Symp*,* 1998**,** *132*, 231.
2. L. Leibler, Macromolecules*,* 1980, *13*, 1602.
3. I. W. Hamley, The Physics of Block Copolymers, University Press, Oxford, 1998, ISBN 0-19-850218-4.
4. M. Thunga, U. Staudinger, B. K. Satapathy, R. Weidisch, M. Abdel-Goad, A. Janke, K. Knoll, Journal of Polymer Science, Part B, Polymer Physics, 2006, *44*, 2776.
5. U. Staudinger, B. K. Satapathy, M. Thunga, R. Lach, R. Weidisch, K. Knoll, Acta Mater*,* 2007, 55 (17), 5844.
6. A. M. Mayes, M. J. Olvera la Cruz, Chem. Phys,1987, *87*, 697.
7. J. Kreßler, Habilitation: "Thermodynamics and Morphology Development of Polymer Blends" 1996, TU-Dresden, Germany.
8. J. M. G. Cowie, in Developments in block copolymers*,* editor: I. Goodman, Applied Science Publishers, London, 1982, Ch. 1.
9. M. W. Matsen, J. Chem. Phy. 2000**,** 113*, 13*, 5539.
10. Y. Zhang, U. Wiesner, H. W. Spiess, Macromolecules, 1995, 28, 778.
11. M. B. Kossuth, D. C. Morse, F. S. Bates, J. Rheo. 1999, 43, 1, 167.
12. F. Morrisson, G. Le Bourvellec , H. H. Winter, J. Appl. Polym. Sci. 1987, 33, 1585.
13. Y. Zhang, U. Wiesner, Macromol. Chem. Phys. 1998, 199, 9, 1771.
14. S. Sakurai, J. Sakamoto, M. Shibayama, S. Nomura, Macromolecules 1993, 26, 3351.
15. G. Holden, E. T. Bishop, N. R. Ledge, J. Polym. Sci. C: Polym. Lett. 1969, 26, 37.
16. U. Staudinger, B. K. Satapathy, M. Thunga, R. Weidisch, A. Janke and K. Knoll, Eur Polym J 2007, 43 , 2750.

5. Synthesis of novel nanocomposites from elastomer based block copolymer by controlling the size of in situ generated sol-gel nanosilica via cross-linking

5.1 Cross-linking of investigated triblock copolymer LN4

The molecular parameters of the triblock copolymer, LN4 is shown in Table 5.1. The samples at different cross-linking dosage are represented as LN4-X and the samples after synthesis of silica inside the cross-linked bulk matrix at different irradiation doses are represented as LN4-Si-X where Si stands for silica and X represents the cross-linking dosage. In this section, cross-linking of triblock copolymer LN4 is discussed on the basis of gel content after irradiation of the samples at different dosages ranging from 0-500 kGy.

Table 5.1 Molecular characterization of LN4

Material	M_n (kg/mol)	M_w/M_n	Total PS content (wt.-%)	PS/(S/B)/PS (wt.-%)	S/B ratio in the random copolymer block	Morphology
LN4	119	1.30	66	16/68/16	1:1	Wormlike

The cross-linking mechanism of PB segments is shown in Figure 5.1. On irradiation first the cleavage of C-H bond takes place which result in the generation of macro radicals on the carbon atom of diene unit. This free radical could react with neighbouring chain to form a cross-link and results in giving a free radical for propagating self-cross-linking in LN4 during irradiation.

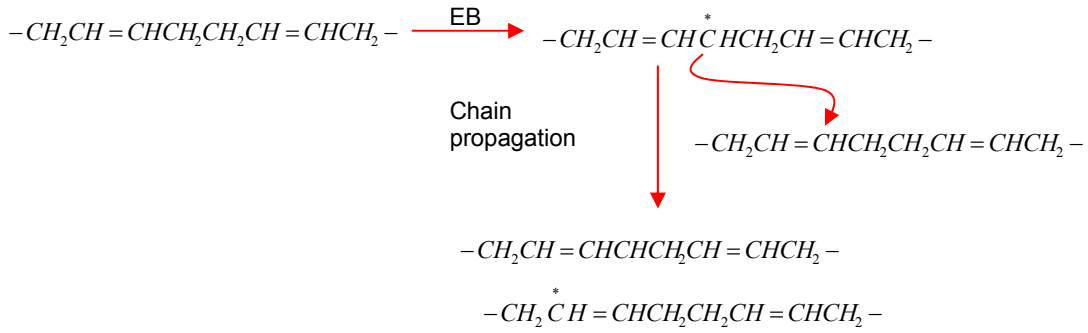

Figure 5.1 Scheme of cross-linking reaction in PB phase.

The irradiation of the samples in the present study are carried out in the electron beam accelerator located in Leibniz institute of polymer research, Dresden, Germany. The design of the electron beam accelerator is shown in Figure 5.2. The most important electrical parameters of an electron beam processing equipment are its acceleration voltage, the electron beam current and the electron beam power. The process parameters are line speed, penetration range and dose rate. When the line speed and dose rate are combined, the total delivered dose can be calculated.

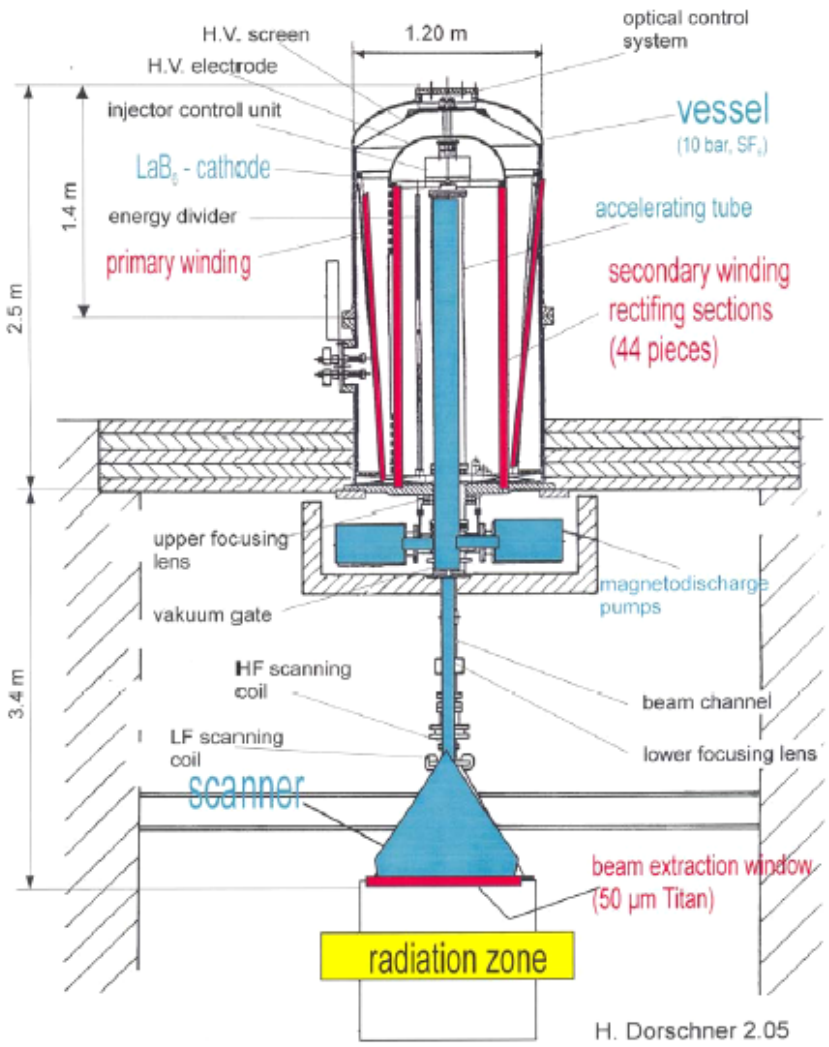

Figure 5.2 Electron beam equipment ELV-2, in Leibniz institute for polymerforschung, Dresden, Germany.

Figure 5.3 depicts the plot showing the gel fraction of LN4 at different radiation dosages. The gel content is increasing upto 150 kGy and on further increase of the radiation dose the gel content does not change significantly. The increase of gel content with the increase in the radiation dose is mainly attributed to the formation of a random three dimensional crosslink network [1]. However, beyond an optimal radiation dose the marginal increase in the gel content upto 92.7 % is ascribed to the balance of various competitive reactions (air oxidation, ether formations and chain scissioning) [2]. Whereas, there are no traces of chemical reactions observed over the surface of the sample, and the transparency in pure LN4 at 1mm thickness was observed to be restored even after irradiation at 500 kGy. It was reported earlier that the cross-linking in copolymers consisting an aromatic ring like styrene segments which are covalently bonded to butadiene segments is mainly controlled by the wt.-% of PS in the copolymer chain architecture [3]. J.P. Manion *et al.* have showed that

the aromatic ring attached to the polymer chain can increase the resistance to radiation damage by serving as 'energy shrinks'[4].

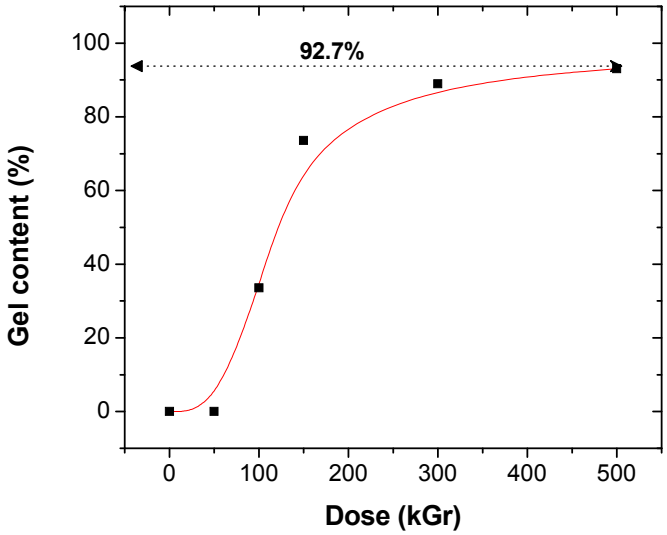

Figure 5.3 Gel content for LN4 irradiated at different irradiation dosage.

Such influences are expected to be similar in both styrene-butadiene random copolymer (SBR) and styrene-butadiene-styrene (SBS) triblock copolymers. However, in the present situation, LN4 is having PB segments in the form of SBR middle blocks which is further constrained between PS outer blocks. This special block copolymer chain architecture can further enhance the high-energy transfer from PB segments to PS segments during irradiation, which ultimately results in better resistance against cross-linking of butadiene.

In order to illustrate a quantitative picture of the cross-linked network form by irradiation of LN4 at different cross-linking dosages, the molecular weight between the cross-links (M_c) is evaluated. M_c is calculated by fitting the tensile data of all the cross-linked and pure LN4 (LN4-0 to LN4-500 kGy) with Mooney-Rivlin model for rubber elasticity where the PS phase is considered as filler inside the elastomeric PB matrix [5,6]. The wt.-% of PS in LN4 is accounted as filler by applying Guth-Gold-Smallwood equation [7] as represented by equation 5.1.

$$\sigma = (2C_1 + \frac{2C_2}{\lambda})(\lambda - \frac{1}{\lambda^2})(1 + 2.5\phi_{PS} + 14.1\phi_{PS}^{\ 2}) \qquad (5.1)$$

And, C_1 can be represented as equation 5.2 [8]

$$2C_1 = \frac{\rho RT}{M_c} \qquad (5.2)$$

Where σ is the tensile stress, ϕ is the fraction of PS acting as filler, ρ is the density of the polymer, R is the gas constant, T is the absolute temperature.

The tensile data is fitted with equation 5.1 as shown in Figure 5.4 and the M_c is calculated by substituting the C_1 value from equation 5.1 in equation 5.2 [8]. The M_c values for all the samples are listed in Table 5.2 and a decreasing trend in M_c is observed with the increase in irradiation dosage.

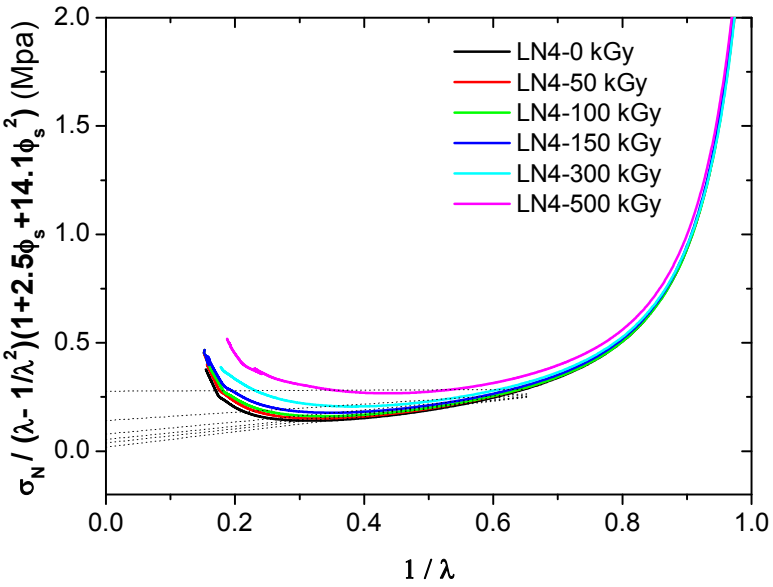

Figure 5.4 Moony-Rivilin plot for cross-linked LN4, irradiated at different dosage. Represents a systematic increase in the σ_N with the increase in irradiation dose

The decreasing trend of M_c between effective cross-links was also calculated in terms of cross-linking density (V_c) by employing Flory and Rehner equation, here V_c includes both chemical and physical interactions and it is determined from equation 5.3 [9,10].

$$V_c = \frac{-1}{2 \cdot V}\left[\frac{\ln(1 - v_r) + v_r + \chi_1 v_r^2}{v_r^{1/3}}\right] \qquad (5.3)$$

Where, χ_1 = polymer–solvent interaction parameter;

V= molar volume of the solvent

ν_r= volume fraction of the rubber in the swollen gel

ν_r was calculated using the following relation

$$\nu_r = \frac{(D_s - F_f A_w)\rho_r^{-1}}{(D_s - F_f A_w)\rho_r^{-1} + A_s \rho_s^{-1}} \qquad (5.4)$$

Where ν_r, D_s, F_f, A_w, A_s, ρ_r and ρ_s are volume fraction of rubber, deswollen weight of the sample, fraction insoluble, sample weight, weight of the absorbed solvent corrected for swelling increment, density of rubber and density of solvent respectively. The calculated V_c at different cross-linking doses were summarized in Table 5.2 and an increasing trend in the cross-linking density with the irradiation dose can be observed.

Table 5.2 Physical and chemical cross-linking densities of irradiated LN4

Sample	$V * 10^{-5}$ g.mol/cc	M_c kg/mol
0	-	64.12
50	-	31.98
100	-	22.52
150	0.22	15.41
300	1.658	8.6
500	3.786	4.4

A decreasing trend in M_c or increase in cross-linking density [Table 5.2] can directly contribute in controlling the volume of the gel during swelling. As the silica particles are generated by conversion of TEOS into silica inside these gels, a direct relation between the growth of silica particles from TEOS inside the swollen gels can be recognized. Therefore, the significance of cross-linking density in controlling the growth of silica particles is studied both qualitatively and quantitatively by making use of AFM , SAXS and TGA techniques and will be discussed in the next section.

5.2 Morphological investigations

5.2.1 Atomic Force Microscopy (AFM)

The viscoelastic phase contrast AFM images of LN4 after cross-linking at 500 kGy is shown in Figure 5.5(a) and the micrographas of LN4-Si-150, LN4-Si-300 and LN4-Si-500 nanocomposites are shown in Figure 5.5(b-d) respectively. In our early communications the physical and mechanical properties of uncross-linked LN4 was studied and correlated to its morphology [11(a,b)]. It was observed that LN4 with symmetric S-(S/B)-S triblock copolymer architecture shows thermoplastic elastomeric nature which arise from weakly segregated wormlike microstructure. The material is showing elastomeric nature even at 66 wt.-% of PS content, which is attributed to the enhanced miscibility between PS outer block in the PS/PB random middle block. From the AFM phase contrast images (Fig 5.5a) it can be observed that LN4-500 is possesses a phase separated microstructure which is unaffected

even after cross-linking up to 500 kGy. However, after sol-gel reaction, spherical shaped silica particles generated with a homogeneous distribution inside the block copolymer matrix without forming agglomerations. Further, the size and distribution of the silica particles are

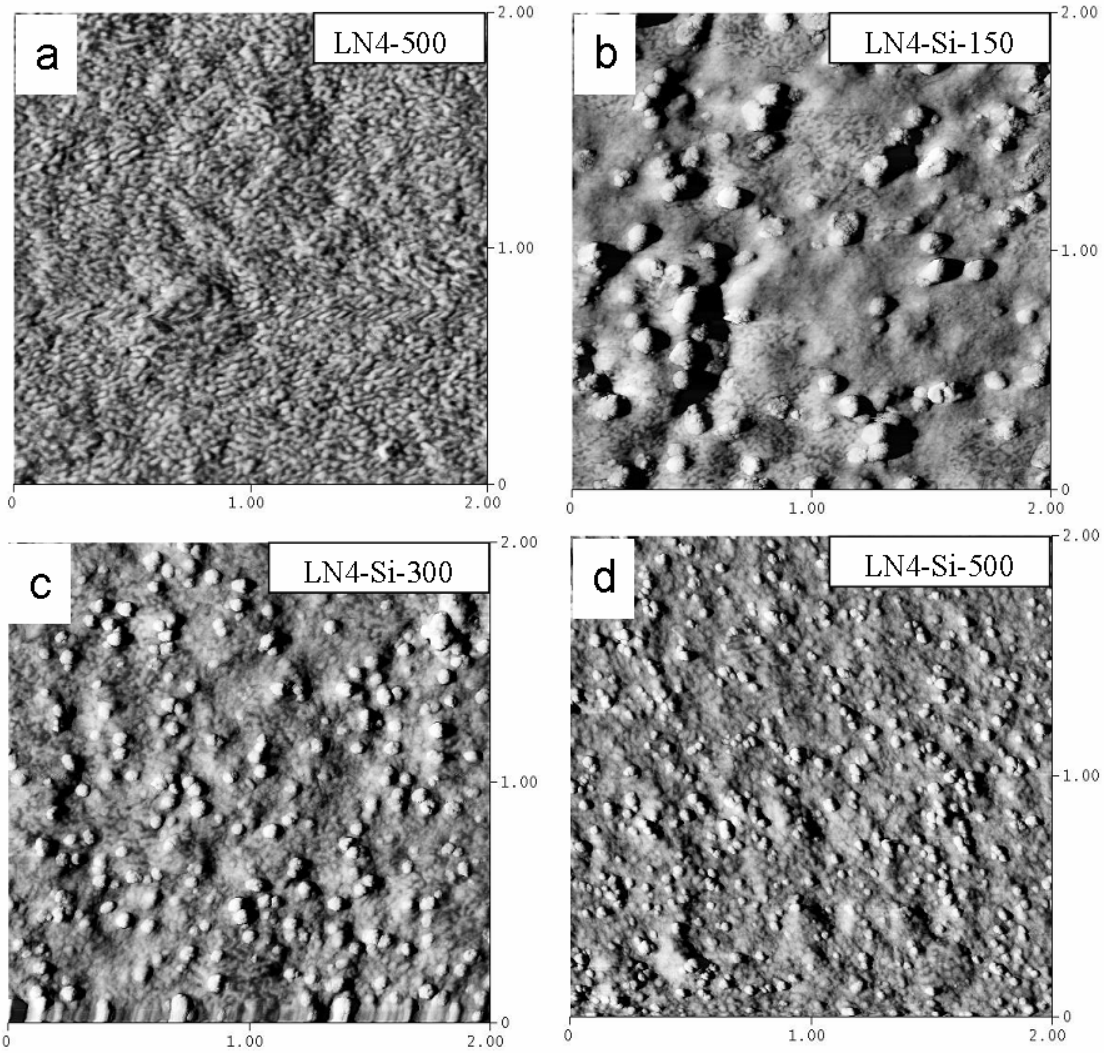

Figure 5.5 AFM images of LN4 and LN4-Si nanocomposites with scale in micrometers. (a)LN4-500 (b)LN4-Si-150, (c)LN4-Si-300 (d)LN4-Si-500

observed to be strongly influenced by the characteristics of cross-linked network, formed during electron beam irradiation. Interestingly, the size of the silica particle is observed to decrease with the increase of the cross-linking density from 150 to 500 kGy. The reduction in size of silica particle is mainly attributed to the reduction in M_c or increase in V due to the increase in irradiation dosage. Hence, the cross-linking density is observed to be crucial perameter in governing the size of silica particles. The decrease in the size of the silica particle was quantitatively investigated by making use of SAXS technique and is discussed below.

5.2.2 Small angle X-ray scattering (SAXS)

The local morphology observed from AFM micrographs is reconfirmed and quantified by studying the bulk morphology using SAXS data. Figure 5.6(a) shows the corresponding raw SAXS data for samples examined in the previous section along with pure LN4. From Figure 5.6(a) it can be observed that for neat LN4 and LN4-500, the SAXS pattern appears to be identical with a single Bragg reflection which is an indicative of phase separated microdomain structure. Appearance of similar scattering pattern in both the samples reveals

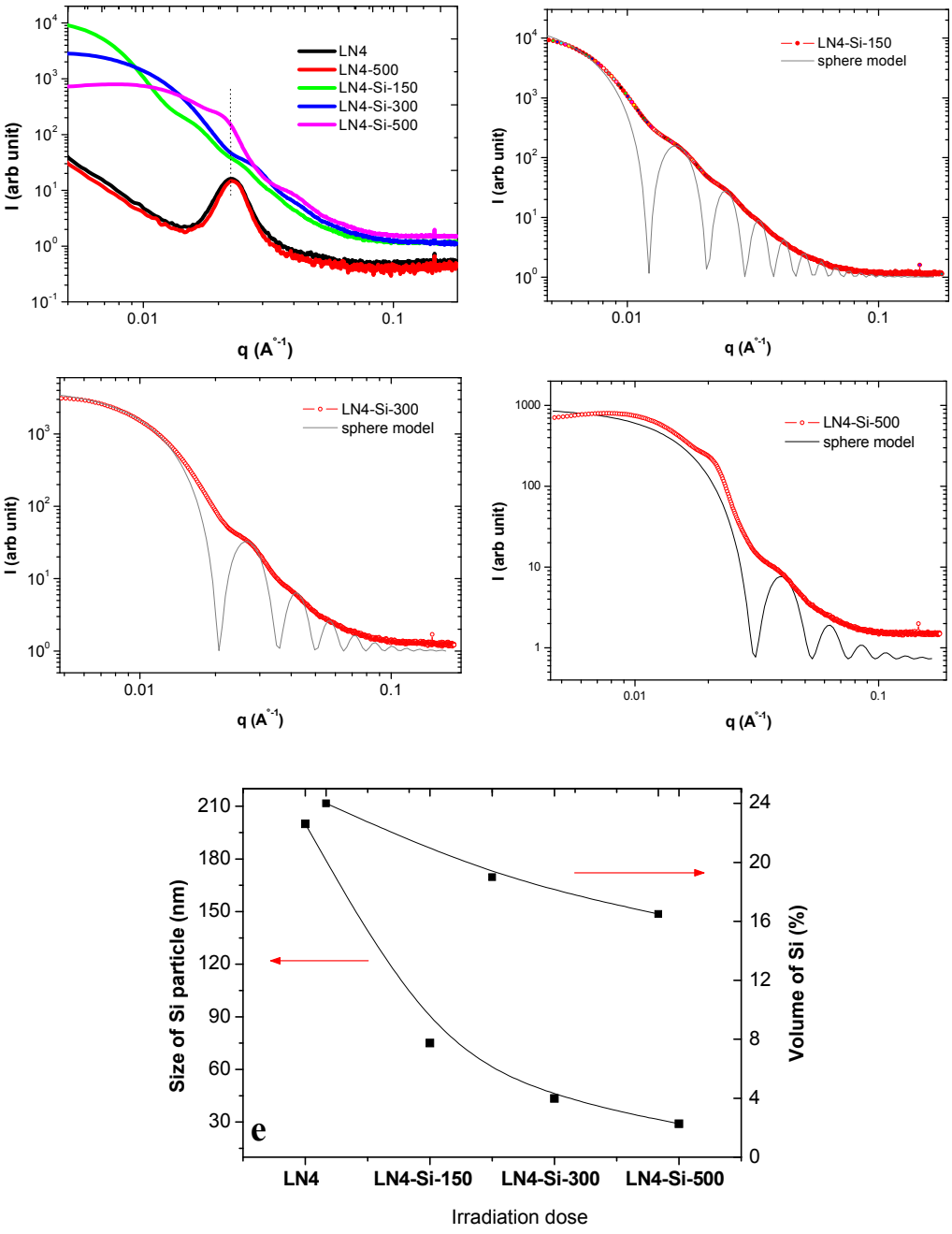

Figure 5.6 SAXS investigations for (a) LN4 and LN4-Si nanocomposites, (b) Sphere model with Gaussian size distribution fitted with raw SAXS data for LN4-Si 150, (c) LN4-Si 300, (d) LN4-Si-500 kGy. (e) Dependency of size and volume % of silica on Irradiation dose.

that cross-linking of PB phase in LN4 is showing insignificant influence on the phase separated microstructure even at 500 kGy dosage. However, synthesis of silica inside cross-linked network causes a dramatic increase in the low-q scattering while the intensity at high q scattering remains nearly unaffected. The distinct variation in low-q scattering with the increase in cross-linking density in nanocomposites is ascribed to the increase in vol.-% of silica generated in side the matrix. So, in order to obtain a quantitative picture about size and vol.-% of the silica particle that is generated during sol-gel reaction, the SAXS data was modeled using the form factor of sphere model with Gaussian size distribution as shown in Figure 5.6(b-d) [12]. The vol.-% of silica generated inside LN4 at different cross-linking densities is attained by normalising the low-q scattering with that of the vol.-% of spherical fillers inside the polymer matrix. On the other hand, through fitting the first and second order peaks from the model to the corresponding peak positions in experimental scattering pattern results in attaining average silica particle size. Similar to the AFM observations, an increase in irradiation dose results in showing considerable influence on both average particle size and vol.-% of silica inside LN4. As shown in Figure 5.6e, a decrease in silica particle size from 200 to 30 nm accompanied with a decrease in vol.-% of silica from 22 to 17 vol.-% can be observed with the increase in irradiation dosage from 150-500 kGy. Such decreasing trend in the size and vol.-% of silica with the increase of cross-linking dosage is attributed to the enhanced network constrains attained through increasing the number of cross-links per unit volume i.e. cross-linking density is directly restricting the growth of silica particles during sol-gel reaction.

From the above experimental results, a schematic illustration of growth of silica inside the phase separated LN4 is shown in Figure 5.7. The synthesis of nanocomposites via *in situ* sol-gel technique takes place in four steps as given below.

1. The elastomers (triblock copolymer LN4) is cross-linked via electron beam irradiation
2. The cross-linked elastomers are swelled in tetraethoxysilane (TEOS)
3. The TEOS which is inside the swollen cross-linked network is converted to SiO_2 gels in presence of either acidic or basic medium during sol-gel reaction
4. The final nanocomposites are attained by drying the samples above room temperature for several days

Thus from Figure 5.7, it can observe that a direct control on the size of the silica generated in side LN4 during sol-gel reaction can be attained very easily by varying the cross-linking density with in the elastomeric matrix. However, the main objective of this work is to control

the material at nanometer scale i.e. to study the significance of the interaction between the nano silica and polymer chains. Such interactions are critically investigated by studying the dynamic mechanical response of these nanocomposites over a broad temperature range

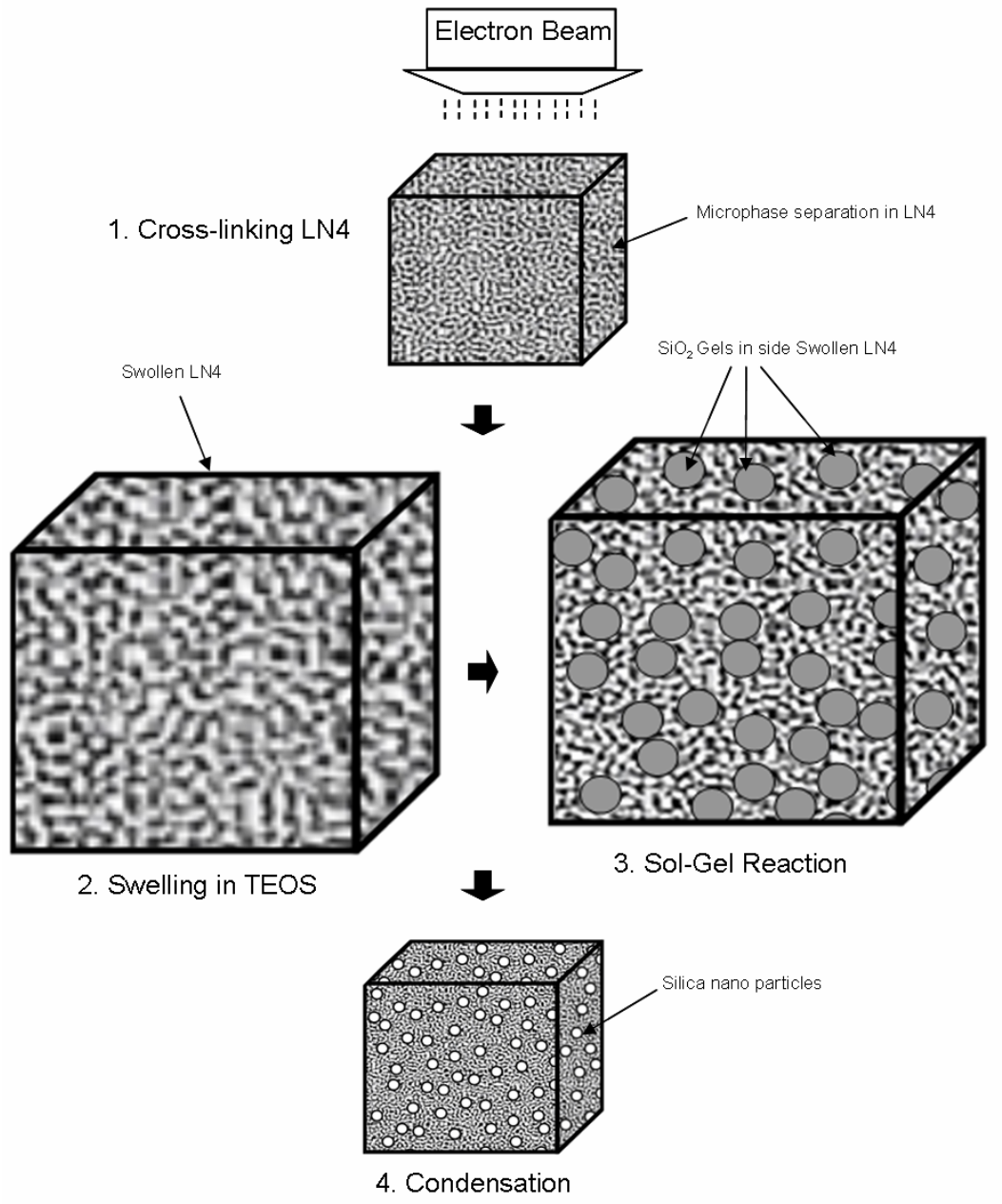

Figure 5.7 Schematic representation of cross-linking and *in situ* sol-gel reaction in LN4

5.3 Dynamic mechanical analysis (DMA)

The dynamic mechanical properties of LN4, LN-500 and LN4-silica nano composites (LN4-150-Si, -300-Si, -500-Si) are measured and the temperature dependency of loss modulus (G'') and storage modulus (G') are shown in Figure 5.8a and 5.8b respectively. As LN4 is a triblock copolymer with heterogeneity in the molecular architecture from PS and PB segments, the thermodynamic incompatibility between PS and PB segments from their

respective microdomains result in showing two distinct glass transition temperatures. In some of our recent communication the phase behaviour of pure LN 4 eas described with the aid of dynamic mechanical properties [11 (a,b)]. The glass transition behaviour of the PB-rich phase T_{g_PB} was readily captured from their loss modulus (G") peaks (Fig.5.8a). A shift in $T_{g\text{-}PB}$ towards higher temperature from -43 °C to -35 °C is observed in pure LN4 after cross-linking at 500 kGy. A considerable shift in T_{g_PB} to words higher temperatures was also observed in LN4-150 and LN-300 similar to LN4-500 (not shown here). The increase in $T_{g\text{-}PB}$ with respect to cross-linking dosage is attributed to the increase in degree of cross-linking. The cross-links in PB phase hinder the segmental motion and this then requires higher temperature for segmental relaxation.

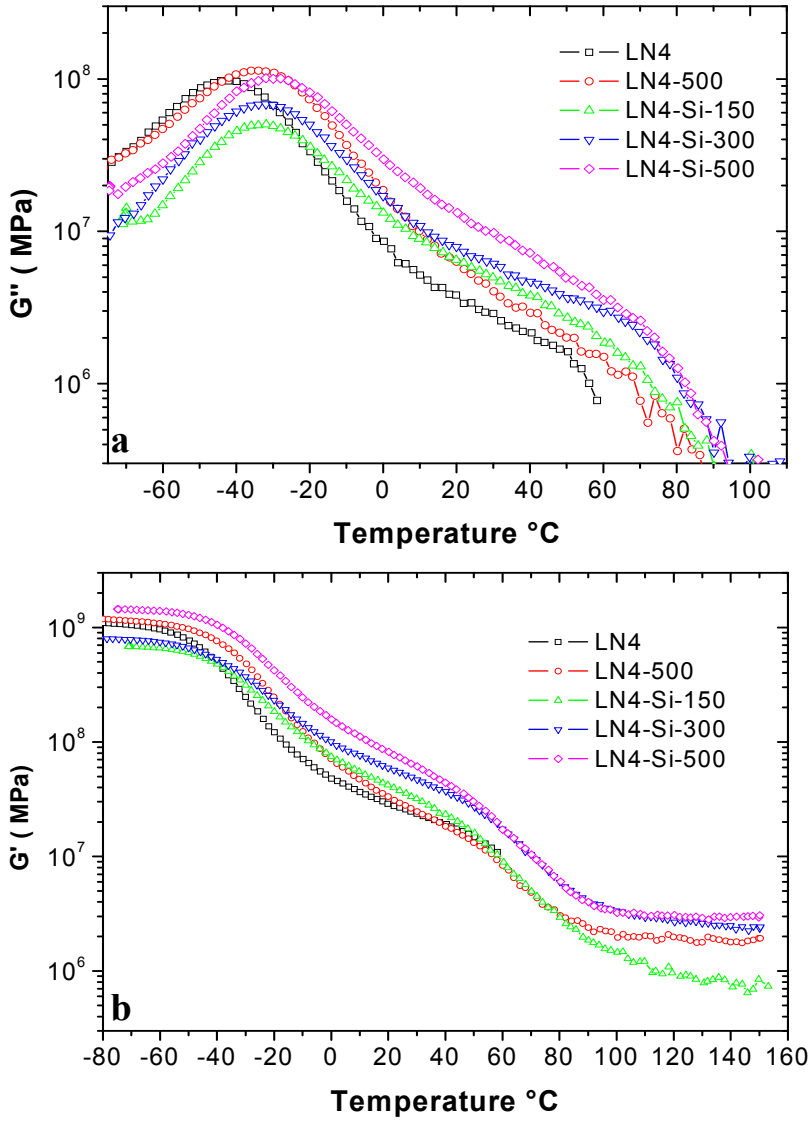

Figure 5.8 Dynamic mechanical property profile for weakly segregated block copolymer LN4 and LN4-Si nanocomposites at different cross-linking dosage(a) loss modulus (G") and (b) storage modulus (G')

On the other hand, the nanocomposites with silica particle at different cross-linking dosage were also showing a shift in T_{g_PB} towards high temperatures. Comparatively, the T_{g_PB} of LN4-Si-500 nanocomposite is staying at higher temperature with reduced peak intensity than LN4-500. The reduced peak intensity for T_{g_PB} in LN4-Si-500 is an indicative of interaction between silica and polymer chains which can hinder the segmental relaxation process [13]. The interaction between the polymer chains and the silica was described as the physical interaction by Y. Ikeda et al. [13]. They showed that the interactions are mainly arising from the entrapment of the polymer chains into the silica i.e. during the sol-gel reaction of TEOS the silica nano particle is initially in the form of swollen gel of SiO_2 network and the neighbouring polymer could get entrapped over the surface of this silica-gel during the condensation process. Such interactions can be clearly seen from the amplitude of the T_{g_PB} peak. As shown in Figure 5.8a the amplitude of the T_{g_PB} is increasing along with a slight shift in peak position towards high temperature with the increase in the cross-linking dosage in the nanocomposites (LN4-Si-150 to LN4-Si-500). Such trend in T_{g_PB} peak can be corroborated firstly with the variation in size and vol.-% of silica particles in the block copolymer matrix which have a direct influence on the interaction between silica particles and polymer chains and secondly, to the self assembling nature of LN4.

As observed from the model parameters from SAXS data, the reduction in vol.-% of silica content is smaller when compared to the reduction in size of the particle, i.e. the vol.-% of silica is decreasing from 24 to 15 vol.-% whereas the particle size is decreasing from 200 to 30 nm. Thus it can be confirmed that the surface area of the silica particle which is interacting with neighbouring polymer chains will be very high in case of LN4-500-Si when compared to LN4-Si-150. So a high interaction between silica particles and block copolymer chains can be expected in LN4-500-Si. Coming to the self assembling nature in LN4, the physical entanglements which arise from entropic and enthalpic interplay between PS and PB chains in LN4 are expected to get disentangled during swelling in TEOS. However, this disentanglement is observed to be influenced by the applied irradiation dosage. i.e. as observed from the AFM and SAXS measurements, at high cross-linking dosage, in LN4-Si-500 the phase separation of LN4 is restored. Whereas at low cross-linking dosage i.e. in LN4-Si-150 and LN4-Si-300 very less traces of phase separation can be observed from the AFM micrographs (Fig 5.5b and c). Thus the PB phase at low cross-linking doses is expected to be more impure due to absence of phase separation which results in decreasing the intensity of T_{g_PB} peak. Whereas at high cross-linking dosage the purity in PB phase is restored resulting in showing an increase intensity for T_{g_PB} peak and on the other hand

presence of nearly 15 vol.-% of silica in the cross-linked matrix results in shifting the T_{g_PB} peak towards high temperature.

Similarly, the elastic modulus G' is also observed to be significantly influenced by the variation in the interaction between silica and polymer chains. From Figure 5.8b it can be observed that for LN4-150-Si and LN4-300-Si, in spite of presence of high silica content when compared to LN4-500-Si (Table 5.3), a substantial reduction in the elastic modulus can be observed in the glassy zone (below T_{g_PB}) . This could be mainly attributed to the disordering of phase separation in LN4 at low cross-link densities as explained above. However, in case of LN4-500-Si, restoring of phase separation of LN4 through cross-linking at 500 kGy is contributing for promoting reinforcing effect from silica in the nanocomposites. In the intermediate temperature range i.e. in between 0-40°C which is recognised as the rubbery zone of PB-rich phase the G' of pure LN4 and LN4-500 are observed to be strongly dependent on temperature. Where as an increase in the modulus with a plateau like behaviour can be seen for the nanocomposites. The elastic modulus in this regime was observed to be controlled by the change in size and content of silica which arise from the corresponding cross-linking densities. At high temperature range i.e., above the $T_{g\text{-}PS}$ (100-150 °C) a rubbery plateau which characterize the cross-link network can be seen and the observed variations in the plateau modulus could be due to collective contribution from cross-linking density and reinforcement from silica in the block copolymer.

5.4 Thermogravimetric analysis (TGA)

The thermal stability and the mode of decomposition of LN4-Si nanocomposites at different cross-linking dosage were comparatively studied with respect to pure LN4. Figure 5.9a and 5.9b represent the thermo gravimetric curves and their derivative curves respectively for pure LN4 and LN4-silica nanocomposites. The decomposition temperatures at different stages and the residue remaining after 750 °C are summarized in Table 5.3. From Figure 5.9a it can be observed that the temperature at 10 %.-wt loss (as represented with an arrow mark) is reaching early for irradiated nanocomposites when compared to pure LN4 and also a nominal decrease in the weight of nanocomposites (LN4-150-Si, LN4-300-Si, LN4-500-Si) can be observed until 360 °C followed by an abrupt drop in the weight loss when compared to pure LN4. The slight decrease in the weight in nanocomposites in between 120-360 °C is due to gradual evaporation of the solvent (TEOS) and 10 wt.-% n-butailamine, which were involved during synthesis of silica in cross-linked LN4 matrix. However, the stability of LN4 is observed to be enhanced by the incorporation of silica

particles i.e. the T_{max} of the derivative curve of LN4 is shifting from 438 to 446 °C (Fig. 5.9b).

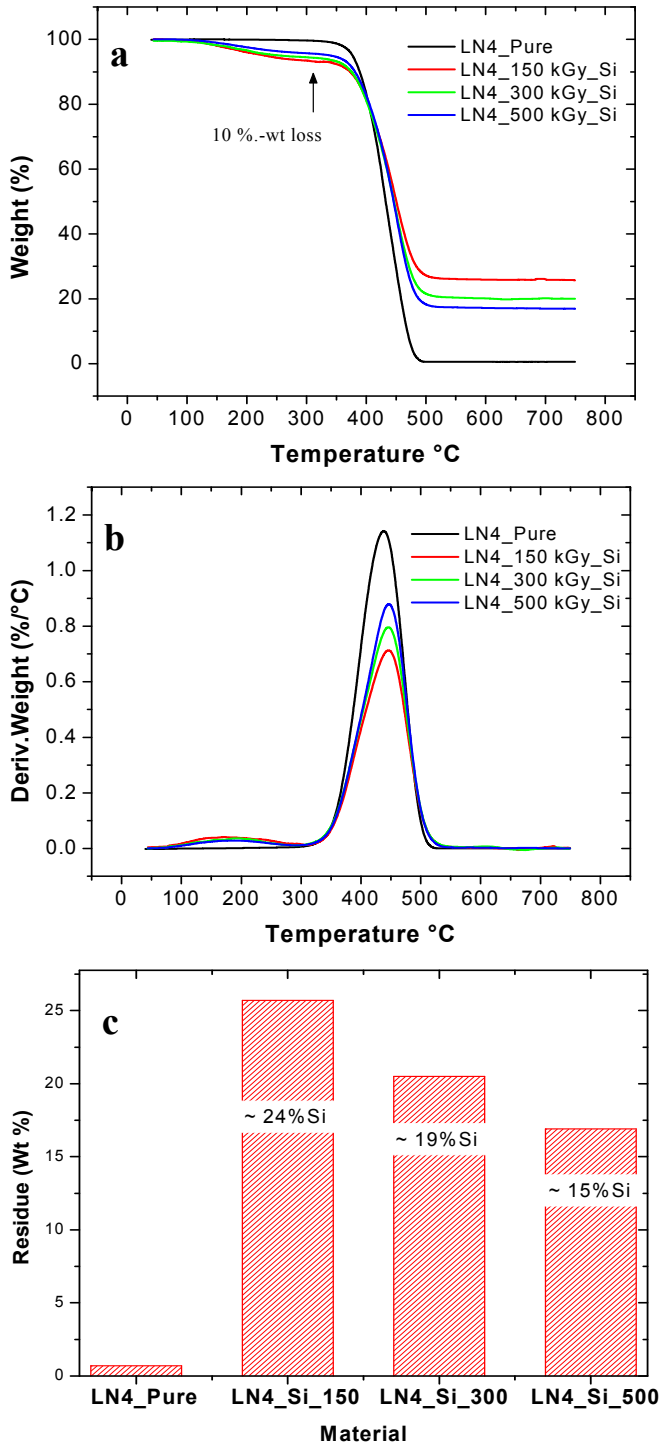

Figure 5.9 Thermo gravimetric analysis (TGA) for LN4 and LN4-Si nanocomposites (a) Thermo gravimetric Weight loss curves (b) Derivative of weight loss curves (c) Residual weight

Such shift in T_{max} was not observed in cross-linked samples with out silica particles (not shown here). The enhanced thermal stability for nanocomposites is attributed to the prominence of interaction between the silica particles with the block copolymer chains.

Table 5.3 TGA investigation on LN4 and LN4-Si nanocomposites

Sample	Degradation temperature (°C)		Residual
	T at 10% wt. loss	T_{max} of derivative curve	
LN4 pure	389	438	0.7
LN4_150 kGy+Si	375	446	23.6
LN4_300 kGy+Si	375	446	19.8
LN4_500 kGy+Si	381	446	16.2

The decrease in intensity of derivative curves with the decrease in cross-linking dosage from LN4-500-Si to LN4-150-Si further qualitatively describes the nature of the interaction as discussed in the DMA section. The residual wt.-% after 750 °C, which was quantised from Figure 5.9a, is shown in Figure 5.9c for different materials after normalizing with the residual wt.-% of pure LN4. As the nano silica particles are quite stable without loss in weight until 750 °C, the residual weight in the nano composites correspond to the wt.-% of silica generated in polymer matrix during sol-gel reaction. The observed wt.-% of silica content at different cross-linking dosages are exactly in accordance with the SAXS results and the decreasing trend in silica content with the increase in cross-linking dosage is reconfirmed from TGA.

5.5 Mechanical properties of nanocomposites (stress-strain behaviour)

The mechanical properties in TPEs from block copolymers are strongly governed by their persisting microphase separated structure [8]. From morphology and DMA analysis it was observed that the microphase separation in LN4 was strongly influenced by the sol-gel reaction. Cross-linking in block copolymers is conventionally adopted to preserve its micro structure. However, the nature of the cross-linked network i.e. the cross-linking density or the amount of gel content formed after cross-linking provides the information about the efficiency of the microstructure that was restored by cross-linking of block copolymers. As shown in Figure 5.3, only above 300 kGy of irradiation dose the gel content is reaching a marginal value of about 92.7 %. Below this the gel content is decreasing with decrease in irradiation dose. The constant value in gel content which is independent of irradiation dose above 300 kGy is attributed to the ability of the cross-links for restoring the microstructure in LN4. Thus at high cross-linking dosage (>300 kGy) one can expect that the micro structure is completely restored even after sol-gel reaction. However, at low cross-linking

dosage i.e. below 300 kGy the disentanglement of the microstructure during sol-gel reaction will be strongly depending on the irradiation dosage

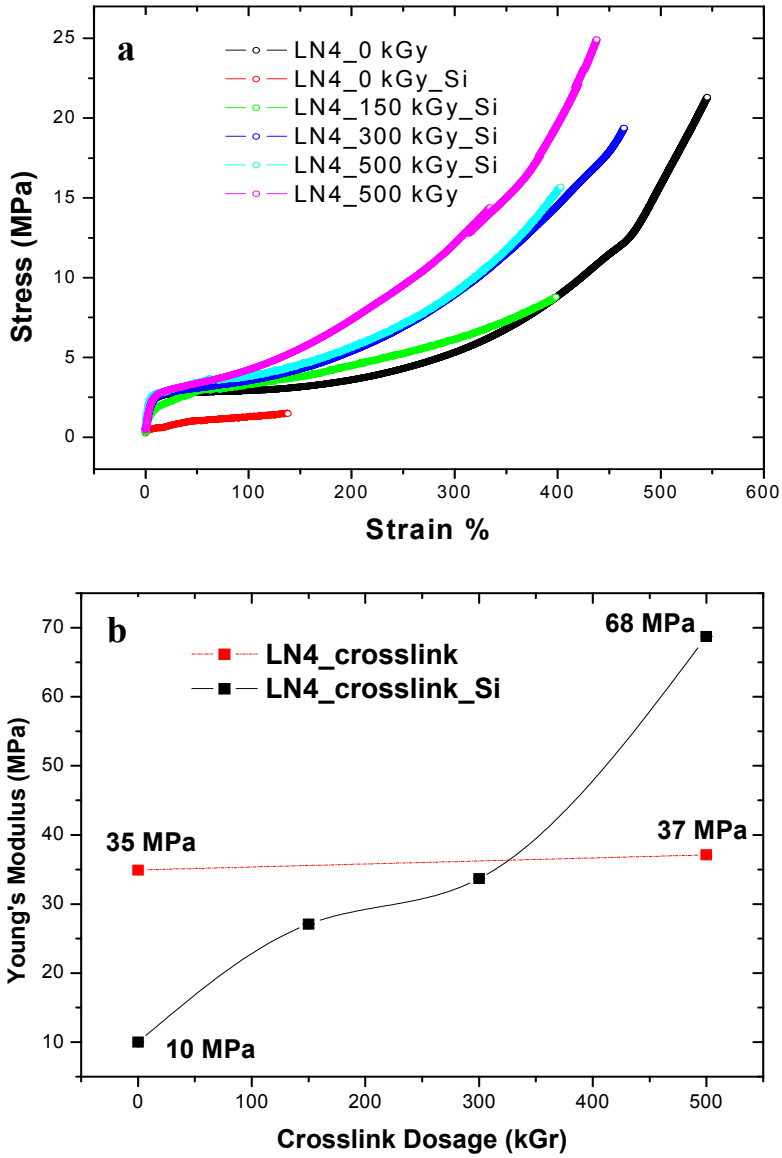

Figure 5.10 Tensile properties of LN4-nanocomposites (a) Stress-strain behaviour of LN4-nanocomposites compared with LN4 and LN4-500. (b) Young's modulus of nanocomposites compared with LN4 and LN4-500

The tensile behaviour of LN4 and LN4-nanocomposites at different cross-linking dosage were shown in Figure 5.10a. Pure LN4 is showing an elastomeric nature due to its inherent microphase separated structure. The stress-strain behaviour of pure LN4 and LN4-500 are only shown in Figure 5.10a for comparing the mechanical properties of cross-linked LN4 with that of LN4-nanocomposites. A gradual enhancement in the stress-strain behaviour was observed in LN4 with the increase in the cross-linking dose. It can be seen that in case of LN4-Si-0, the materials is having weak mechanical properties. Such weak response in the material behaviour can be attributed to the absence of cross-links within the phase separated

structure which results in generating a complete disordered structure during sol-gel reaction. Whereas in case of samples with cross-linking, the average volume of microphase separated structure after sol-gel reaction will be increasing with the increase of corss-linking dosage. Such enhanced ability to restore the phase separation even after sol-gel reaction is showing a strong influence on the stress-strain behaviour of these nanocomposites. Further the variation of cross-linking dosage in the nanocomposites is showing a significant influence on the Young's modulus when compared to cross-linked LN4 with out silica particles. From Figure 5.10b a nominal increase in the Young's modulus from 35 to 37 MPa can be observed with the increase in cross-linking dosage in pure LN4 to LN4-500.

However, in case of LN4-nanocomposites, the modulus values are staying below the pure material which is partially due to the absence of microphase separated structure. On the other hand, the modulus of nanocomposites is enhanced above 300 kGy of cross-linking dosage (Figure 5.10b). Such increasing trend in the Young's modulus is attributed to the inherent phase separated structure that was restored by high cross-linking dosage above 300 kGy. Thus a synergetic effect from the collective deformation of the microstructure in LN4 along with finely dispersed silica particles results in enhanced Young's modulus in LN4-Si-500. However, at extended strain %, the tensile strength of nanocomposites is staying well below the Stress-strain behaviour of LN4-500. Usually, nano inclusions in polymers could result in enhancing the stiffness by sacrificing the ductility. However, in the present study, the nanocomposites are showing a low stiffness and ductility when compared to cross-linkind (LN4-500) (Fig 5.10a). Such unusual stress-strain behaviour is attributed to the absence of strong interaction between the polymer matrix and Silica nanoparticle. The reason behind these unusual mechanical properties is still unclear and this prompted for a detailed study about the interactions between the polymer chains and silica particles. As an extension of the present investigations, a silane coupling agent is used to increase the chemical interactions between LN4 block copolymer chains and silica particles and these extended studies are still under going.

5.6 References

1. H. Kudoh, M. Celina, G. M. Malone, R. L. Clough, Radiat. Phys. Chem. 1996, 48, 55
2. V. Vijaybaskar. PhD thesis: IIT-Kharagpur, India, 2005
3. R. Basheer, M. Dole. Macromol. Chem. 1982, 183, 2141.
4. J. P. Manion, M. Burton, J. Phys. Chem 1952, 56, 560.
5. M. Mooney, J Appl. Phys 1940, 11, 582.
6. R.S. Rivlin, Rheology, Vol. I, Academic press New york, 1956.
7. E. Guth, J.Appl. Polymer Sci, 1963, 7, 861.
8. G. Holden, E.T. Bishop, N.R. Lege, J. Polym. Sci. C, Polym. Lett, 1969, 26, 37.
9. P. J. Flory, J. H. Rener, J.Chem.Phys, 1943, 11, 521.
10. J. E. Mark, Rubber Chem.Technol ,1982, 55, 762.
11. (a) M. Thunga, B. K. Satapathy, U. Staudinger, R. Weidisch, Abdel-M. Goad, A. Janke, K. Knoll, J. Polym Sci, Part B, Polym. Phys., 2008, 46, 329.
    (b) M. Thunga, B. K. Satapathy, U. Staudinger, R. Weidisch, Abdel- M. Goad, A. Janke, K. Knoll, J. Polym. Sci., Part B, Polym. Phys., 2006, 44, 2776.
12. Reduction and Analysis of SANS and USANS Data using Igor Pro, S. R. Kline, J Appl. Cryst., 2006, 39, 6, 895.
13. Y. Ikeda, A. Tanakaa, S. Kohjiya, J. Mater. Chem., 1997, 7, 1497.

6. Thermoplastic elastomers on the basis of multigraft copolymers and electron beam irradiation

The results of this chapter have been published in:

Kautschuk Gummi Kunststoffe Journal, 2008, 11, 597-605

6.1 Investigated Materials

The synthesis of the investigated tri and tetrafunctional multigraft (MG) copolymers with polyisoprene (PI) backbone and polystyrene (PS) branches is described by Uhrig and Mays [1]. The schematic representation of the molecular architecture for tetrafunctional and trifunctional multigraft copolymers are shown in Table 6.1a and b respectively. The molecular characteristics of tetrafunctional and trifunctional multigraft copolymers are shown in Table 6.2 and 6.3 respectively. The samples are represented as MG-n-β where n and β represents the junction point functionality and number of branch points per molecule respectively. All the multigraft copolymers from MG-4-3.3 to MG-4-8.5 in Table 6.2 are having nearly 16 wt.-% of PS content in the chain architecture, whereas it is nearly 6 wt.-% in case of MG-3-4.3 in Table 6.3.

Table 6.1 Molecular architecture of (a) tetrafunctional multigraft copolymers, (b) trifunctional multigraft copolymers

a. Tetrafunctional multigraft copolymer	**b.** Trifunctional multigraft copolymer
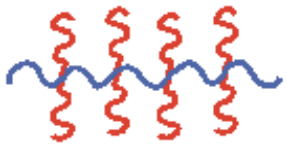	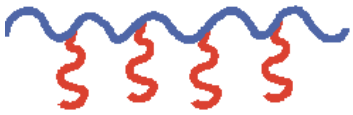

Table 6.2 Molecular characterization of tetrafunctional multigraft copolymers

Material	Branch points	Molecular weight M_w (kg/mol)
MG-4-8.5	8.5	980
MG-4-6.2	6.2	730
MG-4-5.1	5.1	620
MG-4-4.2	4.2	526
MG-4-3.3	3.3	430

Table 6.3 Molecular characterization of trifunctional multigraft copolymers

Material	Branch points	Molecular weight M_w (kg/mol)
MG-3-4.3	4.3	601

The investigations were done on solution cast films which were prepared from a non-selective solvent (toluene). The solvent was allowed to evaporate slowly over 7-14 days at room temperature. The films were then dried to constant weight in a vacuum oven at 120 °C for three days. The resulting films were about 0.2 to 0.3 mm thick.

6.2 Morphological Characterization

6.2.1 Transmission electron microscopy (TEM)

The morphologies of tetrafunctional multigraft copolymers are observed by TEM and the micrographs for MG-4-8.5 and MG-4-5.1 are shown in Figure 6.1 a and b respectively. It could be observed that the investigated tetrafunctional multigraft copolymers are showing microstructure very close to disordered lattice which generally appears near the spinodel decomposition state. However, microphase separation can be observed with wormlike PS microdomains in PI matrix. The observed morphologies are in accordance with the earlier studies from Gido and co-workers [2,3], where it was reported that the tetrafunctional multigraft copolymers with 9 vol.-% of PS content are showing similar morphology with a meshlike structure. From Figure 6.1 it can be observed that the state of ordering is decreasing with the increase of number of branch points. In the previous studies, the morphologies from tetrafunctional multrigraft having broad range of PS concentration (36 to 67 vol %) are observed to be consistent with the predicted phase diagram from Milner [4].

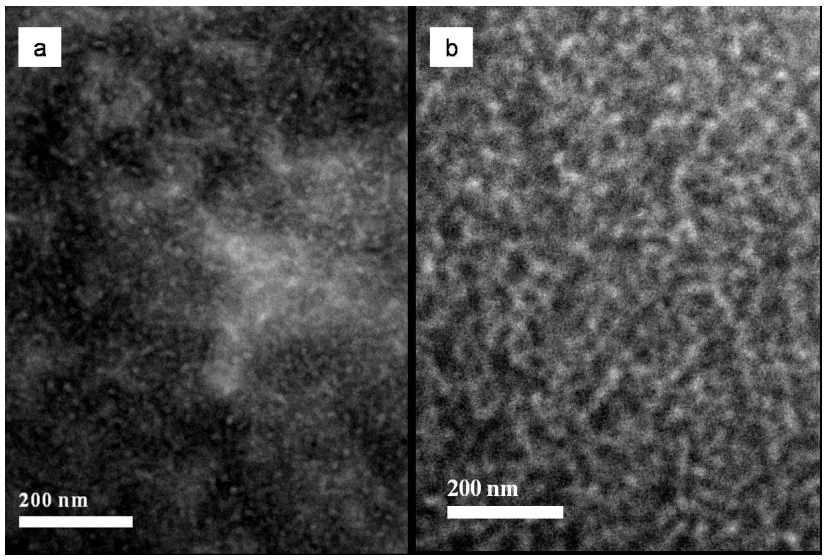

Figure 6.1 TEM micrographs of tetrafunctional multigraft copolymers with 16% of PS: (a) MG-4-8.5, (b) MG-4-5.1

But at low PS content below 21 vol % they are not in agreement with the theoretical phase diagram. Similarly, in the present study, the series of multigraft copolymers from MG-4-8.5

to MG-4-3.3 with ~ 16 wt.-% of PS are expected to form cylinders of PS in PI matrix. However, the observed morphologies are contrasting to Milner theory and the state of ordering is further dependent on number of branch points. Such deviations in the phase behaviour can be mainly attributed to significance of repulsive enthalpic interactions between PS and PI segments. Such interaction between PS and PI segments is crucial in governing the stretching strength for the PS and PI chains to get confined into their respective microdomains during the formation of well ordered structure. In order to predict the morphologies of tetrafunctional multigrafts by Milner theory, a miktoarm star of PI and PS A_2B_2 (I_2S_2) is considered as a constituting block copolymer [2]. So, in the present tetrafunctional multigraft copolymers as the PS content is regularly arranged along the PI backbones, the PS content at individual branch point i.e. in individual I_2S_2 star block is only a fraction of over all PS content in the chain architecture. Further, with the increase in number of branch points, the fraction of PS content at individual branch point will be considerably less. Thus due to the presence of 16 wt.-% of PS at different graft points ranging from 3.3 to 8.5, the enthalpic interaction which contributes for forming well ordered structures will be significantly influenced. With the increase in the number of branch points from 3.3 to 8.5, such interactions will further become insignificant which results in increasing the tendency to form weak ordered structures. The bulk morphology from these tetrafunctional multigraft copolymers was studied by using SAXS and will be discussed in the following section.

6.2.2 Small angle X-ray scattering (SAXS)

The SAXS pattern for the investigated tetrafunctional multigraft copolymers with different number of branch points is shown in Figure 6.2. From these SAXS patterns it could be observed that all the samples exhibit a strong primary peak followed by a weak and broad secondary peak. The nature of these scattering profiles correspond to the inter particle scattering which results from the irregular arrangement of domain of a specific shape [3]. The average distance between the domains D is calculated from the observed primary peak for all the multigrafts. D for Mg-4-3.3 was observed to be 25 nm and it is decreasing linearly with the increase in the number of branch points. D for Mg-4-8.5 is observed to be 22.7 nm. However, the state of ordering for all the multigraft copolymers can be compared with the nature of the second order peak in the SAXS pattern. For clear observation of such weak second order peaks the SAXS date is plotted between Iq^2 vs q as shown in the insight of Figure 6.2. The intensity of the seconded order peak is observed to be slightly strong in multigraft copolymers at low number of branch points (Mg-4-3.3) when compared to multigraft copolymers at high number of branch point (Mg-4-8.5). The stronger intensity of

the second order peak for Mg-4-3.3 when compared to Mg-4-8.5 reveals that the multigraft copolymers are having well ordered phase separated structure at low number of branch points when compared to multigraft copolymers with high number of branch points. Thus the number of branch points in the chain architecture is showing a significant influence on the phase behaviour of the multigraft copolymers. With the increase of number of branch points per molecule, the ability to form well ordered morphology is hindered due to the kinetic limitations imposed by the large number of junction points and high molecular weight [4].

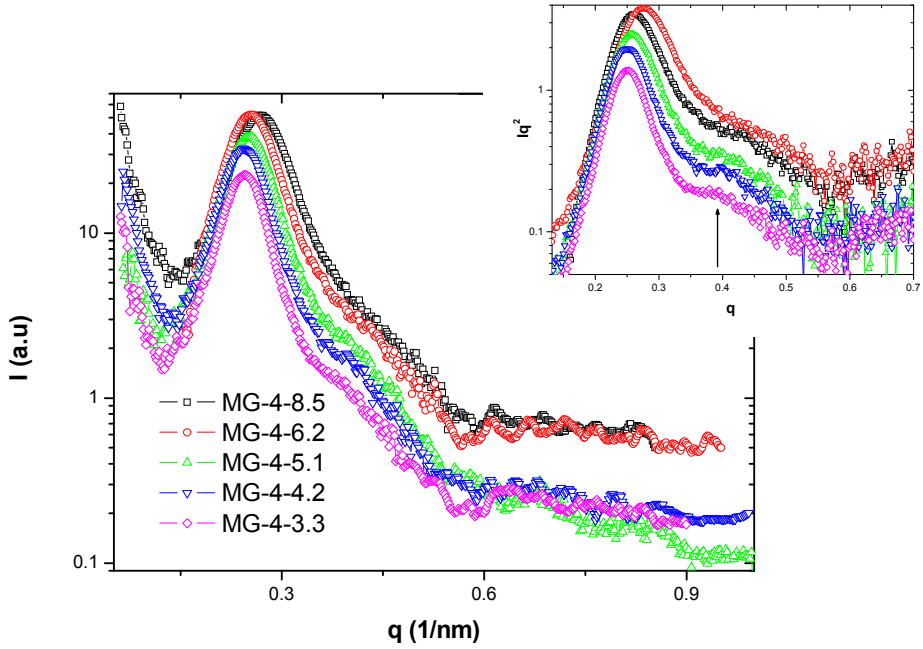

Figure 6.2 SAXS profiles of MG copolymers with different number of branch points. The inset shows the plot between Iq^2 vs q.

6.3 Dynamic mechanical thermal properties of Multigraft copolymers

Storage modules E' and loss modules E'' have been measured as a functions of temperature for the investigated multigraft copolymers and are shown in Figure 6.3. Over the whole temperature range (-80 °C to 100 °C) the multigraft copolymers are showing an increase in the modulus value with the increase in number of branch points in the chain architecture. The T_{g_PI} is observed to be partially identical for all the muligraft copolymers with the pronounced peak in the DMA curves at -40 °C. The T_{g_PI} was observed to shift to higher temperature when compared with the T_g of pure PI which is around -75 °C. This shift in T_{g_PI} to higher temperatures reveals that the PS segments on PI backbone is showing a considerable influence in the segmental relaxation of the PI. However the glass transition of the PS phase is observed from DSC analysis (not shown here) and the T_{g_PS} is ascribed to be over a broad temperature range which is due to presence of only 16 wt. -% of PS in PI phase.

As the M_w and the wt. -% of PS is similar in all the samples, the T_g of PS is expected to stay at a constant value. The T_g of the PS was theoretically calculated from the Allen-Fox equation and is expected to be at 89 °C. The presence of two distinct T_g's for PS and PI phases reconfirms the observations from SAXS studies, that the muligraft copolymers are forming phase separated structures with PS micro domains in the PI matrix. The number of branch points in the molecular architecture is showing a considerable influence on the storage elastic modulus E'.

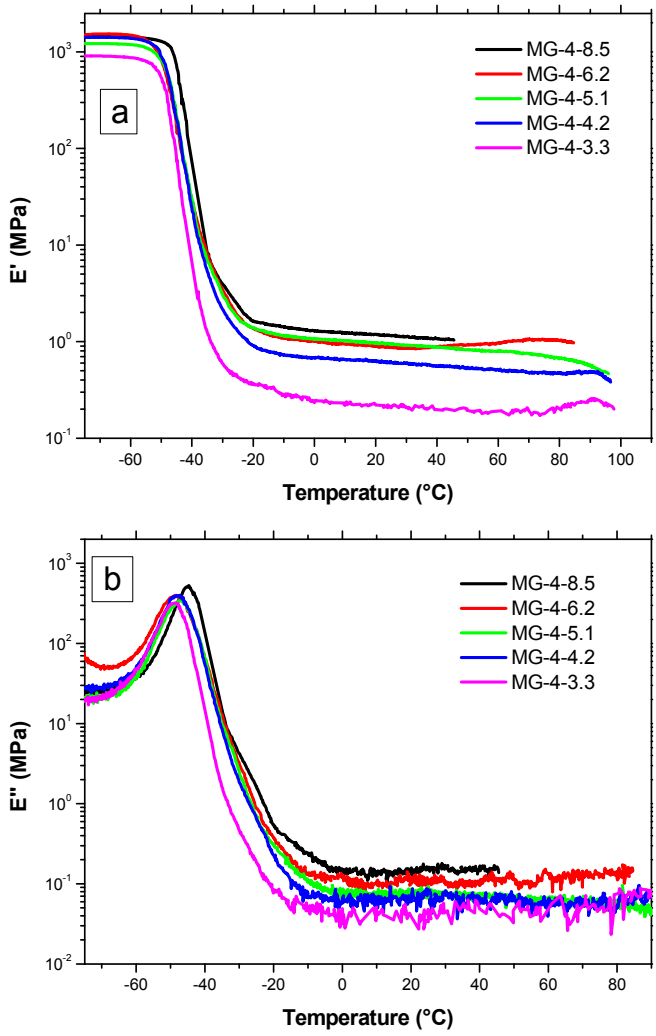

Figure 6.3 DMA of tetrafunctional multigraft copolymers (a) Temperature dependency of storage modulus (E') (b) Loss modulus (E'')

With the increase in the number of branch points, the constrains on the soft PI back bone will be increased. Such rigid constrains on soft PI backbone will enhance the elasticity in the chain architecture. Thus, an increase in the elastic modulus is observed in both glassy and rubbery regime of PI phase with the increase of number of branch points.

6.4 Rheological properties of mulitgraft copolymers

The rheological properties for of the investigated multigraft copolymers are studied in order to describe the segmental, chain and terminal relaxation process with respect to the number of branch points. The master curves of storage modulus (G'), loss modulus (G''), and tan δ for the multigraft copolymers with different number of branch points which are constructed based on TTS principle are shown in Figure 6.4(a-c). The dynamic mechanical spectra which is constructed over the broad frequency range was divided into three regimes i.e. the glassy zone, chain relaxation zone and terminal zone, starting from high frequency regime to low frequency regime. As the master curves are constructed by superpositioning the frequency sweeps which are measured from the temperature above T_{g_PI} and far below T_{g_PS}, the observed relaxation process remains largely dependent on the soft PI phase. However, as the PS phase is remaining as a hard plastic microdomain inside the soft PI matrix and the M_w is increasing with the increase in number of branch points, the influence of such PS micro domains and M_w on various relaxations of PI chains can be readily captured from the master curves of multigraft copolymers. From the master curves it could be observed that in the glassy zone at high frequency the segmental relaxation is insensitive to the change in number of branch points and M_w. However, in the chain relaxation regime the multigraft chain architecture is showing a significant influence on the relaxation process. From Figure 6.4b it could be observed that the multigraft with a large number of branch points is showing a slight extension in the entanglement plateau towards low frequencies. Such extension in the entanglement plateau is attributed to the hindrance in the relaxation process due to high M_w and increased number of tethered junctions on the chain architecture at high number of branch points. In the low frequency regime a non-terminal behaviour can be observed from the magnitude of the slopes of the moduli (G', G''). The low frequency regime is reflecting the existence of additional relaxation modes from the phase separated structure. The dynamic mechanical spectra for damping factor (tan δ) are shown in Figure 6.4c. From the master curves of tan δ it could be observed that the multigraft copolymer with a low number of branch points (MG-4-3.3) is showing a high value of damping in both chain relaxation and terminal regimes.

However, with the increase in the number of branch points the samples are showing more elastic response with low tan δ values. The high damping value which corresponds to the viscous nature of the multigraft copolymer at less number of branch points (MG-4-3.3) is mainly because of less number of constrains on PI backbone from the PS grafts when compared to multigrafts with high number of branch points. As the PI phase is having

comparatively less number of constrains from the PS grafts, it can show high energy dissipation per cycle, which shows high tan δ value in the mechanical spectra after segmental relaxation.

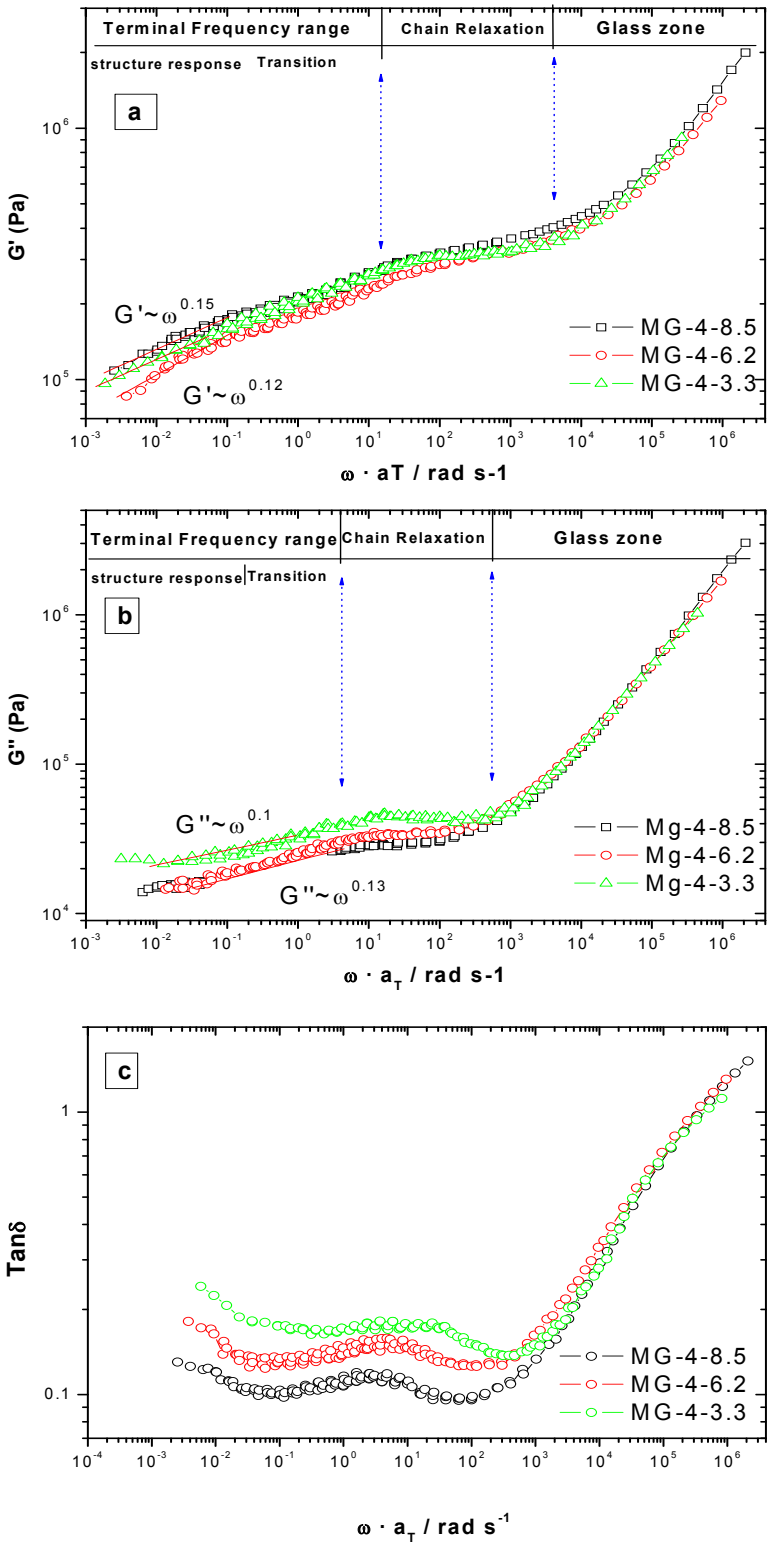

Figure 6.4 Master curves obtained for the investigated multigraft copolymers: (a)Frequency dependency of storage modulus G', (b) loss modulus G'' and (c) Tan δ at T_0=20 °C

6.5 Mechanical Properties

6.5.1 Influence of number of branch points

The mechanical properties for the investigated tetrafunctional multigraft copolymers are characterised from their tensile behaviour as shown in Figure 6.5. These tetrafunctional multigraft copolymers are showing excellent stress-strain behaviour with high strain at break upto 1450% which is far exceeding the values of commercial TPEs (Styroflex, 650%; Kraton, 1080%). From Figure 6.5 it could be observed that the ultimate stress and strain are influenced by the number of branch points. However, the influence of the overall M_w in the chain architecture should be considered very less because in general TPEs from S-B-S and S-I-S triblock copolymers which are having nearly similar PS wt.-% with a reasonable high M_w, i.e. above 100 kg/mol are showing mechanical properties independent of M_w [5].

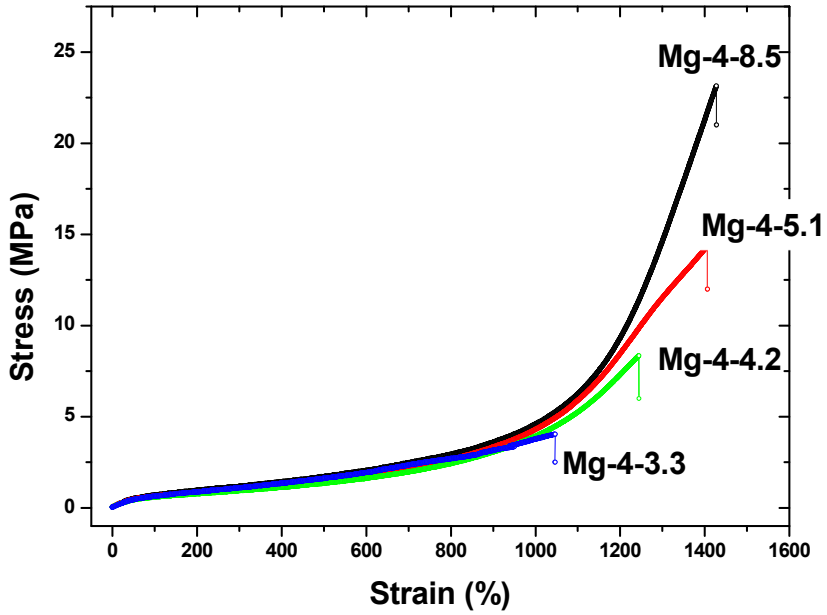

Figure 6.5 Stress-strain behaviour of tetrafunctional multigraft copolymers: Influence of number of branch points

The investigated multigraft copolymers are having M_w far exceeding 100 kg/mol. Thus the observed tensile properties are unaffected by the overall M_w. For clear understanding of the reason behind the superelastic performance of multigraft copolymers, the molecular architecture of multigraft copolymers is comparing constructively with the molecular architecture of commercial thermoplastic materials (triblock copolymers). A schematic representation of the suggested molecular arrangement for this tetrafunctional multigraft is shown in Figure 6.6. As observed from the stress-strain behaviour the superelastic nature in multigraft copolymers is mainly influenced by the chain architecture. From Figure 6.6 it could be observed that the PS grafts which are covalently bonded to the PI backbone can

aggregate to form domains. At room temperature where the material is showing superelastic nature, the PS micro domains are hard and glassy and immobilize the PI backbone which is constrained in between the PS microdomains. Such PS microdomains act as reinforced fillers which are connected very strongly to the PI chains [6]. So a direct control over the growth of PS fillers can be achieved by varying number of PS junction points over the PI back bone.

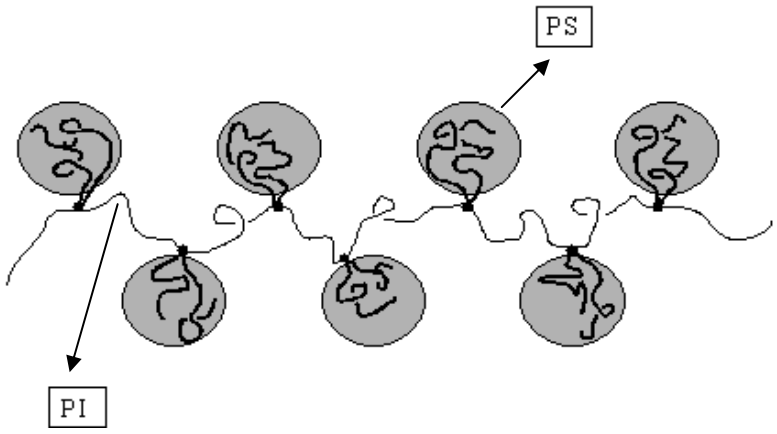

Figure 6.6 Schematic representation of chain conformation in tetrafunctional multigraft copolymers

The physical cross-linking between the PS microdomains and PI phase is directly proportional to the number of branch points in the chain architecture. Thus a highly cross-linked network between PS domains and PI phase can be expected in the multigrafts with high number of branch points.

The stress-strain behaviour of tetrafunctional multigrafts in Figure 6.5 can be divided into two different zones with respect to the strain, i.e. the tensile strength of the materials below and above 750% of strain. At low elongations (below 750% of strain) the stress strain curves appear to have same strength, this observation was reflecting the wt.-% of PS incorporated in the PI matrix which is nearly 16 wt.-% of PS in all the multigraft copolymers. Mostly the physical entanglements within the PI chains and between the PI chains with PS microdomains will show a predominant influence over tensile properties within this low strain. However, at larger strains (above 750% of strain) where the tensile strength starts increasing with the number of branch points, the physical entanglements will be completely stretched and the chemical crosslink became crucial in governing the stress-strain behaviour. According to the case theory when all the chains in the network are substantially of same length and are stretched equally then the enhancement in the mechanical properties can be expected [7]. As the PS grafts are regularly arranged with

equal spacing between the junction points, a nearly ideal network with equal PI chain lengths between the junction points can be expected. Secondly, at high number of branch points, the chemical junction points between PS and PI act as chemical cross-links and the density of these chemical cross-links will be considerably high at high number of branch points. Thus the equal PI chain lengths with highly cross-linked network are able to redistribute uneven stress by permitting slippage of the highly extended chain and retaining the strength of the overall network towards higher strains. As observed from Figure 6.5 the multigraft copolymer Mg-4-3.3 failed at 1050% of strain which is 400% less than Mg-4-8.5. As Mg-4-3.3 is having lower number of cross-linking junction points on the soft PI chains, the network failed at lower ultimate stress and strain. A linear increase in ultimate stress and strain is observed with the increase in the number of branch point which is attributed to the influence of such chemical cross-links between PI and PS phases. Thus the chemical cross-links in the soft phase are crucial in enhancing the strength with high strain at break. In the following section the mechanical properties of a trifunctional multigraft copolymer are discussed where the number of chemical cross-links are increased by selectively crosslinking the soft PI phase by means of electron beam irradiation.

6.5.2 Influence of Cross-linking dosage

The stress-strain behaviour of a trifunctional multigraft copolymer with 4.3 branch points and 6 wt.-% of PS in PI phase is studied by selectively crosslinking the PI phase at different crosslinking dosage using electron beam irradiation technique. The schematic representation of the molecular architecture and molecular parameters are shown in Table 6.1(b) and 6.3 respectively. The trifunctional multigraft copolymers with 6 wt.-% of PS in the chain architecture are showing high strain at break at 3200%. As expected from the previous studies, by increasing the chemical cross-linking points in the PI phase, an enhancement in the mechanical properties can be observed right from the starting of strain window (Fig. 6.7). An increase in the ultimate stress and strain could be observed at 50 kGr of cross-linking dosage. However on further increase of the cross-linking dosage above 50 kGr, the strain at break is observed to decrease. This increase in the stress-strain behavior at low cross-linking dosage (50 kGr) is in accordance with the Bueche theory [8], which states that, in the filled elastomeric phase when the filler particle is firmly attached to the elastomer network then the enhancement in the tensile strength can be achieved by the redistribution of stress by the filler particle when the elastomer chains are broken during deformation and secondly, through absorption of the energy which is released during the chain rupturing by the filler particle. In the present case at 0 kGr the multigraft is showing high strain at break due to the redistribution of the stress by the PS domains which are connected covalently to

the PI backbone. On the other hand by cross-linking the PI phase at 50 kGr dosage, the cross-linking density in the multigraft copolymers is expected to reach a maximum value, because above this cross-linking dosage the material is becoming more rigid with a substantial reduction in the strain at break. Such variation in the material property is attributed to either degradation in the the material or chain scissioning which are normally observed due to a high cross-linking dosage [9]. However, a discussion about chain scissioning and degradation in the material is out of scope for the present work.

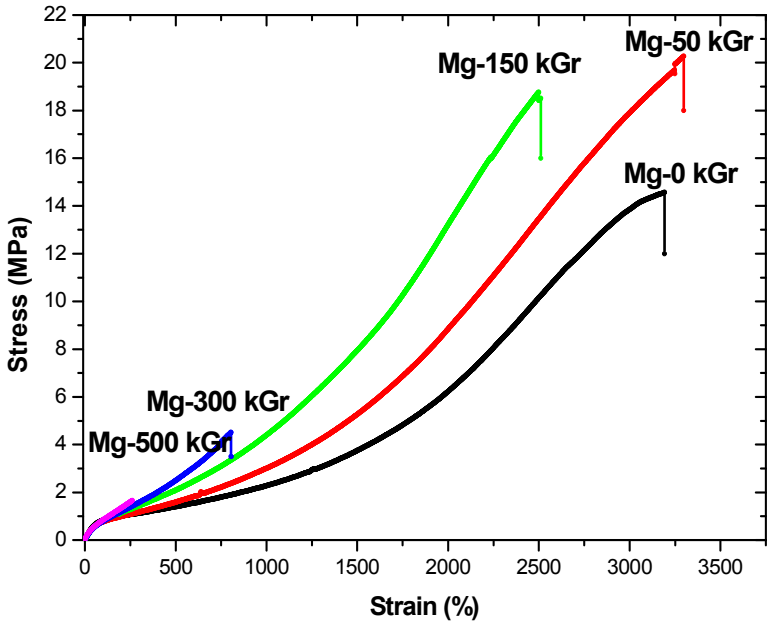

Figure 6.7 Stress-strain behaviour of trifunctional multigraft copolymers: Influence of crosslinking dosage

At this saturation state, the enhancement in the cross-linking density results in making PS microdomains to be confined more firmly within the PI cross-linked network, which results in decrease of the mobility of the PS microdomains at high elongations. Such filled PS microdomains which are firmly attached to the cross-linked elastomer network contributes in increasing the strength of the material by collectively participating in the deformation process and redistributing of the stresses during deformation process. Thus the load bearing capacity is increased even at higher elongations by increasing the chemical cross-linking density in the PI phase.

6.6 Modelling of stress-strain curves

The experimentally observed tensile behaviour of tetra and trifunctional multigrafts are modelled by using the Mooney-Rivlin model for rubber elasticity. The ratio of chemical to physical cross-links (C_1/C_2) is observed to be the governing factor for describing the

tensile behaviour. Figure 6.8 shows the influence of the number of branch points or M_w of tetrafunctional multigraft copolymers on the chemical and physical entanglement modulus C_1 and C_2 values respectively. The modulus values are extracted by fitting the tensile data of the tetrafunctional multigraft copolymer shown in Figure 6.5 with Mooney-Rivlin model for rubber elasticity by considering the PS as filler phase [10-12].

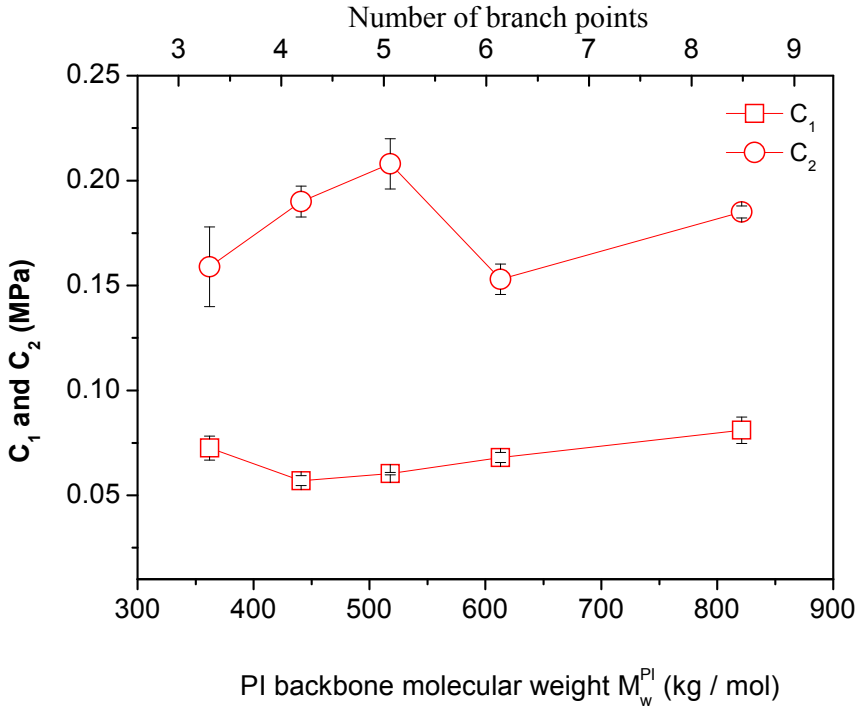

Figure 6.8 Mooney-Rivlin fit parameters for tetrafunctional multigrafts: Influence of number of branch points

A nominal increase in the chemical modulus is observed with the increase in the number of branch points in the chain architecture. Whereas C_2 was observed to increase up to 5 branch points and on further increase of the number of branch points results in showing a decreasing trend. A gradual increase in the C_1 value with the increase in branch points was attributed to the increase in the number of chemical cross-links between PI backbones with PS microdomain. On the other hand at less number of branch points, i.e. below 5, the entanglement effect is significantly increasing the C_2 value. However, at high number of branch points on PI backbone above 5 results in stiffening the PI backbone which contributes in decreasing the influence of physical entanglements (C_2) on mechanical properties. From Figure 6.5 and 6.8 it could be observed that the enhancement in the mechanical properties can be achieved by increasing the chemical cross-linking modulus C_1, i.e. by creating more number of chemical cross-links the stress-strain behaviour could be further improved. As expected, the enhancement in the stress-strain behaviour in

trifunctional muligrafts by cross-linking using electron beam can be observed from Figure 6.7. The increase in the number of cross-links due to electron beam irradiation is verified by fitting stress-strain curves with Mooney-Rivlin model and the fit parameters C_1 and C_2 are shown in Figure 6.9. A linear increase in the chemical crosslink modulus C_1 can be observed along with a gradual decrease in the C_2. The increase in the C_1 value with the cross-linking dosage is in accordance with the above expectations.

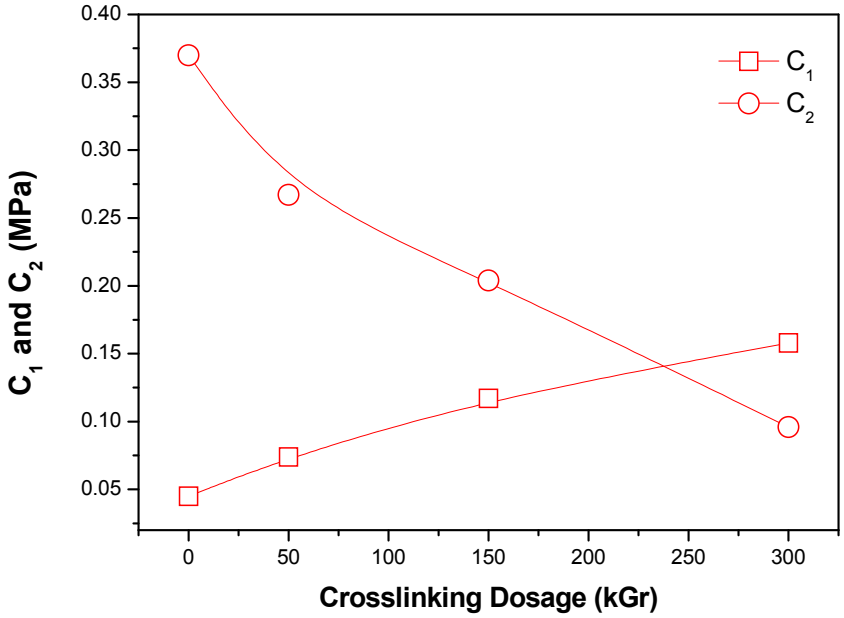

Figure 6.9 Mooney-Rivlin fit parameters for trifunctional multigrafts: Influence of crosslinking dosage

However, with the increase in the cross-linking density in the PI network, the significance of the entanglement effect (C_2) on the tensile behaviour is reduced due to the improvement in the stiffness of the network from high cross-linking points. Further, it reveals that the influence of physical entanglements on mechanical properties can be reduced by increasing the stiffness of the multigraft network by increasing the cross-linking density. Thus the physical entanglements and chemical cross-links are having a significant influence on the super elastic nature of multigraft copolymers.

6.7 References

1. D.Uhrig, J.W. Mayes, Macromolecules, 35, 2002, 7182.
2. F. Beyer, S. P. Gido, C. Buschl, H. Iatrou, D. Uhrig, J.W. Mays, M. Chang, B. A. Garetz, N. Balsara, N. Beck Tan, N. Hadjichristidis, Macromolecules, 33, 2000, 2039.
3. Y. Zhu, E. Burgaz, S. P. Gido, U. Staudinger, R. Weidisch, D. Uhrig, J. W. Mays, Macromolecules, 39, 2006, 4428.
4. S. Milner. Macromolecules, 27, 1994, 2333.
5. G. Holden, E.T. Bishop, N. R. Lege, J. Polym. Sci. C, Polym. Lett., 26, 1969, 37.
6. R. Weidisch, S. P. Gido, D. Uhrig, H. Iatrou, J. W. Mays, N. Hadjichristidis Macromolecules, 34, 2001, 6333.
7. L. C. Case, Macromol. Chem. 37, 1960, 243.
8. F.Bueche, J. Appl. Polymer Sci., 7, 1963, 1165
9. P. Ausloss, Fundamental Processes in Radiation Chemistry, John Wiley and Sons, New York, 1968
10. M. Mooney. J. Appl. Phys, 1940, 1, 582.
11. R. S. Rivlin. Rheology, Vol. I, Academic press New york, 1956.
12. E. Guth, J. Appl. Polymer Sci. 1963, 7, 861.

7. Conclusions and outlook

The present work deals with the investigation of rheological and mechanical properties of triblock copolymers, multigraft copolymers and block copolymer based nanocomposites. The study is focused on the following four topics for enhancing the the physical and mechanical properties of the investigated materials.

1. The influence of molecular chain architecture on phase behavior of linear styrene-(styrene/butadiene)-styrene S-(S/B)-S triblock copolymers and their binary blends was studied
2. The influence of molecular weight (M_w) on physical and mechanical properties of linear symmetric S-(S/B)-S triblock copolymers was critically investigated
3. A novel nanocomposites from elastomer based block copolymer by controlling the size of in situ generated sol-gel nanosilica via cross-linking were synthesised
4. Enhancement of material behaviour in TPEs on the basis of multigraft copolymers and electron beam irradiation was studied.

The phase behaviour of S-(S/B)-S triblock copolymers was initially investigated by studying the influence of chain architecture on physical and mechanical properties. It has been shown that control on the ultimate block copolymer morphology, can be achieved by blending triblock copolymers LN3 and LN4 with asymmetric and symmetric molecular chain architectures respectively. Blends of LN3 and LN4 are observed to be miscible at all blend compositions forming single phase separated morphologies. An unusual morphology with PS-nodes in the cylindrical morphology in the composition range from 40-70 wt. % of LN3 has been observed for the first time in this work which is expected to be due to the influence of the miscibility between the PS end-blocks in LN3 and LN4, and thus reiterates the thermodynamic feasibility of a phase singularity. The ODT behaviour of LN4 is studied by T-SAXS and was reconfirmed by rheology. The SAXS profiles of LN4 in the disordered state are observed to fit consistently with the Leibler structure correlation function for ABA triblock copolymers. The T-SAXS results reveal that with the increase in the complexity in the molecular architecture the phase behaviour is mainly controlled by the entropic term. Rheological observations from the master curves reveal that LN3 is phase separated in the observable temperature range, whereas LN4 is showing an ODT temperature within the experimental temperature range. The ODT is observed to increase linearly with LN3 content. The ODT in the triblock copolymer blends is observed to be governed by M_w difference between the PS end blocks from LN3 and LN4 which are organized in the PS-rich phase

during phase separation process. A co-surfactant effect which arises due to the M_w difference between the PS end-blocks of LN3 and LN4 in the PS rich phase is expected to play a vital role in controlling the segregation strength in the blend composition. A visible change in the composition dependence of ODT was observed after 40 wt.-% content of LN3 in the blends suggesting a change in segregation strength with LN3 content in LN4.

while restoring to the synthesis techniques instead of blending block copolymers for developing new block copolymers with desited property profile. The significance of M_w governing the material behaviour of S-(S/B)-S linear triblock copolymers with high overall PS-content was critically studied. Physical and mechanical properties of these triblock copolymers can be tailored by varying the overall M_w at a constant molecular architecture and the wt.-% of PS. A threshold M_w for attaining microphase separation could be located between 149 to 187 kg/mol. Phase separation with lamellar structure is achieved through increasing M_w for S-(S/B)-S linear triblock copolymers even at 80 wt.-% of PS. The interplay between enthalpic and entropic interactions between the PS and PB block in S-(S/B)-S triblock architecture is observed to be governed by the S/B ratio in the random SB middle block. A high PS content in the SB middle block is reducing the χ parameter which is compensated by increasing the M_w to facilitate phase separation. The triblock copolymers with disordered structure show terminal relaxation behaviour, whereas those with an ordered lamellar structure show non-terminal flow behaviour in the low frequency regime. The persistent lamellar structure within the measured temperature and frequency range leads to an increase in the complex viscosity with a solid like melt behaviour as obtained from the master curves of $|\eta^*|$ and tan δ respectively. The presence of phase separation in triblock copolymers with high M_w results in an extended relaxation time of the polymer chains in the melt. The rheological response obtained from the master curves indicates the sensitivity of phase separation in the block copolymers. Triblock copolymers with high toughness and large strain at break while having high PS-contents above 80 wt.-% can be designed by controlling parameters like block composition, chain architecture and M_w.

Additionally, enhancement in the material behavior of elastometic TPE from block copolymer was attained by synthesis of *in situ* nano silica inside the elastomeric polymer network. An easy access for controlling the size of the silica nano particles in triblock copolymer (LN4) through *in situ* sol-gel reaction was achieved by varying the cross-linking density. The molecular characteristics of the three-dimensional cross-link network are found to be crucial in controlling the growth of silica particles within the block copolymer matrix during sol-gel reaction. In LN4 as the phase separation between PS and PB phases are

strongly influencing the physical and mechanical properties, it is necessary to restore the phase separation in order to attain reinforcement effect from silica. The phase separation in LN4 was completely preserved by cross-linking above 300 kGy, whereas below that the microstructure gets disentangled through swelling in TEOS during sol-gel reaction. Presence of phase separation even after *sol-gel* reaction along with silica nano particles in LN4-500-Si contributes in reinforcing effect for the hybrid nanocomposites. The swelling volume of cross-linked LN4 in TEOS is observed to be a prominent factor in controlling the wt.-% of silica generated inside the polymer matrix. From TGA, it was observed that the wt.-% of silica content is increasing with decreasing cross-linking density. High swelling volume in the gels at low cross-linking density results in increasing the wt.-% of TEOS converting to silica particles with a substantial reduction in size of particle. Therefore application of this new technique in conventional elastomers having homogeneous nature can provide an access to tailor the physical and mechanical properties of their hybrid nanocomposites through varying the size of the nano particles. Thus, in this work a novel material concept in preparing hybrid nanocomposites was proposed, where the desired properties can be scaled by varying the size and content of the inorganic fillers through varying the cross-linking density inside the organic polymer matrix.

Lastly, the work is focused to understand reason for super elastic nature in multigraft copolymers by studying the interrelation between the chemical architecture and physical properties in multigraft copolymers. Under this topic multigraft copolymers with a soft PI back bone which is regularly grafted with PS arms was studied. Selective cross-linking of PI phase was also adopted for studying the influence of cross-linking in these super elastic materials. An increase in the number of PS branch points on the PI backbone in the chain architecture and selective cross-linking of the PI phase are showing significant influence on enhancing the mechanical strength of the multigraft copolymers. Rheological studies on tetrafunctional multigrafts reveal that at high number of branch points the material shows longer relaxation time. On the other hand the multigraft copolymers show a high damping factor (tan δ) at low number of branch points. The stress-strain behaviour of tertrafunctional multigraft copolymers reveal that the chemical connectivity between PS and PI phases is playing a vital role in controlling the mechanical properties. Enhancement in the tensile properties is achived through increasing the number of PS graft points on PI backbone. The fit parameters C_1 and C_2 from the Mooney-Rivlin model for rubber elasticity reconfirms the significance of number of branch points in controlling the stress-strain behaviour. A direct control over the chemical crosslinks in the muligraft copolymers is attained through selective

crosslinking of the PI phase by making use of electron beam irradiation technique. Crosslinking of PI phase which is reinforced with PS microdomains in trifunctional multigraft copolymers results in enhancing the Chemical crosslinks in the PI phases which contributes for enhancing the physical entanglements between PS and PI phases.

In ordered to completely clarify various problems that arise during the course of this work, it is necessary at this point to leave some perspective works that should be considered as an outlook. Initially, the study is dealing with the phase behaviour in the LN3, LN4 and their blends, the existence of the transition at particular blend composition is successfully discussed. However, in order to clearly describe the nature of these highly persistent meta-stable morphologies in blends. A detailed molecular lever study is necessary, In order to reveal such interesting fact from the microscopic structures at nano scale ordering, it is necessary to study the molecular level orientation of the morphology during uni-axial tensile deformation of the sample. Online measurement of FT-IR spectra during deforming the sample could be employed for perusing the required information. Further Rheo-SAXS measurements in the melt state can provide an tool for reconfirming the observation from solid state FT-IT studied.

Future investigations are necessary for describing the though response from triblock copolymewith high M_w. Application of fracture mechanical concepts on these materials could give significant impact for attaining a relation between the observed microstructure with the ultimate mechanical properties. Concerning the nanocomposites topic, a weak tensile response is observed for the block copolymer based nanocomposites. Such unusual tensile properties are attributing to the weak interactions between the nano particles and the polymer matrix. Further investigations are necessary to enhance such interactions for attaining better reinforcement effect from the nanoparticles.

8. Acknowledgements

First of all, I would like to thank my supervisor Prof. R.Weidisch, for introducing me to this exciting field. His esteemed guidance, critical comments and generous co-operation throughout this investigation helped me to meet all the challenges during the course of the research. He has given an excellent opportunity to explore new areas in my work.

I want to express my gratitude to Prof. G. Heinrich from IPF Dresden, for accepting me as his graduate student and for his timely suggestions and strong co-operation throughout the project work. I also thank Prof. M. Stamm from IPF Dresden for his valuable suggestions and extending the SAXS facilities in IPF for my research work.

I would like to thank my group members, Dr. Bhanani K. Satapathy and Dr. U.Staudinger, who constantly motivated me and encouraged me through out my research work. Their stimulating suggestions inspired my passion for my work. I extend my sincere thanks to Mr. M. Ganß, Dr. Y. Duan and Mr. R. Schlegel for their timely help and providing a friendly environment during my stay in Jena.

I wish to express my grateful appreciation to the members from the other working groups at IPF who also helped me during my research work. Dr. R. Vogel for his suggestions during rehological characterization, Mr. A. Janke and Mr. P. Volodyn for helping in AFM investigations, Mr. T. Hofmann and Dr. D. Jehnichen for helping me in SAXS measurements. Dr. R. Häßler and Mrs. L Häussler for carrying out DSC, DMA and TGA measurements. Mr. H. Kunath and Mrs. M. Franke for giving me training in microtoming techiniques for preparing samples for AFM and TEM investigations, Dr. U. Gohs for his kind assistance during crosslinking the block copolymers with electron beam irradiation technique.

I sincerely thank my colleagues from MF group, Dr. K. Schneider, Mrs. U. Reuter, Mr. Scheibner and Mrs. M. Kretzschmar for helping me with mechanical testing. I specially thank Dr. A. Das and Dr. V. Vijayabaskar from IPD for many scientific discussions and helping me in Sol-Gel synthesis and cross-linking techniques. I thank Prof. Jena-U. Sommer and Dr. B. Nandan for their useful discussions in phase behavior of block copolymers.

I would like to acknowledge the BASF AG, especially Dr. K. Knoll, for the productive support and providing the block copolymer samples. I am obliged to the group members of Prof. Uhrig and Prof. Mays from Oak Ridge National Laboratory in Tennessee and Prof. Gigo from University of Massachusetts in Amherst for their co-operation in providing multigraft copolymer samples.

I deeply acknowledge my indebtedness to my parents for their incredible support at many difficult times. I also thank my wife Mrs. Madhavee latha, and all my family members on this occasion, who have extended their love, affection and care to me during the entire period of my research work. Above all, I thank and pray the Almighty for having given me enough strength and good health to complete the research with self satisfaction.

9. Curriculum vitae

Personal Details:

Name : Mahendra Thunga
Birth place : 24.04.1980 in Eluru, India
Nationality : Indian
Sex : Male

Permanent address : 25-4-23, KSR Street, NR pet
Eluru 534006
Andhra Pradesh, INDIA

E-Mail Adress :mahendrathunga@gmail.com, mahendra.thunga@uni-jena.de

---

Educational Qualification:

Ph.D.

(Since March 2005) **Rheological and mechanical behaviour of nano structured triblock, multigraft copolymers and nanocomposites**.
Supervisor: Prof. Dr.-Ing. habil. Roland Weidisch
Prof. Dr.rer.nat.habil. Gert Heinrich

Institute of Materials Science and Technology, Friedrich-Schiller-University Jena. A registered student of Faculty of Mechanical Engineering, Technische University Dresden and Leibniz-Institute of Polymer Research, Dresden.

M.Sc **Applied Polymer science**
(2003- 2005) Martin-Luther-University, Halle-Wittenberg, Germany

B.E **Mechanical Engineering**
(1997- 2001) Madras University, India

Research Interest:

1. Polymer nanocomposites synthesis and characterization
2. Phase transitions in nanostructured polymers
3. Mechanical characterization of copolymers
4. cross-linking studies for filled thermoplastic elastomers (electron beam and chemical ways)
5. synthesis of hybrid nanocomposites via Sol-Gel techniques
6. Fracture mechanics

Research specialization:

1) Rheology and phase transitions of nanostructured polymers

2)Mechanical testing techniques- fracture mechanics

3)Scattering techniques-Small angle X-ray scattering (SAXS), in-situ Rheo-SAXS

4)Crosslinking-Electron beam and chemical crosslinking

5)Microscopy-
Atomic force microscopy (AFM), Transmission electron microscopy (TEM)

Ultramicrotoming for AFM and TEM samples.

6)Sol-gel techniques-Synthesis of SiO_2 nanoparticles in the polymer matrix.

7)Material processing
Compounding, Extrusion, Single-screw and twin-screw extruders, Injection moulding, Compression moulding for producing samples in lab scale.

---

10. Publications

1. **M. Thunga,** U. Staudinger, B. K. Satapathy, R. Weidisch, M. Abdel-Goad, A. Janke, K. Knoll, "Influence of molecular architecture of S-(S/B)-S triblock copolymers on rheological properties", ***J. Poly. Sci. B. Polym. Phy.***. 44 (2006) 2776-2788.
2. B. K. Satapathy, U. Staudinger, R. Lach, **M. Thunga**, R. Weidisch, "Influence of phase miscibility on crack propagation kinetics of nanostructured binary S-(S/B)-S triblock copolymer blends" ***Macromol. Rapid Commun***. 2006, 27, 1814-1820.
3. U. Staudinger, B. K. Satapathy, **M. Thunga**, R. Weidisch, A. Janke, K. Knoll: Enhancement of Mechanical Properties of Triblock Copolymers by Random Copolymer Middle Blocks. ***European Polymer Journal*** 43 (2007) 2750–2758
4. M. Ganß, B. K. Satapathy, **M. Thunga**, R. Weidisch, P. Pötschke, A. Janke, "Temperature Dependence of Creep Behavior of PP-MWNT Nanocomposites", ***Macromol. Rapid Commun***. 2007,28, 1624-1633.
5. U. Staudinger, B. K. Satapathy, R. Lach, **M. Thunga**, R. Weidisch, K. Knoll, "Influence of Phase miscibility and morphology on crack resistance behaviour and kinetics of crack propagation of nanostructured binary styrene-(styrene/butadiene)-styrene triblock copolymer blends ", ***Acta Materialia***,. *55, Issue 17*, *2007*, *5844-5858*
6. **M. Thunga**, B. K. Satapathy, U. Staudinger, R. Weidisch, K. Knoll, "Dynamic mechanical and rheological properties of binary triblock copolymer blends" ***J. Poly. Sci. B. Polym. Phy.***. 46 (2008) 329-343
7. M. Ganß, B. K. Satapathy, **M. Thunga**, R. Weidisch, P. Pötschke, D. Jehnichen, "Structural interpretations of deformation and fracture behaviour of polypropylene / multiwalled carbon nanotube composites", ***Acta Materialia***, 56, 2008, 2247-2261
8. **M. Thunga**, R. Schlegel, U. Staudinger, Y. Duan, R. Weidisch, G. Heinrich , J. Mays, N.Hadjichristidis.''Thermoplastic elastomers on the basis of multigraft and block-double-graft copolymers and electron beam irradiation'' ***Kautschuk Gummi Kunststoffe***, November 2008
9. Y. Duan, E. Rettler, K. Schneider, R. Schlegel, **M. Thunga**, R. Weidisch, H.W. Siesler, M. Stamm, J. W. Mays, N. Hadjichristidis ''Deformation Behavior of Sphere-Forming Trifunctional Multigraft Copolymer''- **Macromolecules** 2008, 41, 4565 - 4568.
10. **M. Thunga**, Bhabani K. Satapathy, Roland Weidisch, Manfred Stamm, Jens U. Sommer, Konrad Knoll''Influence of chain architecture on phase behavior of styrene-(styrene/butadiene)-styrene triblock copolymers and their binary blends'' ***European Polymer Journal,*** 2009, 44, 3790-3796
11. **M. Thunga**, U. Staudinger, M. Ganß, R. Weidisch, K. Knoll, "Influence of molecular weight on rheological properties of linear symmetric S-(S/B)-S triblock copolymers" ***Macromolecular Chemistry and Physics***, 210, 2009, 179-188
12. S. Kalaivani, V. Vijayabaskar, **M. Thunga**, M. Stephan, H. Dorschner, G. Heinrich, A. K.Bhowmick, U. Wagenknecht, "Effect of irradiation temperatures on nitrile rubber nanocomposites" ***Plastics, Rubber and Composites***, 2009, 38, 39-45

13. J.-T. Zhang, **M.Thunga**, S.Petersen, R. Bhat, X. Liu, R. Weidisch, A. Fahr, K. D. Jant. „Temperature-Sensitive simultaneous interpenetrating polymeric network with improved mechanical properties and shrinking kinetics" ***Adv. Eng. Materials*** 2009, 11, 12-19.
14. Y. Duan, **M. Thunga**, R. Schlegel, K. Schneider, E. Rettler, R. Weidisch, H.W. Siesler, M. Stamm, J. W. Mays, N. Hadjichristidis "Morphology and Deformation Mechanisms and Tensile Properties of Tetrafunctional Multigraft Copolymers" ***Macromolecules 2009,*** 42, 4155–4164
15. M. Ganß, B. K. Satapathy, **M. Thunga**, U. Staudinger, R Weidisch, J Hempel, M Rettenmayr, D. Jehnichen, A Garcia-Marcos, Hans H. Goertz, "Morphology and mechanical response of S/B star block copolymer - layered silicate nanocomposites" ***European Polymer Journal*** (Accepted: doi:10.1016/j.eurpolymj.2009.05.021)
16. **M. Thunga**, A. Das, R. Weidisch, G. Heinrich, "Controlling the size of *in situ* sol-gel nanosilica in S-(S/B)-S triblock copolymer'' ***Composites Science and Technology*** (submitted)
17. M. Ganß, B. K. Satapathy, **M. Thunga**, R Weidisch, K. Knoll, "Molecular weight controlled systematic brittle-to-semiductile-to-ductile transition in S-(S/B)-S triblock copolymers" ***Polymer*** (submitted)
18. R. Schlegel, U. Staudinger, **M. Thunga**, R. Weidisch, G. Heinrich, D. Uhrig, Jimmy W. Mays, N. Hadjichristidis, "Investigations on mechanical properties of PI-PS multigraft copolymers ***European Polymer Journal*** (submitted)

11. Abbreviations

PB	Polybutadien
PI	Polyisopren
PS	Polystyrene
N	Total degree of polymerisation
M_n	Number average molecular weight
M_w	Weight average molecular weight
χ	Flory-Huggins interaction
SAXS	Small angle X-ray scattering
D	Domain thickness
DMA	Dynamic mechanical analysis
ε	Strain
f	Composition of block copolymer
G′	Dynamic storage shear modulus
G″	Dynamic loss modulus
GPC	Gel permeation chromatography
ΔG	Gibbs's free energy
ΔS	Entropy change
ΔH	Enthalpy change
ISR	Intermediate segregation regime
λ	Wave length and relaxation time
ODT	Order-disorder transition
OsO_4	Osmium tetroxide
SSL	Strong segregation limit
σ	Stress
σ_y	Yield stress
tanδ	Dynamic loss tangent
TEM	Transmission electron microscopy
AFM	Atomic force microscopy
T_g	Glass transition temperature
TPE	Thermoplastic elastomer
WSL	Weak segregation limit

$I(q)$	Scattering intensity
$S(q)$	Structure factor
De	Deborah number
η	Complex viscosity
τ	Shear stress
TTS	Time-temperature-superposition
a_T	Shift Factor
ω	Angular frequency
KGy	Kilo gray
MG	Multigraft
C_1	Chemical cross-linking modulus
C_2	Physical cross-linking modulus
E'	Tensile elastic modulus
E"	Tensile loss modulus
V_c	Cross-linking density variables
M_c	Molecular weight between cross-links
ρ	Density of polymer
R	Real gas constant
T	Temperature
EB	Electron beam
$H(\lambda)$	Relaxation strength
ν_r	Volume fraction of rubber
D_s	Deswollen weight of the sample
F_f	Insoluble fraction of gel
ρ_r	Density of rubber
ρ_s	Density of solvent